THE UNIVERSITY OF CHICAGO

FEEDBACK AND FITNESS IN THE HEAT SHOCK RESPONSE

A DISSERTATION SUBMITTED TO
THE FACULTY OF THE DIVISION OF THE BIOLOGICAL SCIENCES
AND THE PRITZKER SCHOOL OF MEDICINE
IN CANDIDACY FOR THE DEGREE OF
DOCTOR OF PHILOSOPHY

COMMITTEE ON GENETICS, GENOMICS AND SYSTEMS BIOLOGY

BY
RANIA GARDE

CHICAGO, ILLINOIS
AUGUST 2023

TABLE OF CONTENTS

LIST OF FIGURES

LIST OF TABLES

ACKNOWLEDGMENTS

To my labmates - Surabhi, Asif, Annisa, Sarah and Luke. Thank you for finding humor in every lab meeting and being my role models of humility. Thank you to our excellent lab technician, Rosario, for learning about everything our lab needed so very quickly, and bringing your passion for recycle and reuse!

Thank you, to the folks at the UChicago Cytometry and Antibody Core Facilities, for your patient and friendly help. The reliable Fortessa 4-15 HTS was vital for my experiments. It was always a pleasure to get trained on a new instrument or ask for guidance.

To my family, for all the phone calls and visits, and love from afar, always. Thank you, to my Baba, for applying all your PhD experiences and managerial expertise to help me get through these years, for the daily calls when things got tough. To Mummy for the work sessions on zoom and for spending time with me in my new home in Chicago. Thank you for taking me to the Lawrence Hall of Science to learn about science, and later, to learn to be a teacher! To my little brother Sawan for the encouragement and insights, and reminding me what being excited about learning and hard-working looks like.

To my co-op friends for being my Chicago family. Coming home to dinner with you each day was always a daily dose of laughter and perspective. I have lived with so many amazing PhDs: Clara delJunco, Andrew White, Jeff Johnston, Eric Potash, Chris Quintanilla, and Kevin Casto. They have all successfully defended and showed me that I can do it, too.

To David for always being available for a chat, for remembering what I'm good at when I forget, for modeling optimism and confidence and work-life balance for me. David, I know you say I earned your confidence, but you took me seriously and believed in me from the first day we met. Now I know exactly what an amazing teacher looks like. I hope I can be half-as-good a teacher as you are next year. I hope to make you proud, and will certainly update you on my progress.

ABSTRACT

Many environmental stressors disrupt protein homeostasis in the eukaryotic cell. To adapt, the eukaryotic cell activates the heat shock response which, in *S.cerevisiae*, involves the induction of 42 target genes, many of which are protein-folding chaperones. The induced target genes, collectively called the heat shock response (HSR), replenish the cell's supply of protein folding machinery, so that there are sufficient chaperones to fold the proteins in the cell. HSR hyperactivity and hypoactivity in human disease states indicates that HSR regulation in both directions is essential for normal cell functioning, motivating this project's primary question: how does a healthy cell respond and adapt to unexpected changes in conditions? What feedback mechanisms tune the HSR level?

In the pilot study presented in Chapter 2, one Hsf1 target, Sis1, is investigated for a potential role in feedback regulation of the HSR. As Sis is necessary to repress Hsf1 during non stress, its induction during stress might be necessary for Hsf1 deactivation. Surprisingly, Sis1 induction is dispensable for Hsf1 deactivation, but instead supports long term fitness. Through this initial study, we developed a long-term quantitative fitness assay, and we came to appreciate that the HSR not only restores homeostasis, but supports cell adaptation and growth resumption.

In Chapter 3, all HSR target genes were screened for their role in feedback regulation. Induction of six Hsf1 target genes impacts Hsf1 activity, though none as dramatically as the Hsf1 target Hsp70, identified previously. Induction of four of the six Hsf1 target genes was important for clearing cytosolic protein aggregates during heat shock, indicating these genes regulate Hsf1 activity by boosting Hsp70 availability. Follow up investigations revealed that the most significant novel feedback regulator, Fes1, is indeed necessary for relocalization of Hsp70 from protein aggregates in the cytosol to the nucleus. In conclusion, all feedback regulation on Hsf1 seems to proceed via the Hsp70-dependent negative feedback loop.

Chapter 4 is an investigation of Sis1's role at orphan ribosomal protein (oRP) aggregates

at the nucleolar periphery. First author Asif Ali found that Sis1 maintains the dynamic, liquid-like state of condensates, and is necessary for efficient condensate dispersal after stress. To investigate whether the Sis1-dependent reversibility of condensates had physiological relevance, Sis1 is transiently depleted from the nucleus during heat shock, then cell fitness is measured. Transient Sis1 depletion during heat shock affects cells' ability to resume growth quickly after heat shock so Sis1-maintained oRP condensates are necessary for efficient growth resumption after stress. This study begins to elucidate endogenous, stress-induced protein aggregates: their contents, function, and the chaperones which mediate their formation and resolution.

We now know that heat shock response feedback regulation architecture is simple, and centered around the Hsp70-dependent negative feedback loop. Its simplicity probably facilitates the conservation of this regulatory mechanism across eukaryotes, which likely receives input from diverse proteins across the cell, in response to diverse stressors.

CHAPTER 1

INTRODUCTION

1.1 Stress Response Pathways: A Re-balancing Act

1.1.1 Responding to stress

A eukaryotic cell exposed to environmental stressors has multiple choices. Should it become quiescent – weathering the storm by shutting down all import/export and energy-consuming processes[112]? Should it commit cellular suicide – apoptosis – or should it attempt to repair cellular damage and adapt to the new environment in spite of unpredictable, sometimes escalating environmental stressors [18,34]? All eukaryotic cells, from a human neuron to a single cell organism like *S. cerevisiae* – encounter these choices.

If a cell acts most aggressively, repairing cell damage and attempting to adapt and survive in ongoing stress, it must be sensitive to the state of the cell, stopping the stress response before overshooting the cell's demand. This choice requires sophisticated sensors and signaling mechanisms.

1.1.2 Proteostasis

Many of the cell's stress responses work towards restoring and maintaining one of the fundamental necessities for cell growth and division – protein homeostasis. Protein homeostasis is the state of balance in a cell, where there is an adequate supply of the cell's protein folding enzymes, called chaperones, to facilitate normal protein folding and repair misfolding mistakes[10]. Examples of disrupted protein homeostasis in human disease states (discussed below) indicate that both a deficit and an excess of chaperones is detrimental to normal cell functioning.

Many factors can disrupt homeostasis. Mistakes, such as mRNAs missing stop codons,

damaged mRNA transcripts, or decreased tRNA availability, are often proofread during translation: ribosomes pause which leads to detection by the cells' ribosome quality control mechanisms [28,50,51]. An increase in ROS in the extracellular milieu (which occurs more often during ageing) damages mRNA transcripts, and also results in protein misfolding[122]. Defects in mitochondrial import also lead to a toxic buildup of mitochondrial proteins in the cytosol[143]. Usually, chaperones can quickly restore protein homeostasis by refolding misfolded proteins and sending erroneous proteins for degradation [42,62,125,142]. However, when disruptions to protein homeostasis are large enough, the cell's standing population of chaperones is not sufficient to restore homeostasis, and stress responses are activated to compensate.

The stress response that responds most specifically to disruptions in protein homeostasis is the "heat shock response" (HSR). In spite of the name, heat isn't necessary to activate the HSR. Any stressor which causes proteostatic collapse, such as nutrient starvation, oxidative stress, and osmotic shock, activates the HSR. In the HSR, the transcription factor, heat shock factor 1 (Hsf1) orchestrates the re-balancing act. Hsf1 must induce chaperone expression just enough to restore a balance between the burden of misfolded proteins and the supply of chaperones to refold these proteins.

1.1.3 Medical relevance

In both cancer and neurodegenerative disorders, Hsf1 activity does not match the proteostatic demands of the cell. Chaperone overexpression wreaks havoc by stabilizing proteins that are incorrectly translated in the cell [106,139]. Because hyperactive Hsf1 must induce more chaperones, it follows that Hsf1 hyperactivity in mammalian cells is correlated with metastatic breast, colon and lung cancer[139]. At the other extreme, in neurodegenerative disorders, insoluble protein aggregates accumulate and inhibit normal cell functioning but Hsf1 is highly unstable and thus Hsf1's chaperone targets are not expressed at sufficient

levels to restore protein homeostasis [113,126]. To understand the misregulation of the HSR in disease states, we study the mechanisms of Hsf1 regulation and adaptation to stress in healthy cells.

1.1.4 Overview of response signaling circuitry

Stress response pathways involve a transient response where the signaling output goes back to basal levels, even if the environmental stress continues; in the network regulation field, this is referred to as perfect adaptation [31,70]. Comprehensive screens of potential network circuitry find that only two circuit types – negative feedback and incoherent feed forward loops – can exhibit perfect adaptation [92]. If we consider proteins that can toggle between not two, but three states, then a third circuit type, called "state dependent inactivation", can achieve perfect adaptation. Famously, this circuit type occurs in the voltage-gated channels of neurons.

In biology, negative feedback loops are commonly found in stress responses. In the UPR in the ER of budding yeast, a negative feedback loop involving the Ire1 target gene and chaperone, BiP, governs the deactivation of the master transcription factor, Ire1[103]. In *E.coli*, expression and stability of the heat stress response factor, σ_{32} , increases in expression and stability upon heat induced changes in the σ_{32} RNA secondary structure, and induces hundreds of genes, including many chaperones which aid in restoring protein homeostasis[95]. Two of the chaperones, GroEL and DNAK, also provide negative feedback on their master transcription factor σ_{32} by directly binding and promoting its proteosomal degradation[74,89,97,110]. The HSR in eukaryotes has many similarities to the prokaryotic response.

1.1.5 HSR activation

The eukaryotic HSR is transient, like most stress responses, and is regulated by a negative feedback loop involving "chaperone titration-away", similar to the *E.coli* HSR. Historically, there were two competing models of Hsf1 activation: one, Hsf1 undergoes conformational changes upon temperature change, and two, that chaperone titration out of the nucleus to the cytoplasm de-represses the nuclear transcription factor Hsf1.

Biochemical and genetic investigations of Hsf1 activation provide unanimous support for the chaperone titration mechanism of HSR activation[68,83]. In non-stress conditions, the chaperone Hsp70 is bound to Hsf1 in the nucleus, repressing its activity. Upon heat stress, transcription, translation and ribosome assembly stalls leading to a sudden accumulation of newly translated, unfolded proteins in the cytoplasm, and unassembled ribosome parts (orphan ribosomal proteins) at the nucleolar periphery [6,30]. These protein aggregates recruit Hsp70, freeing Hsf1 to induce its transcriptional targets in the nucleus. A recent investigation found that in a library of stressors which all activate Hsf1, the necessary component for Hsf1 activation is always ongoing protein synthesis, supporting this model where Hsp70 recruitment to newly-synthesized, unfolded proteins is necessary to de-repress Hsf1 [133]. Hsf1 induces expression of 42 genes with diverse roles across the cell, including translation regulators, degradation machinery and cytosolic and mitochondrial chaperones [102].

1.1.6 HSR deactivation

After just 15 minutes of stress, the HSR turns off, and HSR deactivation, like HSR activation, involves Hsp70. Ultimately, Hsf1-induced Hsp70 binds and deactivates Hsf1 in a negative feedback loop, but induced Hsp70 does not immediately deactivate Hsf1 [68]. First, the Hsf1-induced Hsp70 population performs chaperone duties in the cytoplasm: it unfolds proteins so they can spontaneously refold, triages protein aggregates by coordinating degradation machinery, and recruits the disaggregase Hsp104, and Hsp90 chaperones [40,42,63]. Once

protein homeostasis is restored, Hsp70 becomes available to bind and deactivate Hsf1 in the nucleus. Thus, Hsp70 availability transmits information about the homeostatic state of the cell to Hsf1.

1.1.7 Chaperone regulators of the HSR

Hsp70 has many co-chaperones (called J domain proteins or Hsp40s) that catalyze ATP hydrolysis and provide client specificity. Therefore, it is possible that J domain proteins (JDPs) may regulate Hsf1 via the Hsf1 regulator, Hsp70. Transient nuclear depletion of each cytosolic/nuclear JDPs revealed that only Sis1 is necessary for the basal repression of the HSR [30]. Ectopically-induced Sis1 relocalization to the nucleolar periphery causes dramatic HSR activation in non-stress conditions and a decrease in Hsf1-Hsp70 binding, implying that nuclear Sis1 is necessary for basal, Hsp70-dependent Hsf1 repression [30].

Imaging of endogenous Sis1 during the HSR supports its important role in Hsf1 regulation. Within seconds of HS, ribosome assembly halts and the ribosome parts, orphan ribosomal proteins (ORPs), rapidly collect into aggregates at the nucleolar periphery. Sis1 relocalizes from the nucleus to these ORP condensates [30]. Hsp70 also relocalizes from the nucleus to ORPs. Sis1 and Hsp70's roles in chaperoning ORPs at the nucleolar periphery is investigated in Chapter 4.

Biochemical studies flesh out the picture of HSR regulation: Sis1 facilitates HSR repression by mediating high affinity binding of Hsp70 to its substrate, Hsf1. JDPs facilitate ATP hydrolysis by Hsp70, which causes a conformational change in Hsp70 to the closed state, which has orders of magnitude higher binding affinity for client proteins [26,65,109,144]. Supporting the simple model we have developed for Hsf1 regulation, the necessary stoichiometric conditions for the 'ultra-affinity' Hsp70-Hsf1 binding (high Hsp70 concentration, low substrate (Hsf1) concentration, and low JDP (Sis1) concentration) exist in the yeast nucleus.

1.1.8 Other modes of Hsf1 regulation

Additionally, there is correlative evidence for Hsf1 regulation by other means: by Hsp90 chaperone-based regulation and by phosphorylation. Here, I summarize these regulatory axes. Originally, the chaperone Hsp90 was believed to negatively regulate Hsf1 by chaperone titration [8,153]. However, there is no evidence for direct binding Hsp90 and Hsf1, followed by dissociation in stress, followed by rebinding during HSR deactivation, which are hallmarks of the chaperone titration mechanism. Hsp90 probably regulates Hsf1 by indirect means. Hsp90 knockdown causes Hsf1 hyperactivity, suggesting Hsp90 does regulate Hsf1, perhaps via one of the many proteins it folds and stabilizes. Hsp90 OE cannot rescue Hsf1 hyperactivity (when Hsp70 is saturated with Hsf1 decoy), so Hsp90 must regulate Hsf1 in an Hsp70-independent fashion [152]. Perhaps, Hsp90 regulates Hsf1-induced gene transcription by remodeling chromatin at Hsf1 target genes [32,71].

Hsf1 regulation by phosphorylation has also been explored. In the mammalian HSR, it is widely believed that Hsf1 is localized as a monomer in the cytoplasm, then gets phosphorylated, trimerizes and relocalizes to the nucleus to induce its target genes, reminiscent of the conserved two-component signaling mechanism passed down from prokaryotes [8,128]. However, cytosolic Hsf1 or HS-triggered Hsf1 trimerization has never been observed in mammalian or yeast cells, in vivo. However, Hsf1 phosphorylation in stressful conditions is conserved across eukaryotes prompting our lab's previous investigations into its role.

In yeast, mimicking constitutive phosphorylation with 116 serine/threonin-to-aspartate mutations increases Hsf1 activity during heat shock, likely because hyperphosphorylated Hsf1 recruits transcriptional machinery more efficiently, suggesting Hsf1 phosphorylation is sufficient for activation of the HSR [152]. However, Hsf1 phosphorylation does not turn out to be necessary for HSR activation. Remarkably, a mutant of Hsf1 with 152 serine/threonine-to-alanine mutations and completely lacking phosphorylation is able to activate the HSR comparably to wild type. This mutant does deactivate earlier than wild type Hsf1, suggesting

that phosphorylation plays a role in sustaining Hsf1 activity. As so many eukaryotic signaling pathways involve kinase cascades, Hsf1 phosphorylation may be a means for diverse cellular processes to communicate with the HSR [47,145].

1.1.9 Potential Hsf1 deactivators

Given Sis1's interesting role in basal Hsf1 repression, the search for Hsf1 feedback regulators among the Hsf1 target genes promises to be fruitful in expanding our knowledge of the HSR mechanism. It is possible that proteins outside of the Hsf1 transcriptome deactivate Hsf1, but given the importance of negative feedback loops and incoherent feedforward loops in transient stress responses, we believe that Hsf1 targets are the most likely regulators of the HSR.

Here, a few illustrative examples of Hsf1 target genes that may influence Hsf1 deactivation, based on their putative functions. (1) Ira2 is a negative regulator of RAS, which coordinates numerous cellular processes, including other stress responses. Therefore, induction of Ira2 represses cAMP/PKA induced stress responses and cell proliferation Hsf1. Hypothetically, if induced Ira2 provides negative regulation on Hsf1 (i.e. once Ras has been completely deactivated) this could be a means of communication between the HSR and other stress responses [123,130]. (2) The JDP Apj1 has a role in nuclear and cytosolic proteostasis, so it could mediate Hsp70-Hsf1 high affinity binding and thus Hsf1 deactivation. (3) Nucleotide exchange factors (NEFs) are also induced by Hsf1 and occupy a central role in the Hsp70 conformation cycle. NEFs facilitate replacement of ADP with ATP, which allows Hsp70 to assume an open conformation and release its substrate. Thus, a NEF could support Hsf1 deactivation by facilitating Hsp70 release of unfolded protein clients in the cytoplasm or nucleus so that Hsp70 could re-bind Hsf1. For example, Hsf1 induces the multipurpose NEF Sse1, which, in addition to its traditional NEF function, recruits Hsp104 to aggregates, and co-chaperones Hsp90 and Hsp70 [1,9]. The NEFs, Fes1 and Sse2, are also induced by

Hsf1.

It is also possible that Hsp70 is the only negative feedback regulator of Hsf1. If this is the case, what do the Hsf1 targets do? Do they all have adaptive roles?

1.1.10 Studying the HSR

The Hsf1-induced set of genes, coined "the Heat Shock Response" (HSR), and Hsf1 itself, are conserved across eukaryotes. Budding yeast is the perfect model organism for studying the HSR – homologous recombination in yeast allows for easy genetic manipulation, and the yeast genome does not have as many redundant gene groups as mammalian genomes do.

To induce the HSR in yeast, we raise the temperature from optimal growing condition, 30°C, to 37°C or 39°C (hot, but survivable). This sudden temperature elevation ('heat shock') disrupts proteostasis. There is no documented irreversible cell damage caused by mild heat stress (<40C). Indeed, WT cells are capable of adapting and growing at an elevated temperature at comparable rates to cells grown at 30°C. Exposing budding yeast to heat stress is an excellent approach to studying proteostasis and adaptation to ongoing stress.

1.2 Transcriptional Regulation in the HSR

Studies of the transcriptional response to heat shock began with *Drosophila* salivary cells, that, when the incubator was mistakenly raised overnight, developed large chromosomal 'puffs' [108]. Ritossa knew that chromosomal 'puffs' had been recently identified as sites of RNA synthesis. By repeating the heat shock treatment, Ritossa found that the puffs occurred predictably at the same loci in the Drosophila chromosomes, suggesting a programmed transcriptional response to heat shock. This discovery made the heat-shocked drosophila cells a model system for studying the mechanics of transcription - hundreds of genes are rapidly and simultaneously upregulated by heat shock (some more than 100-fold), and Drosophila's elongated interphase chromosomes (called polytene chromosomes) allow

for fluorescence microscopy of transcriptional machinery along promoters and open reading frames during transcription [17,76].

Today, the well-established modes of transcriptional regulation are (1) local chromatin accessibility, (2) the regulatory DNA upstream of each gene (number and strength of transcription factor binding sites) (3) and "3D" chromatin architecture. Here, I review the mechanics of transcriptional induction and how these three phenomena cause variation in induction of Hsf1 target genes.

1.2.1 Local chromatin accessibility

Inactive genes are occupied by nucleosomes in *S. cerevisiae*. Before transcription by RNA polymerase, histones are acetylated and then displaced by histone remodeling machinery, allowing transcription factors to access their specific DNA binding sequences (though transcription factors can induce genes at low levels even when genes are nucleosome bound)[141]. Here, local chromatin remodeling at Hsf1 target genes is reviewed.

18 of the 42 Hsf1 induced targets are induced by Hsf1, in non-stress and stress [124]. Their promoters are maintained in a constitutively nucleosome-free state by the pioneer transcription factor, Reb1, which binds specifically in the enhancers of these genes and recruits chromatin remodelers (SWI/SNF and RSC complexes) and transcriptional machinery (Mediator and RNA Polymerase II) [102,149,150]. Hsf1 is bound at these genes during non-stress. During heat shock, Hsf1 occupancy increases further at these gene's promoters, and gene expression increases as well.

24 genes are induced by Hsf1 only during heat shock; they do not depend on Hsf1 for their basal expression [124]. Nucleosomes occupy the promoter regions of these 24 genes in non-stress conditions. Upon heat shock, Hsf1 itself acts as the pioneer transcription factor by recruiting chromatin remodelers to evict histones and recruiting Mediator and Pol II to initiate transcription [64]. As nucleosomes are evicted, even more Hsf1 binds; both decreased

nucleosome occupancy and strength of the underlying specific Hsf1 binding sequence becomes more strongly correlated with the induction of each target gene as heat shock progresses [102].

1.2.2 DNA sequence

Hard-coded DNA sequence is the most well-studied determinant of local transcription factor binding. Previously, we determined that the Hsf1 DNA binding consensus motif is TTCnnGAA: the MEME motif-analysis algorithm was used to generate sequence that generated the most agreement among DNA sequences with high Hsf1 occupancy (based on genome-wide Hsf1 ChIP-seq) [81,102].

The regions flanking the Hsf1-specific DNA motif may also influence Hsf1 binding. With the stress-induced transcription factor Msn2, the sequences flanking Msn2's specific DNA binding motif interact with the IDR of Msn2 and influence Msn2's binding sites genome-wide [16,59].

1.2.3 3D Genome architecture

Hsf1's target genes make many short intragene contacts upon their induction. Enhancer-promoter looping brings distal enhancers and its bound transcription factors in proximity to specific coding genes, and promoter-terminator contacts concentrate transcriptional machinery for efficient gene transcription [49,138]. Interactions of the 5' UAS with the protein coding region (called gene 'crumpling') has also been observed during transcription of Hsf1 target genes [22]. Though its functional role is not defined, mammalian studies suggest crumpling may aid RNA polymerase progression along the gene [72]. It is still unclear how much intragene contacts vary from gene to gene or impact the diversity in the transcriptional dynamics of Hsf1 target genes.

Dramatic contacts between Hsf1 target genes on different chromosomes are another type of 3D chromatin rearrangement. In the initial seconds and minutes of heat-shock, as Hsf1

occupancy increases across the genome, Hsf1-induced genes coalesce with Hsf1 and transcriptional machinery into two liquid-like condensates. These condensates represent the first instance of active transcriptional hubs ever observed in yeast [23,24]. When Hsp70 rebinds and deactivates Hsf1, condensates disperse – the Hsp70 binding site on Hsf1 (ΔCE2) resulted in constitutive Hsf1 clustering in heat shock and non-heat shock, loss of intergenic clustering, and loss of transcriptional machinery recruitment (Med15). Loss of the NTA (IDR) of Hsf1 depleted Hsf1 condensate formation, even in HS; though Hsf1 did occupy HSR genes, it was not able to recruit Med15 and target gene transcription was depleted. These transient foci have not been observed in any other transcriptional regulon in yeast. However, the stress-induced transcription factor, Msn2, in yeast can be manipulated to form transient stress-induced foci in vivo, by reorganizing the IDR sequence of Msn2 so that its aliphatic residues are more clustered (Naama Barkai, Q-Bio Conference, 2023). In summary, the transient Hsf1 clusters that form upon HS are sites of heightened intergenic interactions and active gene transcription [23].

It is possible that the subnuclear localization and coalescence of Hsf1 target genes may correlate with their raw transcription level or dynamics. A Taq-I 3C screen of intergene contacts between all Hsf1 targets during stress will provide conclusive answers. For the few Hsf1 target genes whose intergenic contacts have been characterized (Hsp104, Hsp82, Ssa2, Ssa4), changes in the frequency of intergenic interactions and intragenic looping/crumpling over the heat shock time course correlate with transcription dynamics [22]. The peak frequency of intergenic interactions and of intragenic interactions also correlates with the raw transcriptional level of each gene, suggesting that transcriptional dynamics are strongly influenced by the timed dissociation of each individual gene from the intergenic clusters and by decreased rate of intragenic looping and crumpling. Hopefully, upcoming studies on transcriptional regulation, especially 3D genome architecture, will shed light on the determinants of the diverse transcriptional dynamics in the HSR.

1.3 Spatial Organization of the Proteostasis Network

Initially, numerous studies attempted to investigate the protein inclusions and compartments that form in human neurodegenerative disorders by ectopic expression of disease-causing human proteins, or engineered temperature-sensitive misfolding proteins. The research on protein quality control compartments are comprehensively summarized in other reviews [69,125]. Here, I review just three protein quality control studies, which identified heat-induced protein compartments and their contents, and laid the groundwork for the proteostasis field.

1.3.1 Initial proteostasis studies

Studies from the Frydman lab tracked the kinetics of protein aggregation, the subcellular location of aggregates, and the post-translational modifications which guide proteins to one compartment or another. They identified a protein compartment that forms within minutes of HS and named it "insoluble protein deposit" (IPOD). Because it contained non-ubiquitinated species and prions, they believed it could be a catch-all protein dump [61]. Simultaneously with IPOD formation, proteosomes and ubiquitinated proteins were targeted to a stress-induced compartment near the nuclear periphery, which they named the juxta- or intra- nuclear quality control compartment (JUNQ or JNQ). After a few hours of HS, perivacuolar inclusions also formed. The kinetics of formation as well the various species found at each site led them to believe that IPOD and perivacuolar inclusions were both overflow spaces to hold insoluble and non-ubiquitinated proteins for when proteosomal degradation was impaired or overwhelmed [61]. Later investigations showed that all compartments appeared to be dynamic and maintained by chaperones, suggesting aggregation is an active and controlled cellular process, not a symptom of cell dysfunction [29]. Many of the chaperones identified at aggregates are induced by Hsf1 during the HSR.

Two years later, a pivotal comparative study revealed that previous investigations which used ectopic misfolded protein reporters to study proteostasis could not be compared directly.

The study found that how ubiquitination affected a protein's destination compartment and how fast the protein was degraded depended on a protein's intrinsic features, and there is a huge diversity of misfolded proteins used across studies [87]. Ectopic misfolded protein reporters in yeast include VHL, a mammalian ubiquitin ligase that misfolds (even at 30°C) without its partner protein, Ubc9ts the temperature sensitive version of the human sumo-conjugating human enzyme, Rnq1 and Ure2, yeast prion proteins, HttQ103 the expanded polyglutamine protein responsible for Huntington's disease, tGnd1-GFP, a truncated version of a yeast dehydrogenase that is constitutively prone to misfolding and aggregation [118]. The differences in ectopic misfolded protein reporters used across studies makes it difficult to apply the results of proteostasis studies beyond their experimental conteext. Nonetheless, these studies will be built upon in future investigations that leverage proteomics to study the endogenous protein composition of stress-induced aggregates.

As introduced in this chapter, the recruitment and release of chaperones from cytosolic HS-induced aggregates determines their availability to repress Hsf1. Therefore, the specific types of protein aggregates where chaperones act and the mechanism of their recruitment and release, are important for understanding Hsf1 regulation. Much more research is needed to identify the proteins that recruit and release Hsf1 regulators from aggregates.

1.3.2 Are aggregates good or bad?: controversy on the function of cytosolic protein aggregates

Questions about the function of protein aggregates emerge from initial proteostasis studies. Are they pre-degradative holding compartments or functioning oases of protein activity during heat shock? Do aggregates set off the proteotoxic stress alarm bells, or is aggregation a stress-management strategy, diminishing the burden of unfolded proteins on the cell? In short, both seem to exist, and a distinction must be made between transient, stress protective aggregates, and persistent, toxic aggregates [3].

Transient stress-induced protein aggregates appear to be stress-protective. A proteome analysis of heat-induced aggregates found 170 different endogenous yeast proteins sequestered at heat-induced protein aggregates; these proteins did not misfold and were found in the soluble fraction of cell lysates after heat shock. (In contrast, the insoluble fraction of cell lysate contains irresolvable protein aggregates and prions that must be removed by degradation.) This study also used a luciferase reporter assay to show that sequestered proteins retain functionality after dissolution, showing that protein aggregates could be stress-protective structures, and invalidating the constitutively misfolded ectopic protein reporters used to study proteostasis previously [135].

Some aggregates that arise in disease states are detrimental to cell fitness. In human diseases, insoluble protein aggregates impair fitness: ectopic expression of the protein responsible for Huntington's prevents the degradation of ectopic misfolded proteins by sequestering the essential yeast chaperone Sis1 [3,96]. More research is needed to understand why an initially reversible stress-protective aggregate becomes an irreversible, toxic aggregate overtime, and what makes it toxic.

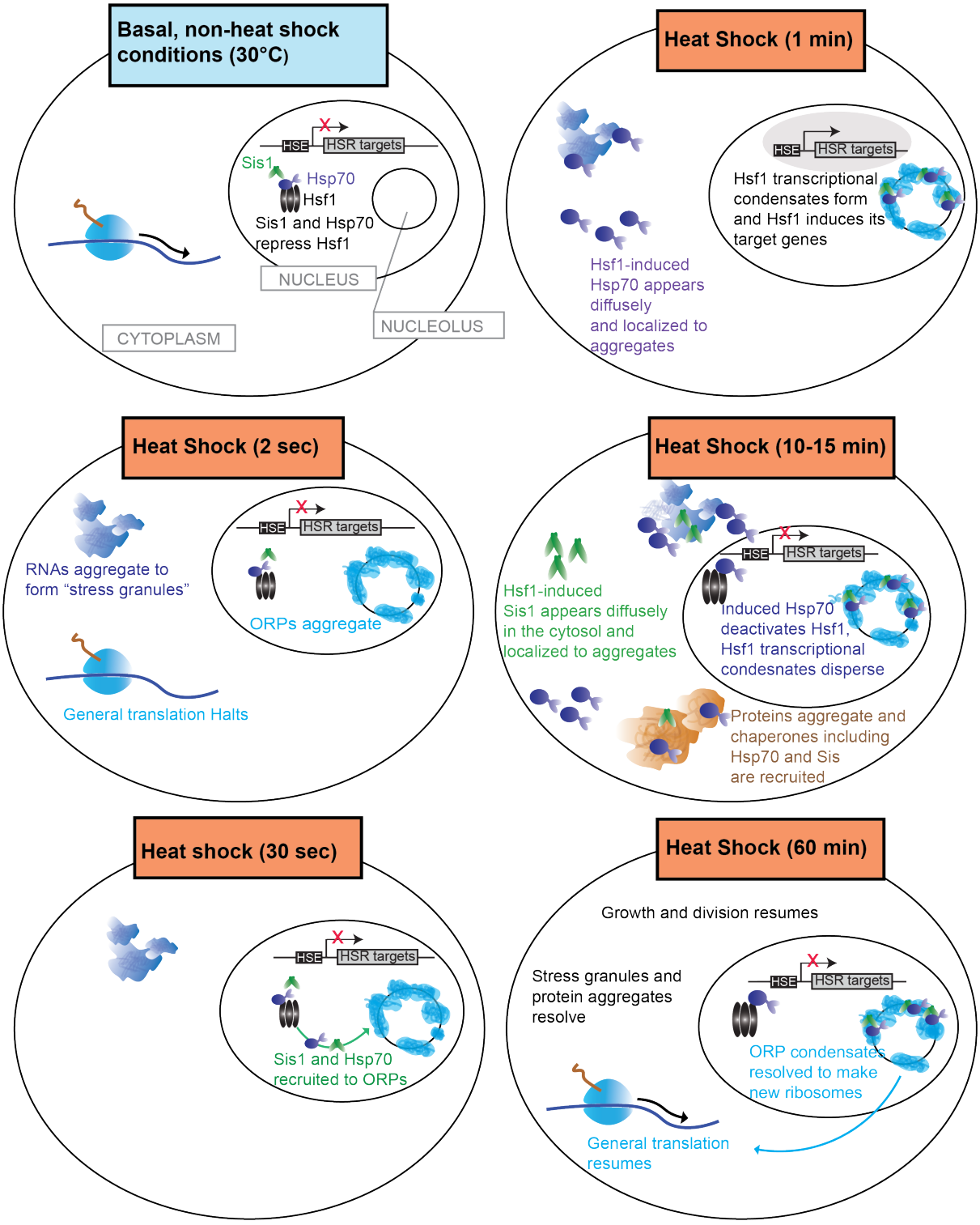

Figure 1.1: An overview of events in the HSR

CHAPTER 2

TRANSCRIPTIONAL REGULATION OF SIS1 PROMOTES FITNESS BUT NOT FEEDBACK IN THE HEAT SHOCK RESPONSE

This chapter was published previously as Garde et al. 2023 [37].

2.1 Abstract

The heat shock response (HSR) controls expression of molecular chaperones to maintain protein homeostasis. Previously, we proposed a feedback loop model of the HSR in which heat-denatured proteins sequester the chaperone Hsp70 to activate the HSR, and subsequent induction of Hsp70 deactivates the HSR [68,152]. However, recent work has implicated newly synthesized proteins (NSPs) – rather than unfolded mature proteins – and the Hsp70 co-chaperone Sis1 in HSR regulation, yet their contributions to HSR dynamics have not been determined. Here we generate a new mathematical model that incorporates NSPs and Sis1 into the HSR activation mechanism, and we perform genetic decoupling and pulse-labeling experiments to demonstrate that Sis1 induction is dispensable for HSR deactivation. Rather than providing negative feedback to the HSR, transcriptional regulation of Sis1 by Hsf1 promotes fitness by coordinating stress granules and carbon metabolism. These results support an overall model in which NSPs signal the HSR by sequestering Sis1 and Hsp70, while induction of Hsp70 – but not Sis1 – attenuates the response.

2.2 Introduction

Under steady-state growth conditions, cells have sufficient protein folding and degradation machinery to maintain protein homeostasis (proteostasis)[58]. However, in response to environmental stressors like a rise in temperature or exposure to oxidizing agents, the cellular

demand for proteostasis machinery outstrips the supply, and cells activate the heat shock response (HSR). The HSR is a highly conserved gene expression program under the control of the transcription factor Hsf1 that coordinately increases expression of molecular chaperones and other proteostasis factors [104]. Implicated in both cancer and neurodegenerative diseases, modulation of the HSR could have powerful therapeutic benefits. Poor prognosis in human cancers – in particular breast and colon cancer – is correlated with hyperactive Hsf1[106,136]. At the other extreme, Hsf1 remains inactive in neurons derived from patients with neurodegenerative disorders despite the presence of protein inclusions and aggregates [20,43,58]. It is unclear how Hsf1 is mis-regulated in these disease states, and even the basic regulatory mechanisms that determine the activation dynamics of the HSR in healthy cells remain incompletely understood.

Due to its high degree of evolutionary conservation, many of the advances in elucidating the HSR and its regulatory mechanisms have come from studying the pathway in budding yeast. In yeast, the HSR comprises 42 genes activated by Hsf1 during environmental stress via binding to cis-acting heat shock elements (HSEs) in the promoter regions of these genes [102]. The Hsf1-induced genes encode a small but diverse set of proteins including chaperones localized to the cytosol, nucleus, endoplasmic reticulum, and mitochondria, translation regulators, and other protein quality control factors. In the absence of stress, Hsf1 is repressed by binding to the chaperone Hsp70, and dissociation of Hsp70 during stress releases Hsf1 to activate the HSR [67,68,84,98,152]. Hsp70 binds to two distinct sites on yeast Hsf1 to mediate the repression [68,98]. Biochemically, Hsp70 can dissociate both yeast and human Hsf1 from DNA [67,84]. However, Hsp70 may repress Hsf1 activity via other mechanisms as well, such as inhibiting interactions with the transcriptional machinery and disassembling transcriptional condensates[23,151].

While Hsp70 can bind to Hsf1 in the absence of any co-chaperones [68,152], the J-domain protein (JDP) co-chaperone Sis1 targets Hsf1 to Hsp70 in the nucleus to promote high-

affinity binding, and nuclear localization of Sis1 is required to repress Hsf1 in the absence of stress[30]. Upon heat shock, Sis1 re-localizes from the nucleoplasm to the periphery of the nucleolus, which may release Hsf1 from Hsp70-mediated repression and initiate the HSR [6,30]. During prolonged stress, induction of the HSR feeds back to once again repress Hsf1, and this negative feedback specifically requires induction of Hsp70 [68]. However, it is unknown whether induction of any other HSR targets, such as Sis1, is also required for negative feedback.

Multiple studies have now implicated dissociation of Hsp70 from Hsf1 as the key regulatory event that activates the HSR, yet the clients that titrate Hsp70 away from Hsf1 following heat shock – i.e. the "ligands" of the HSR – remain unidentified. Long assumed to be heat-denatured mature proteins [75,91,152], it is notable that not a single endogenous eukaryotic protein has been shown to unfold following heat shock at the sublethal temperatures that elicit the HSR[148]. In fact, the protein aggregates that do form following physiological heat shock have been shown to largely consist of reversible biomolecular condensates that play an adaptive role in the stress response rather than proteotoxic aggregates[55,107,135]. Moreover, several studies have demonstrated that depletion of amino acids or treatment with cycloheximide substantially diminishes the output of the HSR following heat shock, suggesting that ongoing translation and/or newly synthesized proteins (NSPs) may drive HSR activation[84,132,133]. Thus, while the identities of the HSR ligands have not been established, NSPs are currently thought to be a major category of HSR activators.

In this study, we incorporate these recent developments into an updated mathematical model of the HSR. First, we develop a new input function for the HSR that explicitly includes protein synthesis and maturation. In this input function, the effect of heat shock is to reduce the protein maturation rate, resulting in an accumulation of NSPs. The NSPs in turn titrate Hsp70, resulting in the release of Hsf1 and activation of the HSR. This new input function allows the model to recapitulate the diminished output of the HSR following

heat shock under conditions with reduced protein synthesis. Second, by incorporating the role of Sis1 in targeting Hsf1 to Hsp70 for repression under basal conditions, we were able to model the induction of the HSR upon depletion of Sis1 in the absence of stress. However, the model predicted that Sis1 does not function as a negative feedback regulator of the HSR. Indeed, genetic decoupling of Sis1 expression from Hsf1 regulation had no effect on HSR dynamics, validating the model prediction. Consistent with its lack of participation in deactivating Hsf1, pulse-label imaging of heat shock-induced Sis1 revealed that Sis1 is spatially localized away from Hsf1, while newly induced Hsp70 partially co-localizes with Hsf1. Finally, we show that while Sis1 is not involved in feedback regulation of the HSR, its Hsf1-dependent transcriptional regulation is required for fitness in the presence of non fermentable carbon sources, and we link this growth phenotype to mis-regulation of stress granules. The new model we present for the HSR incorporates a revised, data-supported activation mechanism while providing further support for the core regulatory circuitry and concise feedback architecture we previously proposed. This work demonstrates that deactivation and basal repression of a pathway need not be achieved by the same mechanism, and that stress response target genes can differentially promote feedback and fitness.

2.3 Results

2.3.1 Modeling the role of ongoing protein synthesis in activation of the heat shock response

Previously, we proposed a model of the heat shock response (HSR) based on a two-component feedback loop consisting of the chaperone Hsp70 and the transcription factor Hsf1[68,152]. In the model, Hsp70 binds and represses Hsf1 under basal conditions. Upon heat shock, unfolded proteins (UPs) accumulate and titrate Hsp70 from Hsf1, leaving Hsf1 free to induce expression of more Hsp70. Once Hsp70 has bound all the UPs, the excess Hsp70 could

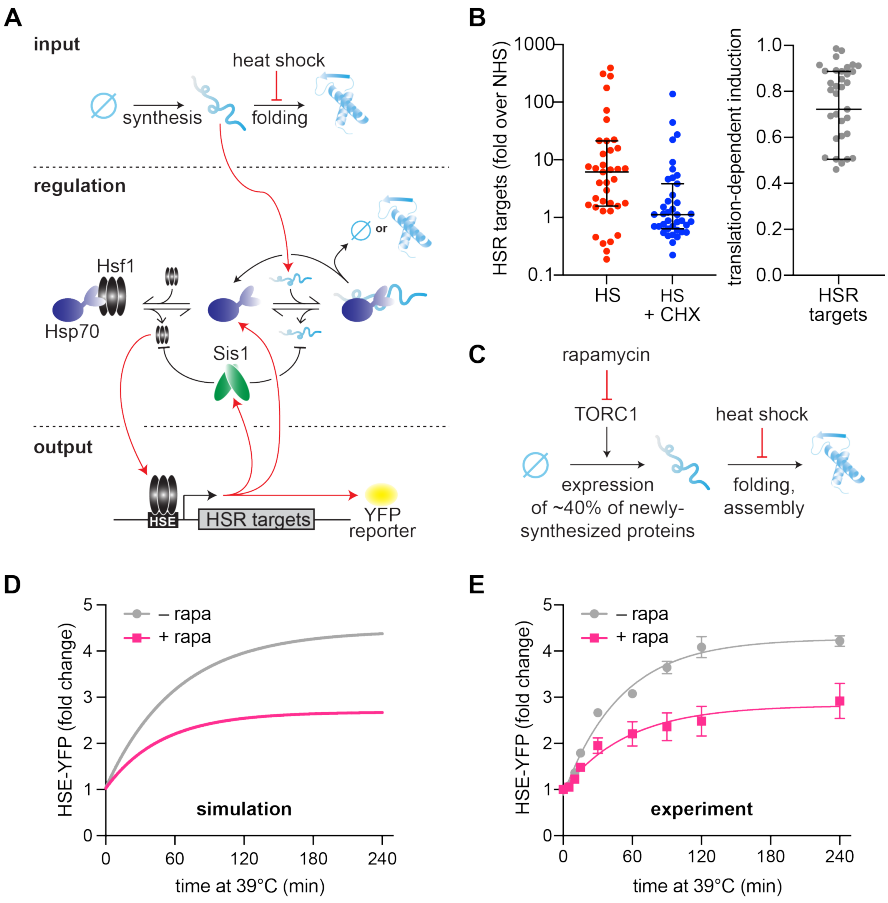

Figure 2.1: Newly synthesized proteins drive full activation of the HSR
A) Schematic of the mathematical model. Heat shock stalls folding of newly synthesized proteins so newly synthesized unfolded proteins accumulate. Hsp70 is recruited to unfolded proteins (red arrow) in turn releasing Hsf1 to induce its transcriptional targets. Among these targets are Hsp70 and Sis1 (and HSE-YFP, our ectopic reporter of Hsf1 activity). Sis1 substantiates Hsf1-Hsp70 binding and substantiates Hsp70-misfolded protein interactions. B) Hsf1 target gene transcript levels, relative to non-heat shock levels. Cells were treated with 200 ug/mL cycloheximide(blue) and subjected to 42ºC heat shock for 20 minutes. Untreated control (red) plotted for comparison(red). Raw data from Triandafillou et al. 2020. 1-transcript levels of CHX-treated over untreated cells = portion of transcriptional induction that depends on ongoing translation (gray). Each data point represents an Hsf1 target gene. C) Model of rapamycin effect. Heat shock stalls newly synthesized protein folding, and newly synthesized unfolded proteins trigger the heat shock response. Upstream, rapamycin inhibits TORC1 which inhibits ribosomal protein production, causing a 40% decrease in newly synthesized proteins. D) HSE-YFP levels during heat shock. Cells pretreated with 10 ug/mL rapamycin before HS (pink), untreated control (gray). Each data point represents the average of the three biological replicates. Error bar is the SD. E) Simulation of HSE-YFP levels during heat shock with or without rapamycin.

then bind to Hsf1 to deactivate the response. This model is capable of recapitulating HSR dynamics following heat shock, but it includes assumptions that are no longer consistent with the current literature.

The input for the original model was heat shock-generated UPs, with the underlying assumption that heat shock causes mature proteins to denature into UPs. However, it is no longer accepted that UPs activate the HSR. Rather, immature newly-synthesized proteins (NSPs) have been suggested to drive HSR activation (Figure 2.1A)[30,44,83,84,133,134]. Supporting this, Hsf1 target gene transcripts were depressed in pH-balanced, cycloheximide-treated cells following heat shock relative to cells heat-shocked while actively translating[132]. Our analysis of these published RNA-seq data indicate that ongoing translation is required for more than 70% of the induction of HSR genes on average (Figure 2.1B). This suggests that NSPs – rather than denatured mature proteins – are major upstream activators of the response.

To account for translation dependent HSR activation in the model, we have implemented an input function in which there is a constant source of NSPs (i.e., a rate of ongoing translation) instead of a single initial input of unfolded proteins ((Figure 2.1A), see methods). NSPs must then undergo a maturation step to become folded. In the updated model, heat shock inhibits the spontaneous folding rate of NSPs, rather than causing denaturation of folded proteins, thereby resulting in an accumulation of immature proteins. During heat shock, NSPs must interact with Hsp70 to either fold or be degraded. Heat shock still activates the HSR by titrating Hsp70 away from Hsf1, but by immature NSPs rather than by UPs.

Using this new input function, we tested the ability of the model to account for the effect of reducing translation prior to heat shock. To do this, we pre-treated cells with rapamycin, which specifically inhibits expression of ribosomal proteins and biogenesis factors by inhibiting the target of rapamycin complex 1 (TORC1)[77] (Figure 2.1C). Together, these genes are estimated to constitute more than 40% of total NSPs in yeast under logarithmic

growth conditions[54]. The model predicts that such a reduction in NSPs should result in a concomitant reduction in HSR output following heat shock (Figure 2.1D). Indeed, using a yellow fluorescent protein (YFP) reporter of the HSR (HSE-YFP) (Figure 2.6), we found that rapamycin-treated cells displayed a substantial reduction in HSR output across the heat shock time course (Figure 2.1E). To verify that the reduction in YFP fluorescence reflects a reduction in transcriptional activation of the HSR (and not due to a reduction in translation of the YFP mRNA caused by rapamycin), we quantified YFP mRNA levels using qRT-PCR. Consistent with the fluorescence measurements, the mRNA was comparably reduced, indicating that the YFP levels accurately report on HSR activation in the presence of rapamycin (Figure 2.6). Together, these results demonstrate that the updated mathematical model can capture the dynamics of the HSR during heat shock and recapitulate the effects of reduced protein synthesis on HSR output.

2.3.2 Modeling the role of Sis1 as a basal repressor of the HSR

Recently, we found that Sis1, a J-domain protein (JDP) and Hsp70 cofactor, participates in repressing Hsf1 activity under non-heat shock conditions by promoting Hsf1-Hsp70 association[30]. Consistent with this result, knockdown of Sis1 resulted in the highest level of activation of the HSR under basal conditions in a genome-wide CRISPRi screen[5]. Moreover, it was independently shown that Hsf1 binds to Hsp70 as a typical client, via the Hsp70 substrate binding domain in a nucleotide-regulated manner [84], further supporting the involvement of a JDP like Sis1. Sis1 was also shown to potentiate the HSR in the presence of exogenous protein aggregates[66]. We incorporated Sis1 into the core circuitry of the model by representing the canonical role of JDPs in substantiating Hsp70-client binding: the Hsp70-client protein dissociation rate is inversely dependent on Sis1 concentration (see methods).

To assess this new model circuitry (Figure 2.2A), we first determined whether it could

recapitulate the known role of Sis1 in preventing activation of the HSR under non-stress conditions. Experimentally, we transiently depleted Sis1 from the nucleus using the anchor away system[30], and monitored Hsf1 activity via the HSE-YFP reporter. Upon nuclear depletion of Sis1, Hsf1 activity increased 2.5-fold compared to untreated control within 90 minutes (Figure 2.2B). Computationally, we simulated the model following instantaneous depletion of Sis1, which induced the HSR without a temperature upshift in agreement with the experimental result (Figure 2.2C). Notably, at later time points, the model failed to capture the sustained increase in HSE-YFP reporter we observed experimentally. This may indicate that prolonged depletion of Sis1 results in a breakdown in proteostasis that sustains HSR activity.

2.3.3 Modeling experimental variability and HSR dynamics across a range of conditions

We implemented this updated mathematical model that incorporates the NSP input function and Sis1-containing circuitry to make predictions about the dynamics of the HSR. First, we repeated our standard heat shock time course – shifting cells from 30°C to 39°C. We performed this experiment 18 times to train the model to include the range of experimental variation on different days (Figure 2.2D). Across these replicates, we observed variation on the order of 20% from experiment to experiment. Replicates performed on the same day behaved more similarly, so we hypothesized that a likely source of this variation could be the initial metabolic state of the cells on different days, reflecting differences in the amount of time they had been in stationary phase or outgrowth prior to initializing the heat shock. These metabolic differences would then be reflected in different rates of protein synthesis. Indeed, varying the rates of protein synthesis in the model yielded heat shock time course simulations that recapitulated the variation observed across the biological replicates (Figure 2.2E). Thus, by modulating a single parameter, the model was able to recapitulate both the

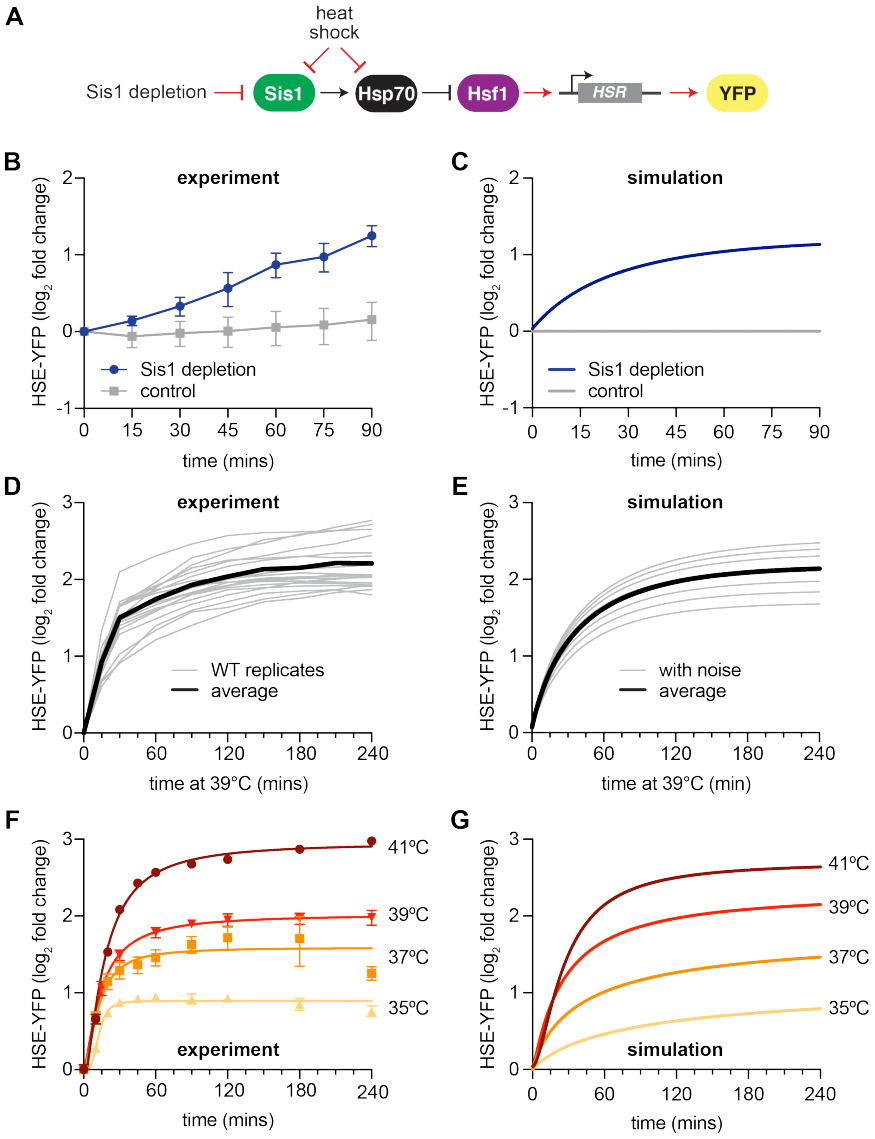

Figure 2.2: New HSR model recapitulates experimental results
A) Model of Sis1 effect. In non HS, Sis1 promotes Hsp70 binding to Hsf1, repressing transcriptional activation of the HSR. Heat shock results in the titration of Hsp70 and Sis1, leaving Hsf1 free to induce the HSR and the ectopic reporter of Hsf1 activity, HSE-YFP (red arrows). B) HSE-YFP levels after nuclear Sis1 depletion (blue) at 30ºC, measured by flow cytometry. Sis1 was ectopically anchored away to cytosol. C) Simulation of HSE-YFP reporter after Sis1 depletion. D) HSE-YFP expression in wild type cells across 18 biological replicates (gray), average (black). E) Simulation of variation in the wild type HSR due to metabolic differences leading to changes in basal translation rate. F) HSE-YFP heat shock time courses at a range of heat shock temperatures between 35ºC and 41ºC. G) Simulation of heat shock time courses. Heat shock at higher temperatures was simulated by a proportional decrease in protein folding rate.

average behavior as well as the experimental variability.

We next performed heat shock time course experiments and simulations at multiple temperatures ranging from 35ºC to 41ºC. When we performed experiments across this temperature range, we observed a rapid induction phase at all temperatures, followed by a slow rise to a temperature-dependent maximal response (Figure 2.2F). Without changing any parameters, the model predicted that cells would reach different steady state levels of HSE-YFP fluorescence in proportion to the increase in temperature, matching the experimental results (Figure 2.2G). Thus, the HSR is a "dose-dependent" response, tuned quantitatively by the temperature of heat shock. Together, these results indicate that the mathematical model recapitulates experimental variation and the dynamics of the HSR across a range of conditions.

2.3.4 Decoupling Sis1 expression from Hsf1 transcriptional activity

Previously, we found that transcriptional induction of Hsp70 is required to deactivate Hsf1 over a sustained heat shock time course, and we therefore deemed Hsp70 a negative feedback regulator[68]. Given that Sis1 promotes Hsp70-mediated repression of Hsf1 under basal conditions, we next tested whether induction of Sis1 is likewise required for Hsf1 deactivation following heat shock. Sis1 is expressed at a moderate basal level under non heat shock conditions, and its transcription is induced during heat shock. Hsf1 is responsible for both maintaining the basal expression level of Sis1 as well as inducing it during heat shock[102,124].

As we had done for Hsp70, we tested the role of Sis1 induction during HS by removing its Hsf1-dependent transcriptional induction, first computationally and then experimentally (Figure 2.3A,B). Notably, while the mathematical model requires Hsp70-dependent transcriptional feedback to recapitulate the wild type response dynamics, it does not include transcriptional induction of Sis1. Thus, the model accurately captures HSR response dy-

namics without a requirement for Sis1-mediated transcriptional feedback. i.e., the model predicts that Sis1 induction is not required for negative feedback (Figure 2.3C).

Experimentally, to maintain the basal expression level of Sis1, we could not simply remove the Hsf1 binding site from the SIS1 promoter since Hsf1 drives its basal expression. Thus, we replaced the SIS1 promoter sequence with the SUP35 promoter (Figure 2.3B). According to our previously published RNA-seq data, SUP35 mRNA is expressed at approximately the same level as endogenous SIS1 mRNA under basal conditions but is not transcriptionally induced during heat shock[102]. To determine whether the SUP35 promoter behaved as we expected, we measured expression of Sis1 by fusing it to P2A-mScarlet (a ribosomal skip sequence that enables fluorescent readout without tagging the protein of interest)[127] (Figure 2.3B). As expected, mScarlet was robustly induced during heat shock when expressed from the endogenous SIS1 promoter, but it showed no induction by heat shock when expressed from the SUP35 promoter (Figure 2.7A). However, we found that SUP35pr-SIS1 cells displayed a moderate growth defect under non-stress conditions in a dilution series spot assay, and basal mScarlet expression from the SUP35 promoter was reduced to half of the level expressed from the endogenous SIS1 promoter (Figure 2.7B,C). To remedy this, we integrated a second copy of SUP35pr-SIS1 into the trp1 locus. In this 2xSUP35pr-SIS1 strain, cell growth is comparable to wild type in a dilution series spot assay, and Hsf1 basal activity matches that of wild type (Figure 2.7C,D). Thus, the 2xSUP35pr-SIS1 strain maintains the initial Sis1 expression level of wild type cells while preventing induction of Sis1 during heat shock.

2.3.5 Transcriptional induction of Sis1 is dispensable for Hsf1 deactivation

To determine whether Sis1 induction plays a role in feedback regulation of Hsf1, we monitored Hsf1 activity with the HSE-YFP fluorescent reporter. If Sis1 induction were necessary for Hsf1 deactivation, we would expect elevated Hsf1 activity during heat shock, similar to the

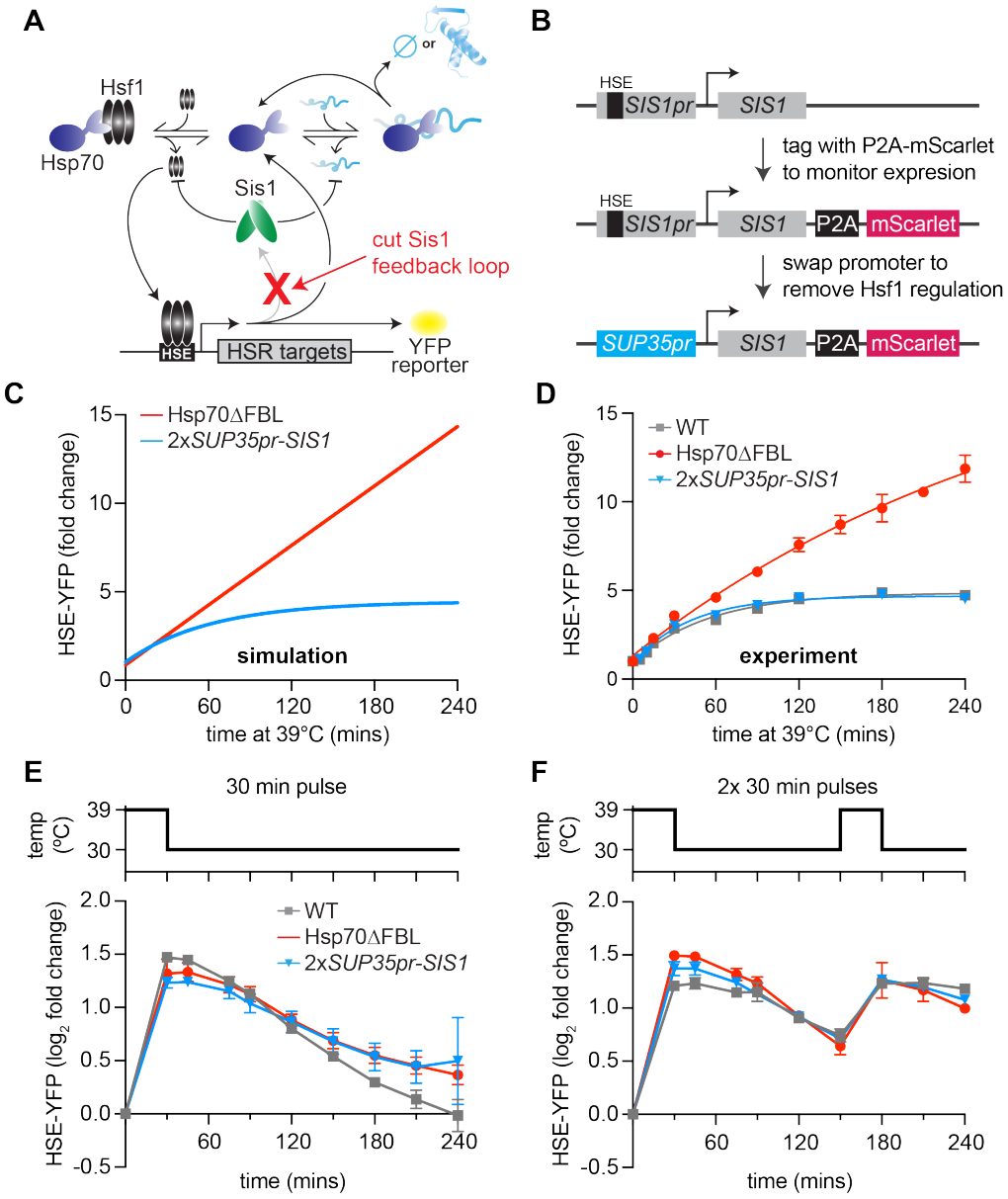

Figure 2.3: Transcriptional induction of Sis1 is dispensable for Hsf1 deactivation
A) Network schematic. Sis1 induction by Hsf1 is cut to test whether Sis1 induction is necessary for normal Hsf1 regulation. B) Generating the non-inducible Sis1 mutant. mScarlet fluorescent protein reports on Sis1 transcription and the Sis1 promoter is replaced with a non-inducible promoter. C) HSE-YFP levels over HS time course, measured by flow cytometry. Each data point represents the average and standard deviation of three biological replicates. D) Simulation of HSE-YFP when Sis1 or Hsp70 is maintained at basal expression level during heat shock. E) HSE-YFP levels during a 30-minute heat shock followed by recovery at 30°C. F) HSE-YFP levels during two 30-minute heat shock intervals, separated by a two-hour recovery at 30°C.

strain we previously engineered to decouple Hsp70 expression from Hsf1 (Hsp70ΔFBL, for Hsp70 "deleted for the feedback loop") (Figure 2.3D). Briefly, in the Hsp70ΔFBL strain, all four paralogous genes encoding cytonuclear Hsp70 in yeast (SSA1, SSA2, SSA3, and SSA4) were deleted, and two copies of SSA2 expressed from the constitutive and Hsf1-independent TEF1 were inserted in the genome. The resulting strain expresses Hsp70 to wild type levels under non stress conditions but cannot induce more Hsp70 upon heat shock. In contrast to the prolonged induction of HSE-YFP displayed by Hsp70ΔFBL cells, 2xSUP35pr-SIS1 cells showed Hsf1 activity dynamics indistinguishable from wild type during heat shock (Figure 2.3D). These data suggest that, despite its role in repressing Hsf1 under basal conditions, Sis1 induction is dispensable for Hsf1 deactivation following heat shock, just as the model predicted.

Since Sis1 induction by Hsf1 is not necessary for Hsf1 deactivation following a single, sustained heat shock treatment, we wondered whether Sis1 induction might be necessary for deactivation of Hsf1 in more dynamic conditions. To test this, we subjected wild type, Hsp70ΔFBL and 2xSUP35-SIS1 cells to various heat shock protocols and measured HSE-YFP dynamics. As we observed with the sustained heat shock, Hsf1 activity in non-inducible Sis1 cells was similar to wild type after a 30-minute heat shock pulse followed by recovery at 30°C (Figure 2.3E). Moreover, HSE-YFP dynamics were also comparable to wild type when non-inducible Sis1 cells were exposed to a two-hour heat shock pulse at 39°C followed by recovery at 30°C (Figure 2.7E). Interestingly, Hsp70ΔFBL showed Hsf1 activity comparable to wild type after the 30-minute heat shock, suggesting that Hsp70-induction is less important for rapid Hsf1 deactivation than during sustained stress (Figure 2.3E). By contrast – and consistent with its hyperactive phenotype following sustained heat shock – Hsp70ΔFBL showed defective Hsf1 deactivation after the two-hour heat shock pulse (Figure 2.7E).

As a final test for defects in Hsf1 regulation in the non-inducible Sis1 lines, we exposed cells to multiple heat shock pulses with two different recovery periods:

[30-minute pulse—15-minute recovery—30-minute pulse] or
[30—minute pulse—2-hour recovery—30-minute pulse]. With the longer 2-hour recovery period, both 2xSUP35pr-SIS1 and Hsp70ΔFBL responded with similar induction dynamics to wild type (Figure 2.3F). This suggests that the 2-hour recovery time was sufficient for the cells to fully reset and respond equivalently to the second pulse. Following the shorter 15-minute recovery period, Hsp70ΔFBL displayed increased Hsf1 activity relative to wild type, while 2xSUP35-SIS1 remained indistinguishable from wild type even in this challenging stress regime (Figure 2.7F). These data demonstrate that Sis1 induction does not serve to tune Hsf1 activity across any of the heat shock protocols we tested.

2.3.6 Induced Sis1 is produced slowly and preferentially localizes to the nucleolar periphery

Given that Sis1 is not necessary for Hsf1 deactivation, we wanted to visualize the heat shock-induced protein to determine its localization. We've previously shown that Sis1 localized in the nucleolar periphery – and away from Hsf1 – upon activation of the HSR [30]. If newly synthesized Sis1 were to likewise localize at the nucleolar periphery, it would not be in physical proximity to Hsf1, explaining its dispensability in the negative feedback loop.

To enable visualization of only newly induced Sis1, we tagged Sis1 with the HaloTag [79] in a strain in which the nucleolar marker Nsr1 is tagged with mScarlet. The HaloTag irreversibly binds to synthetic ligands that contain a haloalkane moiety that can be attached to fluorescent dyes or remain non-fluorescent and block subsequent labeling. To image protein induced during heat shock only, we first incubated cells with the non-fluorescent ligand 7-bromoheptanol to block HaloTag conjugation to pre-existing Sis1 (Figure 2.4A)[86]. Then we pulse-labeled with the fluorescent ligand JF646 and started the heat shock simultaneously: JF646 thus exclusively marked heat shock-induced Sis1. We imaged newly synthesized Sis1-Halo over a heat shock time course and quantified both the induction dynamics and lo-

calization with respect to the Nsr1 nucleolar marker. Sis1 induction was undetectable until 10 minutes after heat shock and then increased linearly until 20 minutes of heat shock when it reached a plateau (Figure 2.4B,C). Moreover, once it became visible, newly synthesized Sis1 preferentially localized adjacent to the nucleolus as determined by a sustained increase in the proportion of Sis1 surrounding the Nsr1 signal (Figure 2.4B,D). Next, we imaged newly synthesized Sis1-Halo in cells expressing Hsf1-mVenus. As recently reported, Hsf1 forms subnuclear condensates during heat shock, and we observe little colocalization between these Hsf1 foci and newly synthesized Sis1 (Figure 2.4E,F)[23]. These data suggest that newly synthesized Sis1 is not spatially positioned to repress Hsf1 and inactivate the HSR immediately following heat shock.

We repeated the pulse labeling analysis for Ssa1-Halo – the SSA1 gene encodes an inducible Hsp70 – as we previously showed that Hsp70 induction is required for HSR deactivation[68]. In contrast to Sis1, we were able to detect newly synthesized Ssa1 after only six minutes of heat shock, and Ssa1 was induced substantially more than Sis1 by 15 minutes (Figure 2.4B,C). Moreover, induced Ssa1 localized to the nucleolar periphery as well as to puncta and more diffusely throughout the cell (Figure 2.4B). Newly synthesized Ssa1 was less concentrated at the nucleolar periphery over the heat shock time course than newly synthesized Sis1 (Figure 2.4D). Moreover, in contrast to Sis1, newly synthesized Ssa1-Halo partially colocalized with Hsf1 (Figure 2.4E,F). The combination of the delayed Sis1 induction relative to Ssa1 and the localization of Sis1 primarily to the nucleolar periphery – and away from Hsf1 – may explain why Sis1 is not a feedback regulator of the HSR.

2.3.7 Sis1 transcriptional regulation confers fitness in non-fermentable carbon sources

Without an obvious role in negative feedback regulation, we investigated whether Sis1 transcriptional regulation by Hsf1 promotes fitness. We quantitatively monitored fitness by

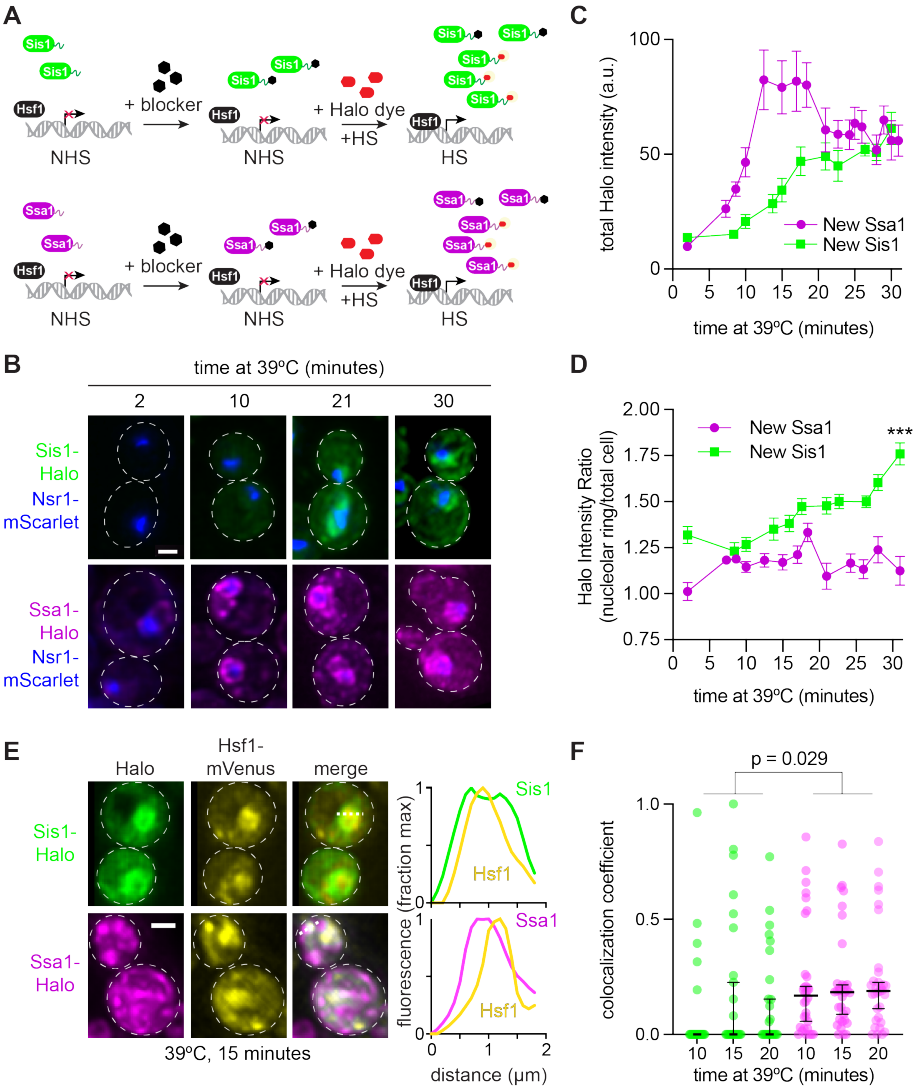

Figure 2.4: Sis1 is induced slowly and localizes away from Hsf1 following heat shock
A) Experiment workflow. Cells were treated with 20uM 7-bromoheptanol (5 min), then 20uM of JF646 Halo-dye at 39ºC. Halo fluorescence marks the population of Sis1 or Hsp70 translated during heat shock. B) Representative deconvolved live cell images. Cells express Nsr1-mscarlet as well as Sis1-Halo or Ssa1-Halo dye. scale =2μm C) Quantification of total cell Halo intensity during heat shock time course. Average +/- SE. n=5-20 cells D) Quantification of mean halo intensity at the nucleolar periphery divided by mean halo intensity in the total cell. Average +/- SE. n=5-20 cells E) (Left) Representative deconvolved live cell images, expressing Hsf1-mVenus and newly synthesized Sis1 or Ssa1. (Right) Normalized fluorescence intensity corresponds to white dotted line across the nucleolus F) Single cell analysis of the fraction of total newly synthesized Sis1 (green) or Ssa1 (magenta) that colocalizes with Hsf1. Median +/- 95% CI (black).

comparing optical density of the 2xSUP35pr-SIS1 strain to the Hsp70ΔFBL strain and wild type in culture using an automated plate reader. Cells were grown for four hours at 30°C, then were either kept at 30°C or shifted to 37°C. All strains showed comparable growth at 30°C (Figure 2.8A). However, while Hsp70ΔFBL was indistinguishable from wild type at 37°C, the 2xSUP35pr-SIS1 strain showed reduced fitness compared to the other strains after the first four hours at 37°C and failed to undergo a diauxic shift once glucose was depleted from the media (Figure 2.5A). This suggests that induction of Sis1 may play a role in promoting growth in the absence of a fermentable carbon source.

To directly test whether Hsf1-dependent regulation of Sis1 promotes growth in non-fermentable media, we grew cells with EtOH/glycerol as the carbon source at 30°C. Indeed, the 2xSUP35pr-SIS1 strain grew substantially slower than wild type or Hsp70ΔFBL in EtOH/glycerol media (Figure 2.5B). Remarkably, the 1xSUP35pr-SIS1 strain – which has a slow growth phenotype in glucose (Figure 2.7C) – completely rescues growth in EtOH/glycerol (Figure 2.8B), suggesting that the 2xSUP35pr-SIS1 strain grows slowly on non fermentable carbon due to the inability to downregulate Sis1 rather than induce it. Consistent with this interpretation, when we increased Sis1 expression even more by adding a second copy of Sis1 under its stronger endogenous promoter, the growth phenotype in EtOH/glycerol was exacerbated to the point that cells failed to grow altogether (Figure 2.8B). Thus, it is not induction per se but the ability to modulate Sis1 expression level according to the metabolic state of the cell that appears to promote fitness.

2.3.8 Transcriptional regulation of Sis1 coordinates stress granules with carbon metabolism

In addition to regulating Hsf1 activity under basal conditions in the nucleus, Sis1 is known to regulate cytosolic stress granules. Stress granules are biomolecular condensates composed predominately of mRNA and translation factors that form in response to a variety of stressors

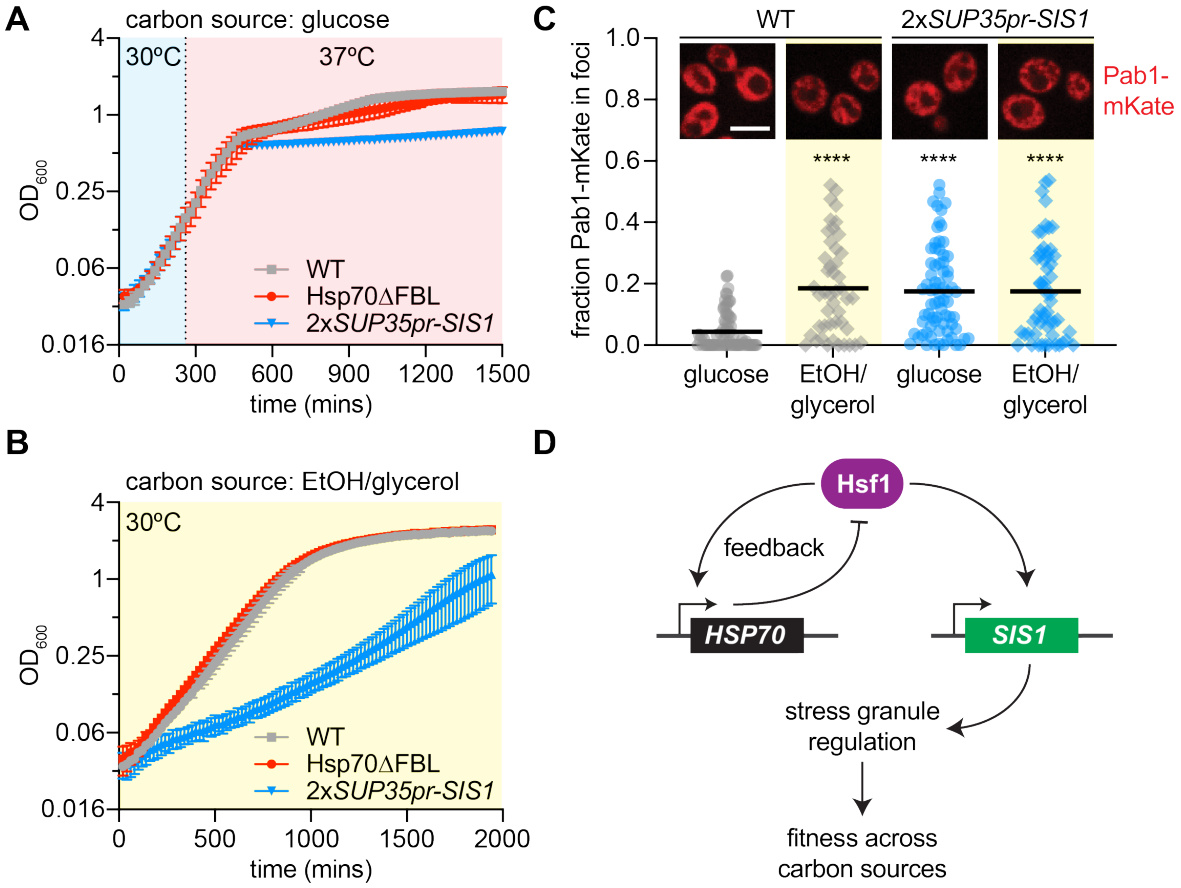

Figure 2.5: Sis1 transcriptional regulation confers fitness under stress
B) Quantitative growth curve of noninducible strains during growth in limited carbon media (2% glycerol 2% EtOH) in non-heat shock (30ºC). C) Single cell quantification of the fraction of Pab1mCherry localized in foci as determined by the FindFoci plugin in Fiji. Inset: Representative deconvolved live cell images captured by lattice light sheet microscopy of cells expressing Pab1mKate. D) Model of the differential roles of transcriptional regulation of Hsp70 and Sis1 in feedback and fitness, respectively.

including both heat shock and glucose depletion. To determine whether stress granules could provide a link between Sis1 regulation and fitness in media lacking glucose, we imaged the stress granule marker Pab1 fused to the mKate fluorescent protein in wild type cells and 2xSUP35pr-SIS1 cells. Pab1-mKate was diffuse throughout the cytosol in wild type cells in glucose media but a fraction formed small granules in EtOH/glycerol media; by contrast, Pab1-mKate was granular in both glucose and EtOH/glycerol in 2xSUP35pr-SIS1 cells (Figure 2.5C). These results suggest there are constitutive stress granules in 2xSUP35pr-SIS1 cells, connecting a known activity of Sis1 in regulating stress granules with its apparent role in carbon metabolic homeostasis. This result suggests that proper regulation of Sis1 expression is required to dynamically regulate stress granules, conferring fitness as carbon source fluctuates in the environment.

2.4 Discussion

In this study, we formally incorporated two recent findings into a mathematical model of the HSR: 1) the role of newly synthesized proteins (NSPs) as a major class of molecular species that drive HSR activation [84,133], and 2) the role of the JDP Sis1 in repressing HSR activity under non-stress conditions by promoting the interaction of Hsp70 with Hsf1 [30]. Importantly, while the addition of these new features makes the model more realistic and enabled accurate recapitulation of experimental perturbations to protein synthesis and Sis1, our results indicate that the core circuitry of the HSR that we previously proposed need not be embellished: the heart of the HSR remains a two-component feedback loop between Hsp70 and Hsf1.

Our previous model, as well as those of other groups, assumed that the HSR is triggered by the denaturation of mature proteins [30,68,99,116,152]. These models simulated the initiation of stress as the instantaneous accumulation of a single bolus of heat-induced unfolded or misfolded proteins that required chaperones for triage, refolding, and degrada-

tion. However, these models are unable to account for the reduction in HSR output observed in heat-shocked cells that had been treated with protein synthesis inhibitors or otherwise cultured in growth conditions with reduced protein synthesis [84,132–134]. To reflect the current understanding that the HSR is triggered, at least in part, by NSPs, we explicitly model translation and subsequent protein maturation/folding. Upon heat shock, the elevated temperature decreases the protein folding rate, thereby resulting in the accumulation of immature NSPs. These NSPs in turn titrate Hsp70 and Sis1, thereby activating the HSR. To test this mechanism, we experimentally decreased the pool of NSPs by pre-treating cells with rapamycin prior to heat shock. Indeed, compared to untreated cells, we observed decreased HSR output in the rapamycin-treated cells following heat shock in the model and in cells, validating the NSP-based activation mechanism. In addition to NSPs, it has been proposed that heat-induced biomolecular condensates of mature proteins and mRNAs may activate the HSR [132]. If/when these putative condensate agonists are identified, they will be incorporated into future iterations of the model.

Regarding the HSR feedback loop, we previously found that in addition to repressing the HSR under basal conditions, induction of Hsp70 is required to deactivate the HSR following a sustained heat shock [68]. Thus, Hsp70 is a negative feedback regulator of the HSR. Given the role of Sis1 in repressing the HSR in the absence of stress and the fact that it is also a transcriptional target of the HSR, we expected that Sis1 too would provide negative feedback. However, after decoupling Sis1 expression from the HSR, we observed no difference in HSR activation dynamics compared to wild type cells, demonstrating that Sis1 induction is dispensable for deactivation of the HSR. Since induction of Hsp70 is required for deactivation of the HSR, it is possible that the increased levels of Hsp70 obviate the requirement for Sis1. Alternatively, the basal concentration of Sis1 may be sufficient to promote Hsf1 inactivation, or induction of another JDP may be required.

Though dispensable for Hsf1 deactivation, we found that Sis1 induction was necessary

for long term fitness during heat shock and in nonfermentable carbon sources, and we linked this to a disruption in the regulation of stress granules (Figure 2.5). Sis1 plays a critical role in disaggregation of stress-induced biomolecular condensates in cooperation with Hsp70 and Hsp104[148], and our results here imply that regulation of Sis1 levels may in turn regulate the condensates that form during heat shock or glucose depletion. In addition to cytosolic stress granules, Sis1 is also targeted to the periphery of the nucleolus during heat shock, where it interacts with accumulated ribosomal proteins that are known to activate the HSR when produced in stoichiometric excess to ribosomal RNA [4,30,134]. The peri-nucleolar localization of induced Sis1 we observed here in the pulse labeling experiments (Figure 2.4B,D) is consistent with a role for Sis1 as an orphan ribosomal protein chaperone [6]. The emerging role of Sis1 in regulating adaptive stress-induced condensates may be among its essential functions.

Our experimental findings imply that Hsp70 induction is still the principal source of negative feedback for the HSR, and that the mechanism of HSR repression during basal conditions may be distinct from the deactivation mechanism following stress. Further investigations should systematically explore whether Hsp70 is unique in its role as a negative feedback regulator or if other Hsf1 targets confer feedback to the HSR either independent of or via Hsp70. With an input function based on the accumulation of NSPs and the inclusion of Sis1 in the regulatory circuitry, the new iteration of the model presented here brings us closer to a mechanistically accurate and predictive understanding of the HSR.

2.5 Acknowledgements

We thank Arvind Murugan and Kabir Husain for use of the cell culture plate reader and the University of Chicago Integrated Light Microscopy facility for use of the lattice light sheet microscope. We also thank Alex Ruthenburg for helpful suggestions and members of the Pincus lab for insightful discussions and critical reading of the manuscript.

2.6 Methods

2.6.1 Mathematical modeling

Mathematical Modeling To model the Hsp70-Hsf1 feedback circuit we have expanded the previous model [30] to explicitly consider the production of unfolded nascent proteins that are folded into their native state with some rate. More specifically, the model consists of four different protein species (Hsf, Hsp, unfolded protein (UP), reporter YFP) and two complexes (one between Hsp and Hsf and the other between Hsp and UP). The differential equations describing the cellular concentration of these species are as follows:

$$\frac{d[HSP]}{dt} = k_2[HSP \cdot Hsf] - k_1[HSP][Hsf] + (k_4 + k_5)\,[HSP \cdot UP] - k_3[HSP][UP] + \beta \frac{[Hsf]^n}{K_d^n + [Hsf]^n}$$

$$\frac{d[Hsf]}{dt} = k_2[HSP \cdot Hsf] - k_1[HSP][Hsf]$$

$$\frac{d[UP]}{dt} = k_{up} - k_{dup}[UP] + k_4[HSP \cdot UP] - k_3[HSP][UP]$$

$$\frac{d[HSP \cdot HSF]}{dt} = k_1[HSP][Hsf] - k_2[HSP \cdot Hsf]$$

$$\frac{d[HSP \cdot UP]}{dt} = k_3[HSP][UP] - (k_4 + k_5)\,[HSP \cdot UP]$$

$$\frac{d[YFP]}{dt} = \beta \frac{[Hsf]^n}{K_d^n + [Hsf]^n}$$

where [] denotes the cellular concentration of respective species. The interpretation of all models here is identical to the original model [152], except for two new parameters - the de-novo synthesis of unfolded proteins $k_{up} = 1\,\mathrm{min}^{-1}\,a.u^{-1}$ and their folding with rate k_{dup} = 0.35 min^{-1}. The rate k_1 = 320 $\mathrm{min}^{-1} a.u^{-1}$ denotes the binding of Hsp to Hsf to create an inactive complex $HSP \cdot Hsf1$, and the complex dissociates with rate k_2 = 0.7 min^{-1}. The rate $k_3 = 112\,\mathrm{min}^{-1}$ a. u^{-1} is the binding of Hsp to unfolded proteins (denoted as UP) to create the complex $HSP \cdot UP$ that dissociates with rate k_4 = 0.1 min^{-1}. The degradation

of UP by Hsp is captured via the rate $k_5 = 0.15$ min^{-1}. The activation of both YFP and Hsp by Hsf is modeled by a Hill equation with $n = 3, \beta = 0.1$ min^{-1} and $k_d = 0.0025$ $a.u.$

The above differential equation model was run with the following initial values (in a.u.) at time $t = 0$

$$[HSP] = \frac{1}{2}, [Hsf1] = 0, [HSP \cdot HSF1] = \frac{1}{250}, [UP] = 0, [HSP \cdot UP] = 0, [YFP] = 1$$

The effect of rapamycin is captured by decreasing the rate k_{up} and trajectories corresponding to different heat shock temperatures are obtained by perturbing the folding rate k_{dup}. To investigate the experiment-to-experiment fluctuations in YFP trajectories we solved the above system by varying the parameter knoaround its nominal value by 20% at the start of the simulation. The impact of Sis1 depletion is captured by destabilizing the HspHsf complex via an increase in the dissociation rate k_2. Finally, the removal of Hsp feedback is realized by removing the Hsfinduced activation term in the equation for $\frac{d[HSP]}{dt}$.

2.6.2 Strain construction

Yeast strains and plasmids used in this study are listed in Table S1. All strains are derived from the W303 parent strain. CRISPR-mediated promoter swapping was performed to create the 1xSup35pr-Sis1 (1701) and 1xSup35pr-Sis1-P2A-mscarlet (1661) strains. CRISPR-Cas9 mediated precise, scarless replacement of the native Sis1 promoter with the 600-bp Sup35 promoter. To construct the final non-inducible Sis1 line (2xSup35pr-Sis1, 1761), we incorporated a second copy of Sup35pr-Sis1 at the tryp locus. In all other cloned lines, genes were tagged at the endogenous locus. Cells were transformed with double-stranded DNA fragments containing 20 bp homologous flanking regions. This method takes advantage of homology-directed repair mechanisms in S.cerevisiae, as described previously [78].

2.6.3 Cell growth

For heat shock time courses followed by flow cytometry, cells were cultured in 1xSDC media overnight at room temperature (synthetic media with dextrose and complete amino acids). Before RT-PCR or cell growth assays, cells were cultured in yeast extract peptone dextrose (YPD) media shaking at 30ºC overnight. Cells were subjected to heat shock at 39°C unless otherwise specified.

2.6.4 HSE-YFP reporter heat shock assays

Three biological replicates of each strain were serially diluted five times (1:5) in 1xSDC and grown overnight at room temperature. In the morning, cells had reached logarithmic phase, and 750 μL of each replicate was transferred to a PCR tube and shaken for one hour at 30ºC to aerate. Then, cells were exposed to heat shock at 39ºC. At the pre-determined time points (0,5,10,15,30,60,90,120,180,240 minutes), 50 μl of cell culture was transferred to a well of a 96 well plate, containing containing 1xSDC and a final concentration of 50 mg/mL cycloheximide to stop translation. After the time course, cells were incubated at 30ºC for one hour to allow fluorescent reporter maturation before measurement. All experiments were performed using C1000 Touch Thermal Cycler (Bio-Rad). Cell fluorescence was measured by flow cytometry and results were analyzed as described below.

2.6.5 Anchor-away assay

Cells were grown overnight as described above. Rapamycin was added to a final concentration of 10 μM, and the time course was started immediately. During the time course, cells were maintained at 30ºC shaking. At the predetermined time points (0,15,30,45,60,75,90 minutes), 50 μL of cells were transferred to a 96-well plate identically to the heat shock assay described above.

2.6.6 Translation inhibition assay (rapamycin pre-treatment)

Cells were grown overnight, and in the morning, shaken at 30°C for 1 hour. Rapamycin was added to a final concentration of 10 μM, and cells were left shaking at 30°C for 5 minutes. Then, the heat shock time course was performed at 39°C as described above.

2.6.7 Flow cytometry

HSE-YFP and mscarlet reporter levels in heat shock time course and rapamycin treatment assays were measured at the University of Chicago Cytometry and Antibody Technology Facility. These measurements were performed using the 488-525 FITC fluorescence filter (HSE-YFP) and 561-PE Dazzle (mscarlet) on the BD Fortessa High Throughput Flow Cytometer. The raw fluorescence values were normalized by side scatter in FlowJo. Then, the median fluorescence value was calculated. Each data point represents the average of three biological replicates.

2.6.8 Dilution series spot growth assays

Yeast strains were grown overnight shaking at 30°C in YPD. In the morning, they were diluted to and final optical density (OD) of 1 and serially diluted 1:10 in water. Each diluted yeast culture was spotted onto 1xYPD plates. Images were taken after two days of growth at 30° or 37°C.

2.6.9 Heat shock quantitative growth assay

Yeast strains were grown overnight at 30°C in 1xYPD. In the morning, they were diluted to OD= 0.1 in 1xYPD. SpectroStar Nano microplate reader was used to measure cell density every 20 minutes. Each data point represents the mean of three biological replicates.

2.6.10 Glucose starvation quantitative growth Assay

Yeast strains were grown for 24 hours in 2% glucose YEP media then diluted to OD=0.1 and grown overnight again. In the morning, cells were diluted to OD=0.1 in 1xYEP containing 2% glycerol, 2% EtOH and growth was monitored every 20 minutes at 30ºC.

2.6.11 RNA quantification and analysis

RT-qPCR was performed as previously described in [23], except for the following: cells were grown at 30°C in YPD (yeast extract-peptone-dextrose) to a mid-log density (OD_{600} = 0.8). Rapamycin was added to a final concentration of 10 ug/mL for 5 min. At this point, a portion of the culture was maintained at 30°C (0 min HS) and the remainder was subjected to heat shock at 39°C for 5, 15, 60, and 120 min. Cells were flash frozen immediately after heat shock, and then harvested. Total RNA was extracted using hot acid phenol extraction method, followed by ethanol precipitation [124]. To determine fold change mRNA levels, mean mRNA levels of heat-shocked samples were normalized to the NHS sample[100]. mVenus forward primer: caacattgaagatggtggtgttc mVenus reverse primer: ctttggataaggcagattgatagg

2.6.12 RNA-Seq analysis

RNA read counts for 39 Hsf1 target genes were collected in a recent paper and reanalyzed here [132]. GSE accession number 152916.

Experimental methods are described in detail in the original paper. In brief, cells were exposed to heat shock at 42ºC for 20 minutes. Cells exposed to heat shock and cycloheximide were treated with 200 ug/mL cycloheximide (CHX) simultaneously upon HS. Each data point represents average read count for a single Hsf1 target gene (two biological replicates). Translation dependence was calculated as 1-(CHX+HS/HS).

2.6.13 Halo-tagging

To image newly synthesized proteins, we incubated cells with blocker (20uM, 7-bromoheptanol) for 5 minutes, washed two times with 2xSDC media and then incubated with 0.4 uM of Halo JF646dye at 39^{o}C, to start HS treatment simultaneously. Under this treatment, only protein induced during heat shock was visualizable. Lattice light sheet microscopy was used to visualize 5-20 cells every 2.5 minutes throughout the 30-minute heat shock.

2.6.14 Lattice light sheet microscopy and quantification

Lattice light-sheet imaging was performed at the University of Chicago Integrated Light Microscopy Core (Intelligent Imaging Innovations) and run in SlideBook 6.0 software. Captured images were deconvoluted using Graphics processing unit–based Richardson-Lucy deconvolution with measured PSFs via Brian Northan's "Ops" implementation (https://github.com/imagej/ops-experiments). 3D reconstructions and videos were assembled using ClearVolume [111]. The mean Halo intensity at the ring around the Nsr1-marked nucleolus was divided by the mean intensity over the total cell.

2.7 Supplementary Materials

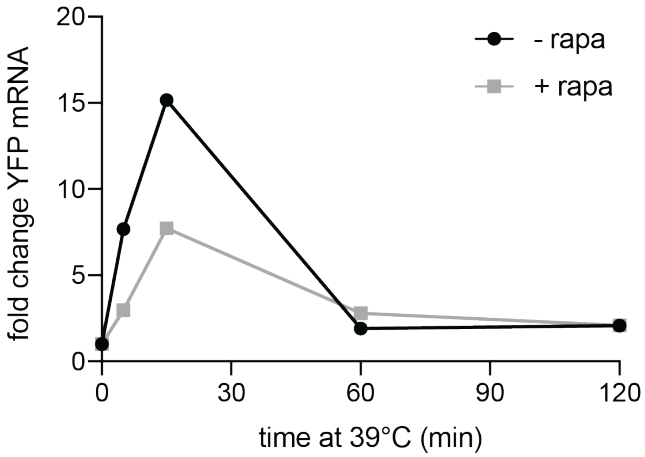

Figure 2.6: Rapamycin reduces HSE-YFP at the mRNA level
RNA levels during heat shock relative to non-heat shock, measured by qRT-PCR. Cells treated with 10 ug/mL rapamycin for 5 minutes before heat shock (gray) and compared to untreated control.

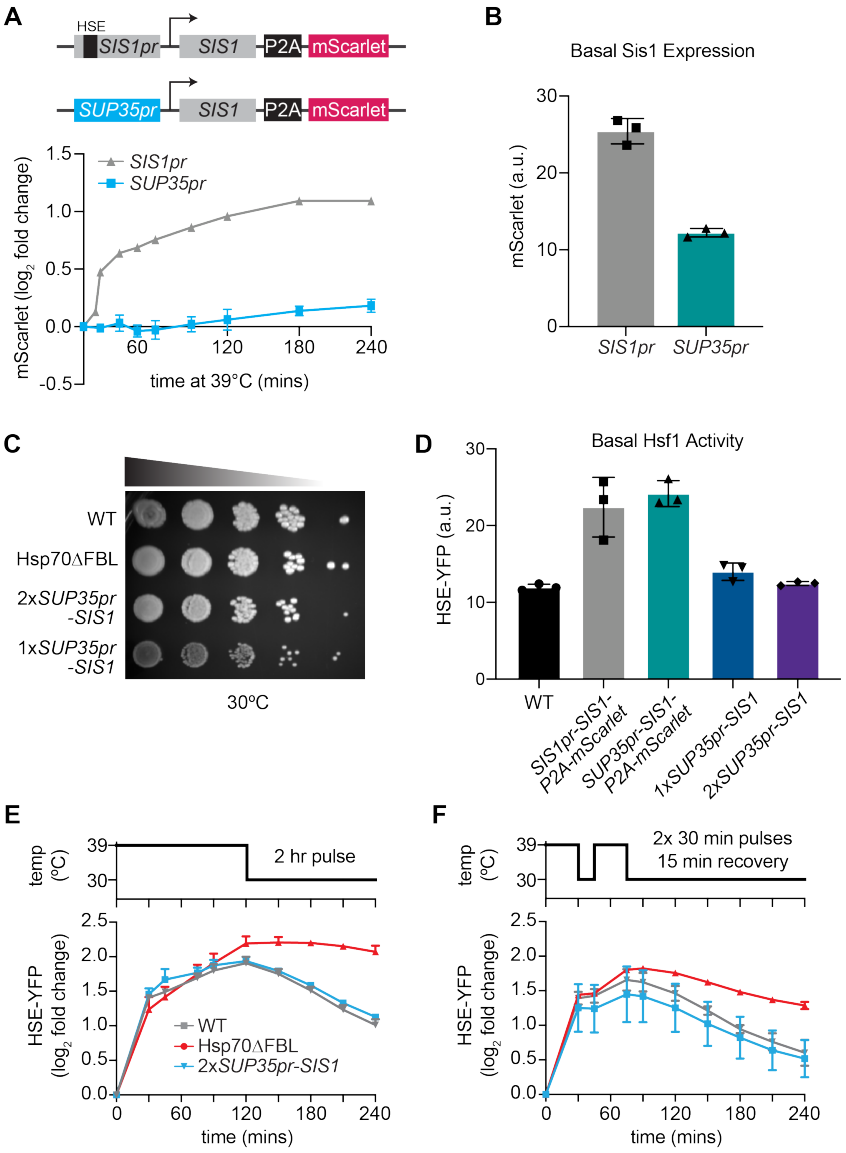

Figure 2.7: Decoupling Sis1 from Hsf1 regulation
A) Heat shock time course of mScarlet levels in WT (gray) and non-inducible Sis1 (blue) lines measured by flow cytometry. The WT line contains a heat shock element (HSE) in the native enhancer sequence, where Hsf1 binds to induce transcription (top, gray line). A non-inducible Sup35 promoter drives Sis expression (bottom, blue line). mscarlet, separated by a ribosomal skip sequence (P2A), reports on Sis1 transcription. B) Raw mScarlet reporter level in non-heat shock, 1xSup35pr-Sis1 and WT lines. C) Dilution series spot assay of all lines. WT, Hsp70ΔFBL, and 1xSup35pr-Sis1 and 2x Sup35pr-Sis1 lines grown for 3 days at 30°C. D) Basal HSE-YFP reporter expression of all lines measured by flow cytometry. E) HSE-YFP reporter during 2-hour heat shock, followed by recovery at 30°C. F) HSE-YFP reporter levels over two 30-minute heat shocks separated by a 15-minute recovery period at 30°C. Average +/- SD, n=3.

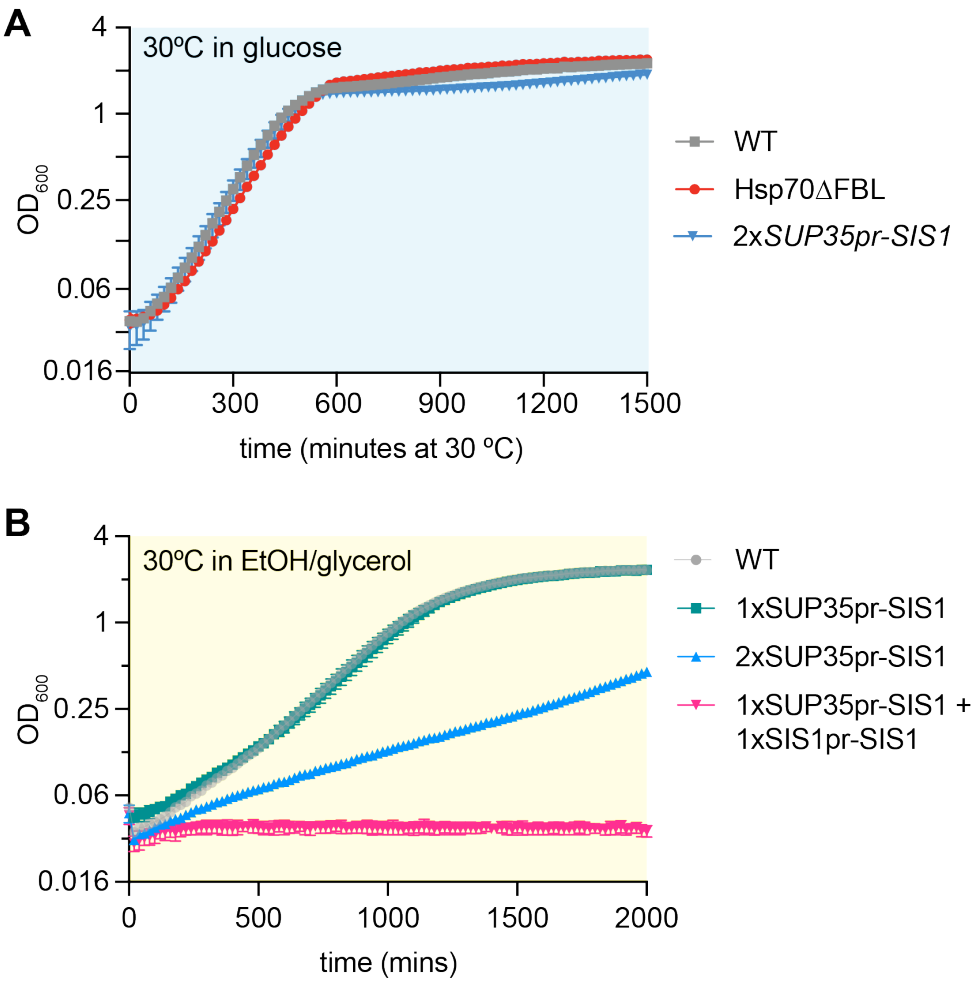

Figure 2.8: Additional growth curves
A) Quantitative growth curve of non-inducible strains in glucose media under non-heat shock conditions. B) Quantitative growth curve of strains with low, medium and high levels of non-inducible Sis1 grown in EtOH/glycerol.

Table 2.1: Cell lines used in Chapter 2

Strain	**Genotype**	**Description**	**Figure**
DPY1701	w303a;4xHSE-Venus::LEU;Sup35pr-SIS1	Sup35pr-SIS1	2.4EF
DPY1368	w303a;HSEv2-Venus::LEU2; SSA1Δ::HYG; SSA2Δ::KAN; TEF1pr-SSA2::HIS; SSA4Δ::NAT; TEF1pr-SSA2::URA; SSA3Δ::BLE	Hsp70ΔFBL	2.3CEF 2.8C,2.5AB
DPY1761	w303a;4xHSE-Venus::LEU;Sup35pr-SIS1;Sup35pr-Sis1::Trp	2xSup35pr-Sis1	3CEF,5AB 2.8CD
DPY1284	w303a; tpk1/2/3-as;TOR1-1(S1972I);fpr1Δ::NAT;TEF2pr-mKate -URA3-4xHSEve-EmGFP; RPL13A-2xFKBP12::TRP; SIS1-FRB::HIS	Sis1-AA	2.1E, 2.2B
DPY144	w303a;4xHSE-Venus::LEU	WT	2DF,3CEF 2.5B,2.6 2.8D
DPY1615	w303a;4xHSE-Venus::LEU;Sis1-ERVB1-mscarlet::KAN	SIS1pr-SIS1-P2A-mscarlet	2.8ABD
DPY1661	w303a;4xHSE-Venus::LEU;Sup35pr-Sis1-ERVB1-mscarlet::KAN	Sup35pr-SIS1-P2A-mscarlet	2.8ABD
DPY1600	w303a; 4xHSE-Venus::LEU; Hsp82-ERVB1-mscarlet::KAN	WT	2.5A,2.6,2.8C
DPY1930	w303a:Halo-Sis1;Nsr1-mscarlet-i::KAN	Sis1-Halo	2.4B-C
DPY1846	Sis1 mVenus:His,Nsr1-mScarI:Kan;ssa1pr-HALO-ssa1ORF::LEU	Ssa1-Halo	2.4B,D
DPY1990	w303a;Hsf1-mVenus::HIS;ssa1pr-HALO-ssa1ORF::LEU	Ssa1-Halo; Hsf1-mVenus	2.4E-F
DPY1991	w303a;4xHSE-mVenus::HIS;Pab1-mKate::URA3	Pab1-mKate	2.5C
DPY1992	w303a;4xHSE-Venus::LEU;Sup35pr-SIS1;Sup35pr-Sis1::Trp;Pab1-mKate::URA3	Pab1-mKate; 2xSup35pr-Sis1	2.5C
DPY2001	w303a;Halo-sis1(N ter CRISPR);Hsf1-mVenus::HIS clone 1	Halo-Sis1; Hsf1-mVenus	2.4E-F

CHAPTER 3

A COMPREHENSIVE DISSECTION OF TRANSCRIPTIONAL FEEDBACK IN A EUKARYOTIC STRESS RESPONSE

This chapter is a manuscript currently in preparation, by Rania Garde and David Pincus.

3.1 Abstract

Cells maintain homeostasis despite fluctuations in the environment by activating stress response pathways. These pathways employ negative feedback loops to transiently induce corrective gene expression programs, but the extent to which individual target genes provide feedback has not been comprehensively measured for any stress response. Here, we disrupt the stress-induced expression of each target gene in the *S. cerevisiae* heat shock response (HSR) and quantify how their induction affects the dynamics of HSR activity and fitness during stress. Remarkably, we determined that regulation of the HSR is dominated by a single feedback loop governed by the chaperone Hsp70. In addition to Hsp70 itself, we found several other target genes that feed into the core Hsp70 negative feedback loop to tune HSR dynamics. The strongest additional regulator we identified, Fes1, supports Hsp70 in deactivating the response by releasing Hsp70 from protein aggregates in the cytoplasm and allowing it to return to the nucleus to repress gene expression. We propose that the simplicity of this central regulatory architecture may allow auxiliary genes to gain and lose membership in the HSR over evolution without influencing the activity of the overall response as organisms adapt to new environmental niches.

3.2 Introduction

Stress response pathways are triggered to adapt to environmental changes and resume growth in ongoing, stressful conditions. To promote cell fitness, stress responses rapidly repair any

damage caused by the stressor, synthesize proteins for growth and division in new conditions, and deactivate processes that are no longer adaptive. Then, to avoid excess energy consumption or overshooting optimal adaptation, the stress response must rapidly turn off. Thus, cellular stress responses themselves must be adaptive. It is unclear how response dynamics are tuned by the induction of downstream effectors. How do stress responses adapt to ongoing changes in stress intensity? To what extent do master stress response regulators integrate feedback from their suite of effectors?

Previously, the heat shock-induced Hsf1 transcriptome was rigorously characterized, revealing just 42 target genes both show increased Hsf1 occupancy in their enhancer region (genome wide ChiP-seq results) and are dependent on Hsf1 for their transcription during heat shock [102]. How do the transcriptional dynamics of individual genes collectively determine the adaptive dynamics of Hsf1 activity?

In eukaryotic cells, Heat Shock Factor 1 (Hsf1) is the master transcriptional regulator of the heat shock response (HSR), a prototypical stress response pathway activated by perturbations to protein homeostasis (proteostasis) – a state of balance between cellular demands for protein folding and the supply of molecular chaperones. When an environmental stressor or internal dysfunction causes an excess of newly synthesized, unfolded, misfolded or mis-targeted proteins to accumulate in the cytosol, Hsf1 transcriptionally induces molecular chaperones to aid in protein folding, disaggregation, and degradation [104] Once proteostasis is restored, molecular chaperones become available to bind and deactivate Hsf1. Hsf1 misregulation in human disease indicates that Hsf1 is tightly tuned in both directions. In aggressive cancers, Hsf1 is often hyperphosphorylated and hyperactive, or overexpressed due to Hsf1 locus amplification [85]. Hsf1 hyperactivity leads to overexpression of Hsf1 targets, including Hsp90 chaperones, which stabilize oncogenic proteins that are prone to misfolding, allowing cancer cells to survive and proliferate [14,139]. On the other hand, in neurodegenerative disorders, aggregates of proteins remain unresolved and sequester chaperones, which

hampers general cellular processes and causes further protein aggregation; in Huntington's disease, Hsf1 is unstable and protein aggregation (disrupted protein homeostasis) is the hallmark of neurons [43]. One therapeutic solution involves ectopic upregulation of Hsf1 activity to induce chaperones that resolve protein aggregates [94] In conclusion, tight regulation of Hsf1 activation and repression occurs in healthy cells.

Hsf1 is regulated by an Hsp70-based negative feedback loop [68,83]. The chaperone Hsp70 is recruited from the nucleus where it directly binds and represses Hsf1 in non-stress, to protein condensates in the cytoplasm and nucleolar periphery [6,30]. This leaves Hsf1 free to bind and induce its transcriptional targets, which include all four Hsp70 chaperones, ssa1, 2, 3, and 4 (referred to collectively as Hsp70). The induction of Hsp70 above basal levels is essential for Hsf1 deactivation: within fifteen minutes of heat shock, Hsf1 is rebound by Hsp70 in the nucleus and Hsf1 transcriptional activity is repressed again [67,68,84]. Thus, Hsf1 is sensitive to the homeostatic state of the cell because the negative regulator of Hsf1, Hsp70, senses cytoplasmic protein homeostasis. In the initial thirty seconds of heat shock, transcriptional machinery, newly synthesized proteins, translational machinery and protein-bound RNAs condense into reversible condensates maintained by chaperones including Hsp70, Hsp40s and Hsp90s and small heat shock proteins (sHSPs) that are Hsf1 targets [6,29,30,147]. Therefore, though Hsp70-based negative regulation is the only significant Hsf1 deactivation mechanism known at this time, other targets (especially Hsp40s and Hsp90 chaperones) are likely to negatively regulate Hsf1 by restoring protein homeostasis. It is possible that most Hsf1 target genes have independent but additive roles in Hsf1 deactivation, or alternatively, induction of most of the Hsf1 target genes may be evolutionarily obsolete.

Here, we characterize how the induction of the full suite of Hsf1 target genes tune dynamic regulation of the heat shock response and cellular adaptation to stress. First, we characterize the transcriptional dynamics of the 42 Hsf1 target genes during heat stress in *S. cerevisiae* by

flow cytometry quantification of a co-cistronic transcriptional reporter. Second, we perturb the transcriptional dynamics and observe how depleting each target gene's induction affects the system as a whole. To deplete the Hsf1-based induction of each target gene, we leverage our previous RNA-seq and Hsf1 ChIP-seq datasets to identify and delete the 9-25 bp Hsf1 binding region in the upstream regulatory DNA, using CRISPR/Cas9. By inhibiting Hsf1-dependent induction of each transcriptional target and observing the effect on the dynamics of Hsf1 activity, we identify feedback regulators of Hsf1. To our knowledge, a comprehensive characterization of an entire transcriptional regulon has never been completed.

Further, we investigate the mechanism of identified negative feedback regulators during heat shock: do they regulate Hsf1 via the known, Hsp70-dependent feedback loop, or via other mechanisms [68]? The phenotype of each induction mutant (state of protein homeostasis and cell fitness) reveals the effect of each target gene's induction on Hsf1 regulation, restoration of protein homeostasis, and cell fitness. Multiple genes emerge as negative regulators that deactivate Hsf1. We discuss how and why the Hsf1 regulon might have evolved such a simple architecture.

3.3 Results

3.3.1 A transcriptome-wide characterization of gene expression dynamics

Previously, nascent transcript sequencing and a genome-wide Hsf1-occupancy ChIP-seq screen revealed that 42 target genes are directly bound by and dependent on Hsf1 for their transcription during the first five minutes of stress (Figure 3.1A)[102]. After identifying the Hsf1 target genes, we wondered what role this small, diverse set of conserved target genes serve. This question is investigated in this study by deleting the Hsf1-based induction of each target gene. However, before genetic manipulation, the expression profile of each gene is measured to establish a baseline. Though the general expression level of these targets was

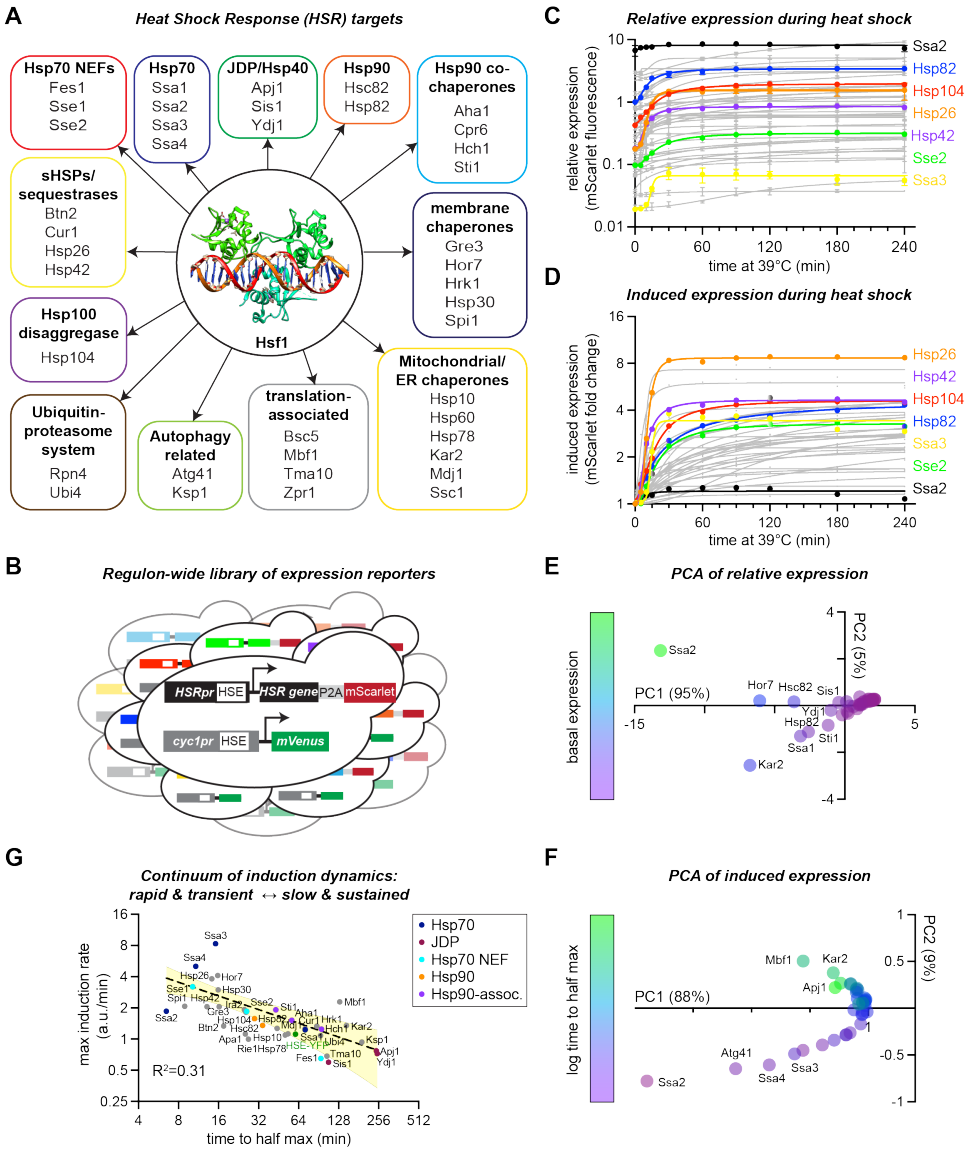

Figure 3.1: Hsf1 induces a range of transcriptional dynamics in its 42 target genes A) 42 genes are directly bound by Hsf1 and dependent on Hsf1 for their transcription (Pincus, 2018). B) Gene expression reporter strategy. A fluorescent reporter of transcriptional dynamics at the C terminal of each Hsf1 target gene, separated by the ribosomal skipping sequence polycistronic skipping sequence (P2A)-mscarlet). A generic, ectopic reporter of Hsf1 activity (HSE-YFP) is also included in each cell line. 42 cell lines, each monitoring one Hsf1 target gene, were cloned. C-D) Relative mScarlet levels (normalized to non-stress WT (C) and fold change mScarlet (D) during HS for all Hsf1 target genes. Average plotted, n=3 along with non-linear curve fits. E-F) PCA of relative transcription dynamics (E) and transcriptional fold change (F), inputting the relative mScarlet expression for each time point for each gene, n=3. G)Maximum induction rate vs. time to half maximum expression calculated with parameter estimates from the non linear curve fits of induced expression. 95% CI (yellow area).

established by RNA-seq and NAC-seq previously, a characterization of target gene transcriptional dynamics at high time resolution throughout heat shock had never been completed before.

To establish the transcriptional dynamics of the Hsf1 regulon in WT cells, we measure the induction dynamics of each Hsf1 target gene during heat shock with a mScarlet reporter of gene expression by flow cytometry. In contrast to expensive and laborious RNA-seq transcript quantification, flow cytometry measurement of a fluorescent reporter enables time course assays with high time resolution. The mScarlet fluorescent protein sequence is preceded by a ribosomal skipping sequence, integrated into the endogenous genome at the 3' end of each Hsf1 target gene to generate one cell line per Hsf1 target gene (Figure 3.1B). Each cell line is exposed to a four-hour heat shock and the fluorescent reporter is measured at multiple timepoints during heat shock. As expected based on previous RNA-seq experiments, the raw expression levels of Hsf1 target genes vary 1000x fold across the 42 gene regulon (Figure 3.1C), and each gene's relative expression level corresponds roughly with transcript levels quantified by RNA-seq and NAC-seq data collected previously [102], corroborating the fluorescent reporter strategy as an accurate readout of transcription. To highlight unique induction dynamics over the large range of gene expression, fold change in mScarlet expression is plotted; fold change induction varies 10x across the regulon (Figure 3.1D). By eye, the induction profiles take a great variety of shapes. Surprisingly, neither gene function nor hard-coded characteristics of genes (strength of Hsf1 binding site, distance from binding site to promoter) explain the variance in transcriptional dynamics between genes (unpublished analysis). Thus, a hypothesis-free strategy was used to parse transcriptional dynamics.

Principal component analysis of the transcriptional induction profiles in the Hsf1 regulon allows us to avoid a priori assumptions about the influences on transcription. We feed the PCA algorithm the mScarlet fluorescence readout of each gene at ten timepoints during heat shock. The analysis reveals that 95% of the variance in relative expression profiles

is explained by principal component 1 (PC1), which correlates well with basal expression level. Surprisingly, the primary determinants of fold change in expression during HS have no significant correlation with relative expression level (unpublished analysis). PCA of fold change expression traces (Figure 3.1D) show that PC1 accounts for 88% of the variation between genes (Figure 3.1F). None of the ten loadings (gene expression at ten time points during each shock) contribute significantly to PC1, however color-coding genes by non-linear agonist-response dose curve kinetic parameters reveals $t_{1/2}$ time until half maximum expression $t_{1/2}$ has a striking correlation with PC1 and PC2 in 2D space. Therefore, $\log_2(t_{1/2})$, emerges as a predictor of the gene induction dynamics. Given that log time to half max can predict induction dynamics, we test commonly-used parameters of induction dynamics for their correlation with $t_{1/2}$. $t_{1/2}$ negatively correlates with the maximum rate of induction (R=0.31) (Figure 3.1G). The negative correlation implies that there are no genes with very high Kds and high maximum induction rates – all genes are induced without delay. The Hsf1 regulon was defined previously by identifying genes induced by Hsf1 within the first five minutes of HS (indicating target genes are directly bound and induced by Hsf1), so it follows that all Hsf1 targets are induced immediately upon heat shock. Additionally, genes with high max induction rates tend to have short time to half maximum. Thus, the more rapidly a gene is induced, the more transient its expression (mScarlet curve plateau indicates gene expression has stopped). A more extensive analysis of these transcriptional dynamics data and comparison to characteristics of gene structure and sequence is likely to reveal more about the 'grammar' of HSR gene regulation.

We conclude that expression levels and induction dynamics vary greatly across the regulon, but one unifying principle stands out: the steeper the gene induction rate, the more transient the gene's induction. This picture of the gene expression dynamics across an entire transcriptional regulon will inform future investigations on HS-induced genome changes [23,24]. These measurements also establish a baseline of transcriptional dynamics in the WT

cell to compare against the target induction mutants that are cloned and studied below.

3.3.2 Identifying Hsf1 feedback regulators

How many Hsf1 target genes feedback on Hsf1 activity? To query the effect of gene induction on Hsf1 activity, we create target gene induction mutants by deleting the strongest Hsf1 binding site in each target gene's endogenous regulatory region (Figure 3.2A). The strongest specific Hsf1 binding sequence, called a heat shock element (HSE), is determined by identifying the motif most similar to the binding consensus sequence (TTCnnGAA) under Hsf1 CHiP-seq occupancy peak for that gene after five minutes of heat shock [102]. The 9-25 bp HSE is deleted by scarless, CRISPR-Cas9 based deletion. The generic Hsf1 activity reporter (HSE-YFP) is also included in each cell line for quantification later on. Though a few genes, including Aha1, Sti1, Ksp1 did not survive after ΔHSE mutation, we successfully deleted the HSE ahead of most Hsf1 target genes.

To understand how deleting Hsf1-based induction affects gene expression during heat shock, the mscarlet profile of the ΔHSE induction mutant is compared to the corresponding WT, mScarlet-tagged line. One Hsf1 target gene provides an illustrative example of the process. Unlike the other Hsf1 target genes, which each have one Hsf1 ChIP occupancy peak, Hsp26 has two. mScarlet profile changes after HSE deletion under the proximal, distal or both peaks of Hsp26 provide an illustrative example of the effects of HSE deletion (Figure 3.2B). Late-stage mscarlet expression is depleted in the proximal HSEΔ line indicating that the proximal Hsf1 binding is necessary for sustained Hsp26 induction during stress (Figure 3.2B, green). On the other hand, deleting the HSE farthest from the promoter (ΔHSE_distal) affects overall gene induction level but not induction dynamics, and deleting both HSEs (ΔΔHSE) has a cumulative effect on Hsp26 expression, almost reducing heat shock-induced expression to zero. The unique changes in Hsp26 expression dynamics after each HSE deletion imply our transcription factor binding site deletion strategy as a highly

targeted technique to control target gene expression dynamics, so we move on to characterize the induction mutants of the other Hsf1 target genes.

mScarlet expression for each ΔHSE mutant is summarized, where mScarlet expression after four hour HS (y axis) is plotted against mScarlet expression in non stress for each tagged gene (x axis) (Figure 3.2C). Most induction mutants had lower gene expression both after four hour HS, and in basal (NHS) conditions (yellow quadrant, (Figure 3.2C). The decrease in HS-induced expression among most induction mutants is expected given that Hsf1 is responsible for these 42 genes induction above basal levels during HS. However, the decrease in basal target gene expression for so many Hsf1 target genes is surprising: our previous studies concluded that only 18 genes are dependent on Hsf1 for basal expression [124]. These results indicate that HSE deletion might perturb local chromatin structure and as a result, affect recruitment of transcriptional machinery or transcription factors. Alternatively, more Hsf1 target genes may be dependent on Hsf1 for basal transcription than previously believed. In our previous assay, nascent transcription in non-stress in the presence or absence of Hsf1 in the nucleus, was measured to determine Hsf1-dependence. However, the nuclear depletion of Hsf1 may have activated stress responses which induced Hsf1 target genes and restored their WT basal expression levels.

To identify the genes whose induction is important for Hsf1 regulation, we measured the generic HSE-YFP reporter during heat shock in each induction mutant. Defects in any Hsf1 activity mutant are a sign that a target gene's induction provides feedback regulation on Hsf1, either directly, by affecting Hsf1 activity in the nucleus, or indirectly, by restoring the cytosolic state of protein homeostasis, which Hsf1 senses via Hsp70 [68]. It is also possible that Hsf1 is sensitive to cellular processes other than cytosolic protein homeostasis, of which we are still unaware. Fold change in HSE-YFP reporter over four-hour heat shock shows Hsf1 activity dynamics vary four-fold (Figure 3.2D), but most HSE-YFP values after four hour heat shock fall within the WT range, indicating that the induction of most Hsf1 targets

neither directly regulates nor indirectly affects Hsf1 activity (Figure 3.2E). Just six genes (blue) have hyperactive Hsf1 activity (fold change in Hsf1 activity above WT).

The three induction mutants with lower than WT Hsf1 activity induction (Figure 3.2E, gray) had lower than WT basal Hsf1 activity levels (Figure 3.2F, black) which artificially depressed their Hsf1 activity induction values, so we eliminate these three genes as candidate feedback regulators of Hsf1. The elevated basal Hsf1 activity of these induction mutants is not surprising: all three genes are dependent on Hsf1 for basal expression, as determined by our initial screen, and have important roles in general protein folding across the cell [90,117,124]. Protein homeostasis probably breaks down when basal Hsf1 binding at these genes is depleted.

To summarize, induction of six Hsf1 target genes affect Hsf1 activity during HS, and are thus candidate negative feedback regulators of Hsf1. As expected, some candidate negative feedback regulators have putative roles in protein homeostasis and degradation (Hsp42ΔHSE, Fes1ΔHSE, Ubi4ΔHSE). However, it is surprising that induction of Hsp70s, Hsp90s and Hsp40s was dispensable for Hsf1 regulation.

3.3.3 Checking for redundancy among Hsf1-induced chaperone families

To determine conclusively whether cytosolic chaperones affect Hsf1 regulation, we ask whether entire groups of Hsf1-induced chaperones are dispensable for Hsf1 regulation. Hsf1 induces all four of the Hsp70 homologs, both of the yeast genome's cytosolic Hsp90 chaperones, and four of the thirteen cytosolic Hsp70 co-chaperones (a.k.a. Hsp40s). Though induction of each individual Hsp70, Hsp90 and Hsp40 chaperone is dispensable for Hsf1 regulation during heat shock, chaperones of each family may have redundant functions, or compensate for one another, obscuring defects in the single induction mutants. We make double and triple mutants to find out.

The Hsp70 chaperone family consists of four homologs with almost identical sequences

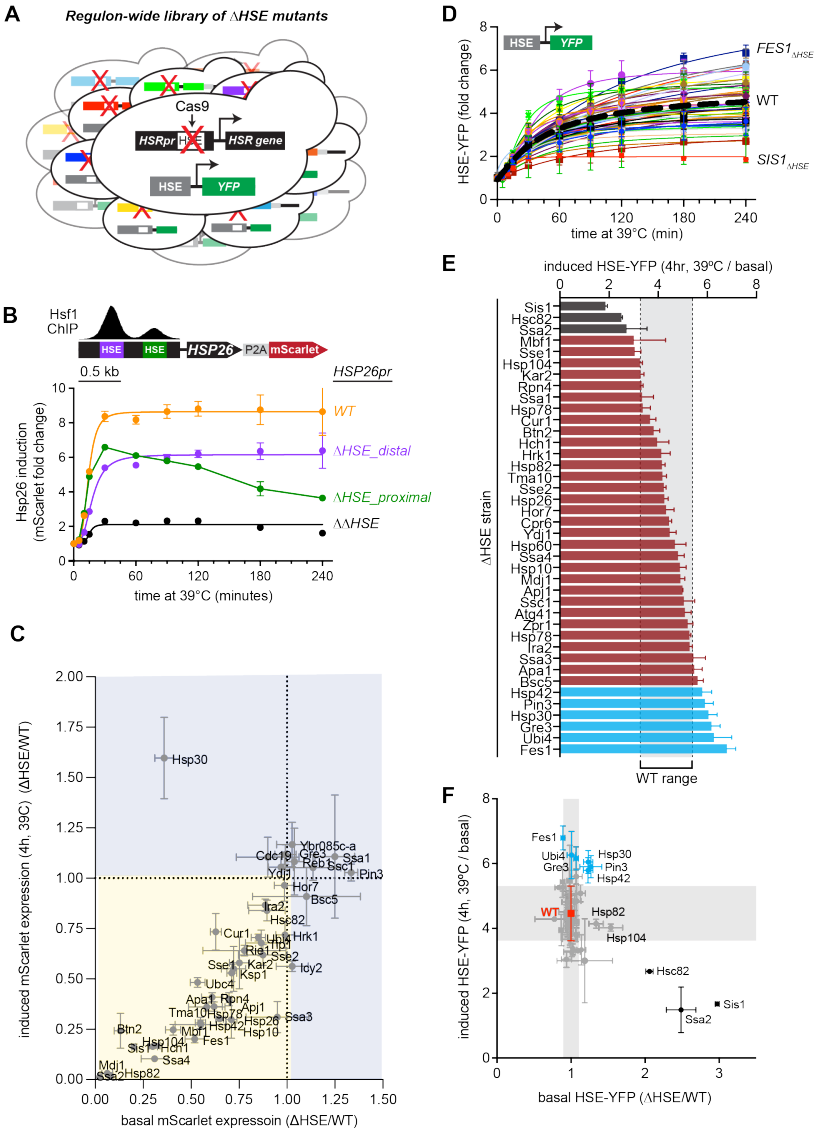

Figure 3.2: Six Hsf1 induction mutants have defects in Hsf1 regulation during heat shock A) Creation of a library of induction mutants. A new set of 42 induction mutant lines were cloned by CRISPR-Cas9-targeted deletion of the 9-25 bp ChIP-seq verified Hsf1 binding site ahead of each target gene. B) Hsp26 has two HSEs which were deleted individually and in combination. Average +/- SD, n=3. C) Summary of HSE deletion effects. Basal mScarlet level in induction mutant (normalized to WT mscarlet-tagged line in non-stress) vs. ratio of induced mScarlet level (after 4 hr at 39°C) in the induction mutant (normalized to WT mscarlet-tagged line after 4 hr HS). D) HSE-YFP fold change over a HS time course for all induction mutants. WT average (black dash line). E) HSE-YFP fold change after 4 hr heat shock at 39°C (autonormalized to non-stress HSE-YFP). WT range (gray), n=20 ($P<0.05$). F) HSE-YFP level after 4hr at 39°C (auto normalized to non-stress WT) vs. HSE-YFP level in non-stress conditions (normalized to non-stress daily control). Average +/- SD, n=3. WT range for reference (gray area) ($P<0.05$).

in the yeast genome. Hsp70s are known to recruit the protein disaggregase Hsp104, unfold proteins of all kinds, and coordinate with Hsp90 and other chaperones to facilitate refolding or degradation; differences between Hsp70 members, in terms of protein localization or function, if any, are still unknown [90]. The relative expression level and induction dynamics of each Hsp70 is distinct: two of the Hsp70 chaperones, Ssa3 and Ssa4, are expressed much less than ssa1 and ssa2 suggesting there may be some redundancy (Figure 3.3A). Among the single Hsp70 induction mutants, only Ssa2ΔHSE has abnormal Hsf1 activity above basal Hsf1 activity (Figure 3.2F), and depleting Hsp70 homologs' induction in combination (Hsp70ΔFBL) leads to significantly hyperactive Hsf1 (Hsp70ΔFBL) (Figure 3.3B). This Hsp70ΔFBL phenotype was the basis for our previous discovery that Hsp70 induction is essential for Hsf1 deactivation during stress [68]. Hsp70s perform redundant roles in Hsf1 regulation, and in combination, are essential for Hsf1 deactivation. We wonder whether any other chaperone families cooperate to regulate Hsf1.

The two Hsp90s in *S.cerevisiae* are both induced by Hsf1, share 97% sequence similarity and have important roles in overall proteostasis and cell fitness [41]. Both are induced to identical levels during heat shock (Figure 3.3C). To delete Hsp90s chaperones' induction simultaneously, we delete both genes at their endogenous locus and place Hsc82 under the non-inducible TDH3 promoter to maintain basal expression at WT level. Hsf1 is slightly hyperactive in Hsp90ΔFBL cells in the initial fifteen minutes of heat shock, but overall, Hsf1 regulation is comparable to WT (Figure 3.3D). It is not surprising that Hsp90 induction contributes little to Hsf1 activity regulation, given our previous findings that Hsp90 OE cannot rescue Hsf1 activity after Hsp70 depletion [152].

Finally, we assay the cytosolic Hsp40s that are induced by Hsf1 and known to assist Hsp70 chaperones in ATP hydrolysis and high affinity client binding – Ydj1, Sis1, and Apj1. Unlike the Hsp70s, the Hsp40s all have similar, slow induction dynamics during heat shock (Figure 3.3E). Sis1 aids Hsp70 in Hsf1 repression in non-stress conditions and its rapid relocalization

to the nucleolar periphery upon stress de-represses Hsf1 (Feder et al. 2021). Sis1 induction during stress is dispensable for Hsf1 deactivation [36]. To create induction mutants of Sis1 and Ydj1, which both rely on Hsf1 for their basal expression, we employed a promoter swapping strategy (instead of deleting the HSE) to maintain endogenous gene expression at basal WT levels (described in Garde et al. 2022, Figure 3.9A). Because recent investigations show Apj1 and Sis1 perform some redundant functions in vivo, but Ydj1 and Sis1 have distinct roles, we were curious whether Hsp40s are functionally redundant in Hsf1 regulation [13,135] To investigate, we simultaneously deplete induction of two J domain proteins at a time in all pairwise combinations. Surprisingly, all double induction mutants, and the triple mutant (JDPΔFBL), have normal Hsf1 activity during stress (Figure 3.3G). Because Apj1 has been implicated in nuclear proteostasis, we wonder whether it had any role in Hsf1 activity regulation or cellular functioning at all [15]. When Apj1 gene is deleted (apj1Δ), Hsf1 is hyperactive in basal conditions (Figure 3.9), and Hsf1 activity increases 9-fold during heat shock, comparable to the Hsf1 hyperactivity defect observed in Hsp70ΔFBL (Figure 3.3H), Apj1 is likely important for maintaining cellular proteostasis in non-stress and stress conditions. Overall, we conclude that Hsp40 chaperones' induction, independently and in combination, is dispensable for Hsf1 regulation.

In conclusion, we find that the Hsp70 family is the only chaperone family that works together to deactivate the HSR. Though the Hsp90 and Hsp40 families are dispensable for Hsf1 feedback regulation, their induction may impact protein homeostasis or overall cell fitness.

3.3.4 Quantifying fitness in Hsf1 target gene induction mutants

In response to environmental changes, cells must repair any cell damage, and adapt and resume growth in ongoing stress. Previous studies show that direct Hsf1 misregulation (via Hsp70) does not affect fitness, suggesting that direct Hsf1 regulation and growth resumption

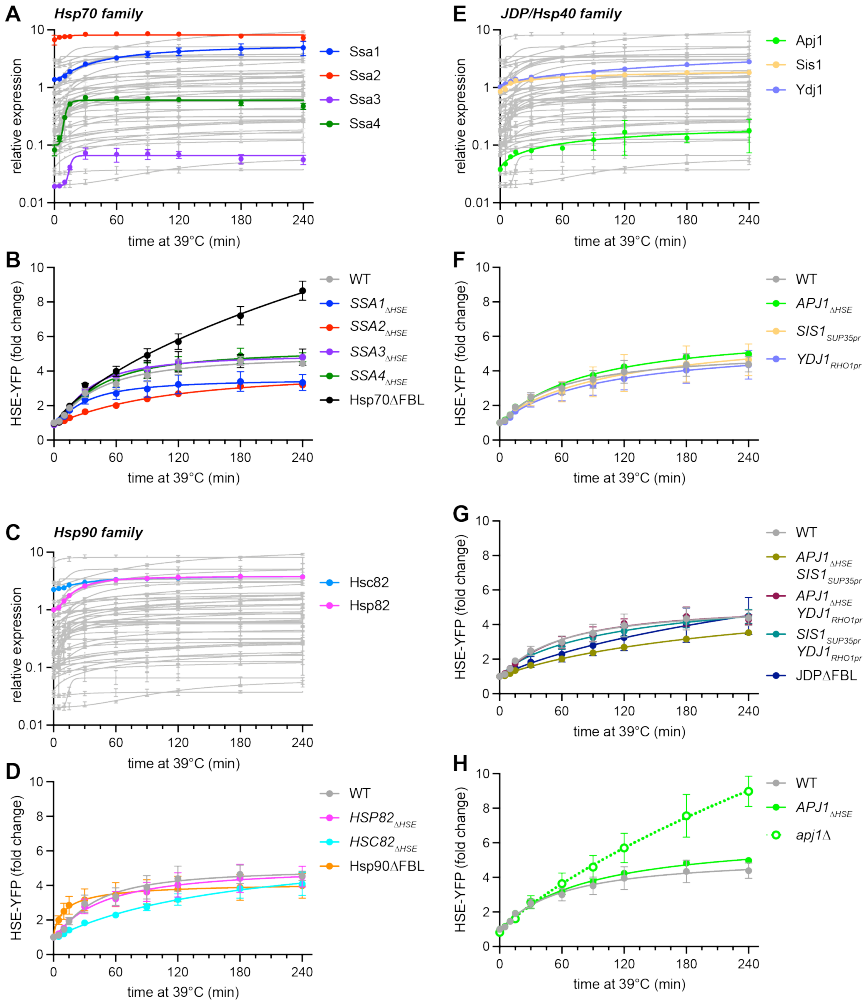

Figure 3.3: The Hsp70 homologs work together to deactivate Hsf1 in stress, but induction of the Hsp40 and Hsp90 chaperone families are entirely dispensable for Hsf1 regulation A) Relative mScarlet level (normalized to basal control) over a 4 hr HS. The four Hsp70 homologs are highlighted, and expression profiles for the remaining Hsf1 target genes are gray. B) HSE-YFP fold change for single Hsp70 induction mutants (ssa1ΔHSE, ssa2ΔHSE, ssa3ΔHSE, and ssa4ΔHSE) and mutant defective in induction of all 4 Hsp70s, Hsp70ΔFBL. C) Relative mScarlet expression over a heat shock time course for each Hsp90 (normalized to basal control). D) HSE-YFP fold change for each Hsp90 induction mutant, and the double mutant, Hsp90ΔFBL. E) Relative mScarlet level over a heat shock time course (normalized to basal control). The Hsp40 chaperones, highlighted, and remaining target genes' expression in gray. F-H) HSE-YFP fold change for each Hsp40 induction mutant (F), for pairwise double Hsp40 induction mutants and a triple Hsp40 induction mutant (JDPΔFBL) (G), and Apj1 induction mutant (Apj1ΔHSE, solid) and Apj1 KO (apj1Δ, dashed) (H). Average +/- SD, n=3.

are distinct and decoupled processes in the cell [68]. Thus, a mutant with Hsf1 activity defect but no fitness defect is likely to have a defect in direct Hsf1 regulation. To determine whether the six induction mutants with Hsf1 activity defects have specific Hsf1 regulation defects or a more general breakdown in cellular processes, we screen for fitness defects in the library of induction mutants. The screen also reveals Hsf1 induction mutants with fitness defects but no other phenotypes, indicating some targets are induced solely to promote cell adaptation and growth resumption in stress.

Our quantitative growth assay reveals dramatic fitness defects in many ΔHSE strains during stress. Four ΔHSE strains have abnormal Hsf1 activity and fitness defects (Figure 3.4C, pink). They likely affect processes that Hsf1 is not sensitive to. Alternatively, they may cooperate to affect cytosolic proteostasis, such that together they indirectly deactivate Hsf1 by restoring proteostasis. Hsp42ΔHSE has Hsf1 activity defects but no fitness defects, reminiscent of our Hsp70ΔFBL strain, suggesting Hsp42 may regulate Hsf1 via the previously established Hsp70-dependent feedback loop (Figure 3.4C), blue)[68]. Five induction mutants - Ubi4, Pin3, Hsp30, Gre3, Fes1 – had defects in cell fitness and Hsf1 activity ((Figure 3.4C), white). We wonder whether these target genes' induction affects cell fitness and Hsf1 activity by restoring cytoplasmic proteostasis, or by affecting some other process that Hsf1 is sensitive to. Excitingly, the function of Pin3, Hsp30 and Gre3 is ill-defined, so this result offers an opening for further investigations into these genes in general. In total, this study finds that induction of ten Hsf1 targets, a quarter of the Hsf1 regulon, has a clear adaptive role in responding to stress (Figure 3.4B).

3.3.5 Investigating the mechanisms behind Hsf1 regulation defects

To determine the mechanism behind the fitness defects, we investigate the slow-growing Hsf1-hyperactive ΔHSE mutants for signs of proteotoxic stress. Disruption to protein homeostasis is the only known process which Hsf1 senses (via Hsp70 availability) [68]. Therefore,

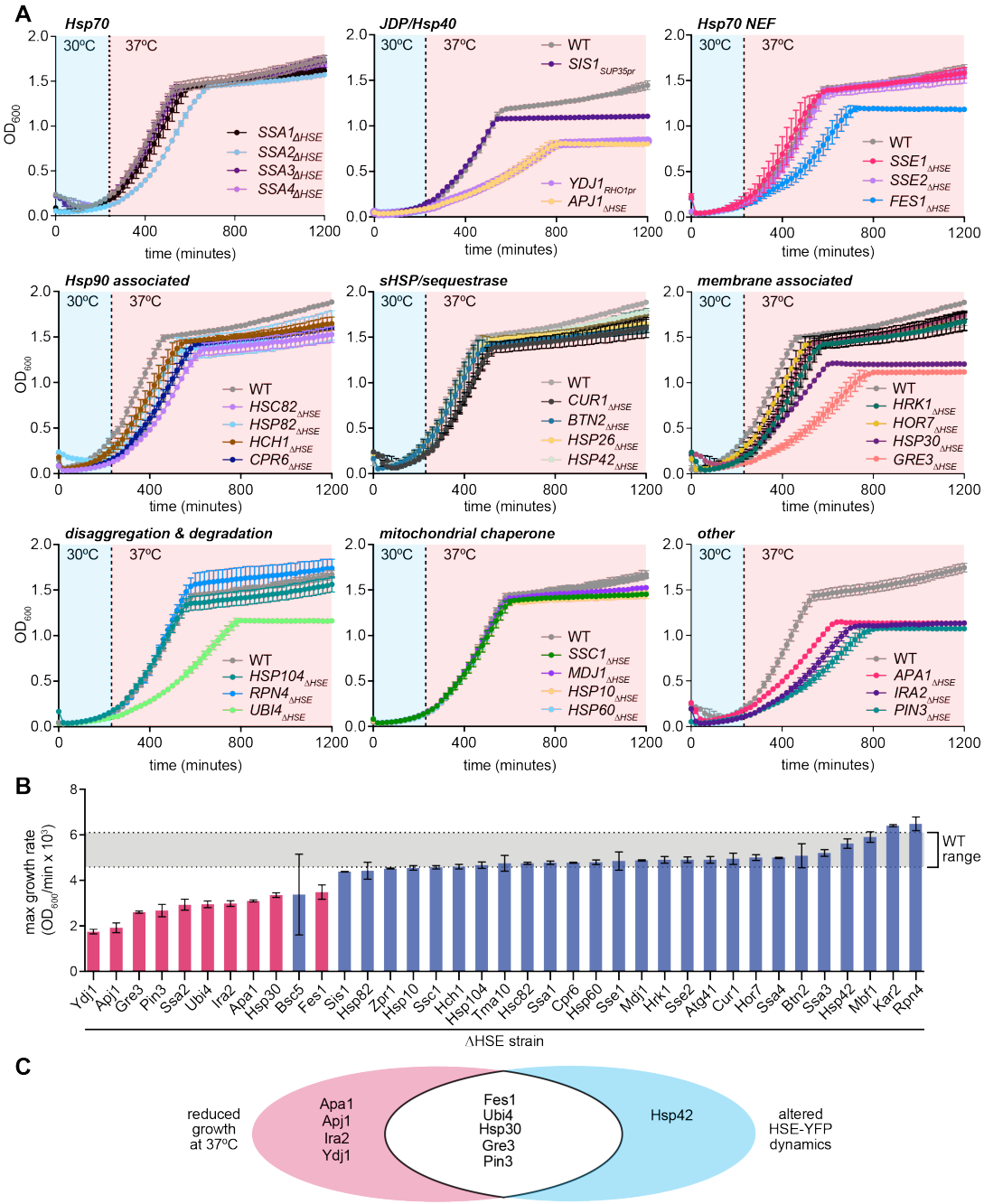

Figure 3.4: The set of ΔHSE induction mutants with fitness defects is partially distinct from the induction mutants with mis-regulated Hsf1

A) Quantitative growth assay of Hsf1 target induction mutants during heat shock (37°C), grouped by known cellular function. Average +/- SD, n=3. B) The log phase growth rate of each induction mutant (maximum derivative of the OD_{600} curve). Average +/- SD, n=3. C) Summary of the induction mutants with slow growth during HS (pink), altered Hsf1 activity (HSE-YFP dynamics) (blue), or both phenotypes (white).

disrupted cytosolic protein homeostasis is a likely cause of the fitness defects in the Hsf1 hyperactive mutants. WT cells exposed to heat shock experience disruptions to protein homeostasis: Hsp104-marked aggregates form and are cleared within an hour (Figure 3.5A) [68]. To determine which fitness defects are caused by persistent disruptions to cytosolic proteostasis, we image an established marker of proteostasis, Hsp104. In contrast, most of the induction mutants that have fitness defects – Fes1, Ubi4, Pin3, and Hsp30 – developed large, persistent foci upon heat shock (Figure 3.5A). Induction of these genes is important for restoring cytosolic proteostasis; Hsf1 is more active in these mutants because it is responding to a larger disruption in proteostasis. The one induction mutant with Hsf1 hyperactivity but no fitness defect, Hsp42ΔHSE, has only a few, small Hsp104 foci, comparable to WT, and reminiscent of the Hsp70ΔFBL strain [68]. The Hsp70 induction mutant (Hsp70ΔFBL) has hyperactive Hsf1, no fitness defect, and Hsp104 foci clearance similar to WT, presumably because the induction of Hsp70 affects Hsf1 regulation, but the induction of extra Hsp70 during HS is dispensable for restoring proteostasis in the cytoplasm. It is likely that Hsp42 regulates Hsf1 activity via the Hsp70 negative feedback loop.

Finally, we follow up on the induction mutant with the most dramatic Hsf1 hyperactivity among the single induction mutants (Figure 3.2E), as well as fitness and proteostasis defects, Fes1ΔHSE. Based on the induction mutant phenotype and Fes1's established role as a nucleotide exchange factor for Hsp70, we wonder whether its induction directly affects Hsp70 and Sis1 localization, which are known to be recruited to Hsp104-marked sites of proteotoxic stress [30,42,68]. Both Ssa1 and Sis1 localized to the persistent cytoplasmic foci that form upon heat stress and persist in Fes1ΔHSE (Figure 3.5C,D,F). Additionally, Fes1ΔHSE has a smaller fraction of nuclear Ssa1 and Sis1, suggesting Sis1 and Ssa1 at cytosolic foci return to the nucleus once released from cytosolic aggregates (Figure 3.5E,G). Given Fes1's known role in releasing Hsp70 from its client proteins, Fes1 induction likely feeds into the Hsp70-dependent negative feedback loop by releasing Hsp70 from aggregated proteins.

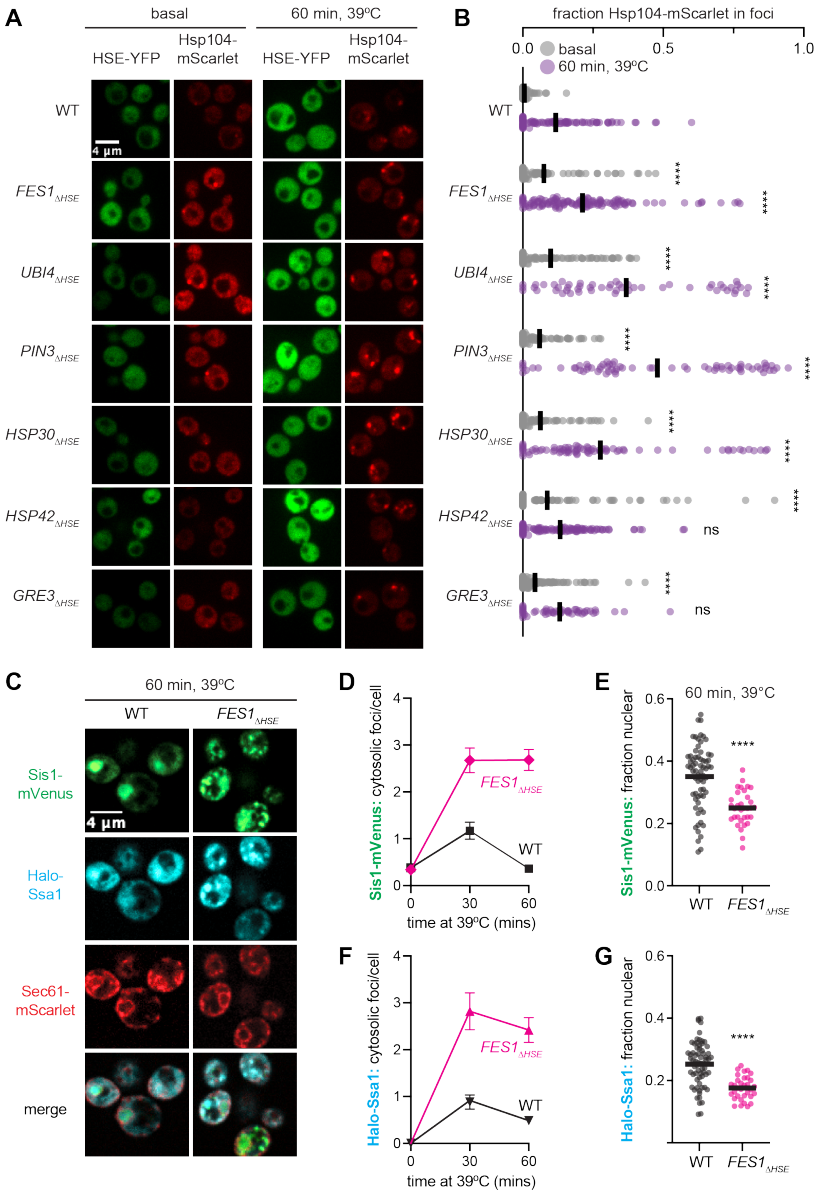

Figure 3.5: Induced Fes1 deactivates Hsf1 by releasing Hsp70 from protein aggregates A) Induction mutants (ΔHSE) expressing the genome-integrated reporter, Hsp104-mKate and the generic reporter of Hsf1 activity, HSE-YFP. Cells were fixed with 4% formaldehyde. B) Portion of Hsp104 signal found at cytoplasmic foci, relative to the whole cell, in non HS (30°C,gray), or 1 hr HS (39°C,purple). Single cell data graphed. Average, n=>25 imaged cells. Two-tailed p-value generated from unpaired t-test ****P<0.0001. C) Induction mutants expressing ssa1pr-Halo-ssa1 (Hsp70-Halo) and Sis1-mVenus, and endogenously tagged membrane marker Sec61. Sis1 and Ssa1 reporter constructs were integrated into the genome. D) Count of proteotoxic stress foci during heat shock at 39°C. Average +/- SD, n=>25 cells. E) Nuclear Sis1 and Ssa1 signal relative to total cell signal. Each data point represents a single cell. Average, n=>25 cells. Two-tailed p-value generated from unpaired t-test **** P<0.0001

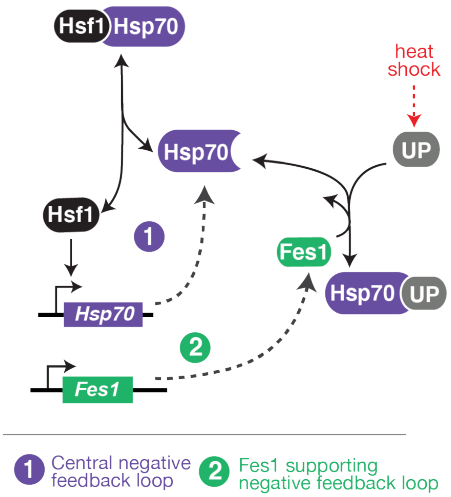

Figure 3.6: Fes1 induction helps deactivate Hsf1 via Hsp70
Heat shock causes a pool of newly-synthesized unfolded proteins (UP) to accumulate in the cytoplasm, which recruits Hsp70 from the nucleus to the cytoplasm. Hsf1 is free to induce its transcriptional targets, including Hsp70. The induction of Hsp70 deactivates Hsf1 in a negative feedback loop. Hsf1-induced Fes1 supports the Hsp70-dependent negative feedback loop by releasing Hsp70 from client UPs, so it can return to the nucleus and repress Hsf1.

3.4 Discussion

Here, we find that feedback regulation in the HSR is strikingly elegant, involving the previously-established, Hsp70-dependent feedback loop. Induction of six Hsf1 target genes had a small but significant deactivating effect on Hsf1. In-depth investigation of the most significant negative feedback regulator, Fes1, indicates it simultaneously supports Hsp70-dependent feedback and restores protein homeostasis. The identification of Hsf1's more subtle negative regulators has great potential for improving our fundamental understanding of protein homeostasis, and guiding new therapeutic applications. Follow-up investigations on the five other Hsf1 feedback regulators are likely to be as revelatory as the investigations on Fes1 conducted here.

Ten Hsf1 targets affect the cells ability to adapt and grow in long term heat stress. Given that the HSR responds to a range of environmental stressors, other Hsf1 targets may perform important functions for HSR regulation or cell adaptation in other conditions.

Even though each target gene is dependent on the single nuclear transcription factor, Hsf1, target gene expression varies widely (Figure 3.1). The Hsf1 target genes have a 1000-fold range in their basal expression levels, ten-fold range in fold change induction during heat shock, and their dynamics of induction vary greatly as well. Once the 3D genome architecture of the Hsf1 targets is characterized, each target gene's architecture and chromosomal contacts can be compared against the gene's expression dynamics, measured here. Hsf1 is known to trigger a transient restructuring of DNA into active transcriptional condensates, but how this restructuring influences transcription levels and dynamics is still unknown [22–24]. Though the HSR has been a model system for understanding eukaryotic transcriptional regulation for more than fifty years, it can now be leveraged to understand the mechanisms of transcriptional variation between genes.

Previously it was established that the deactivation of the HSR required Hsp70 induction and binding Hsf1 in the nucleus, but it was unclear whether any induced Hsf1 targets mediated relocalization of Hsp70 to the nucleus, or substantiated Hsp70 binding to Hsf1 to deactivate it [30,68]. To identify the negative feedback regulators of the HSR, we deleted the previously identified Hsf1 binding site ahead of each target gene, and screened for Hsf1 activity defects during heat shock in the library of induction mutants. We find that Hsf1 activity fold change is significantly higher than WT in six Hsf1 target gene induction mutants, most significantly Fes1ΔHSE. Fes1 induction is necessary for the release of Hsp70 and Sis1 back to the nucleus to repress Hsf1 (Figure 3.5C,D). Thus, Fes1 induction negatively regulates Hsf1 via the previously discovered negative feedback regulator, Hsp70[68]. The Fes1-mediated release of Hsp70 from cytosolic condensates allows Hsp70 relocalization to Hsf1 in the nucleus, is an important part of the Hsf1 deactivation mechanism (Figure 3.6). It is possible that the Fes1-dependent release of Hsp70 is the initial trigger for the entire dissolution of Hsp104-protein aggregates, but more work is needed to define the timeline and players involved in each stage of restoring protein homeostasis.

Surprisingly, the Hsp40 chaperones (Sis1, Apj1, and Ydj1) that are induced by Hsf1 are dispensable for Hsf1 regulation individually and in combination (Figure 3.3)[37]. Given that Sis1 is necessary for the basal repression of Hsf1 and is integral to HSR activation, it is unexpected that Hsp40s are not involved in Hsf1 deactivation [30]. However, this result provides a long-awaited reason for why Hsp70 (1000:1) must be induced beyond its high basal levels for Hsf1 deactivation [26,68].

Hsf1 targets which do not affect Hsf1 regulation still may have a functional role in the cell; to find targets that support growth resumption or other processes that affect fitness in long term stress, we measure cell growth across the library of induction mutants. The screen revealed that the induction of four Hsf1 target genes have a role solely in overall fitness during heat shock (Apa1, Apj1, Ira2, Ydj1). Most of the induction mutants with Hsf1 regulation defects had growth defects as well (5 out of 6). One induction mutant, Hsp42ΔHSE, had hyperactive Hsf1 initially during HS (Figure 3.5), but no defects in growth.

How does Hsp42 affect proteostasis and Hsf1 regulation? In this study, we find that Hsp42 induction is not necessary for Hsp104-aggregate clearance, or overall cell fitness. Hsp42 is a protein sequestrase, necessary for protein condensate formation in the cytoplasm [29]. It is believed that Hsp42 shields aggregated proteins from degradation and chaperone machinery, so that chaperone and degradation systems are not overwhelmed by a sudden accumulation of newly-synthesized upon stress. Consistent with the idea that Hsp42 shields Hsp70 from aggregate proteins when the burden of aggregates is large, Hsp42ΔHSE has especially hyperactive Hsf1 in the initial minutes of heat shock and Hsp42 KO cells are especially sensitive to Hsp70 depletion [52]. It is likely that induced Hsp42 directly buffers the recruitment of Hsp70 to cytosolic aggregates upon HS, which we know does not affect cell fitness but does affect Hsf1 activity. We hope further investigations can document the chaperones which are Hsf1 target genes – Sis1, Btn2, Hsp104, Hsp42, Fes1 – as they arrive and depart from protein aggregates. Which proteins arrive first and which are necessary for the recruitment

or release of the others?

To investigate the mechanism behind the slow growth phenotype in the hyperactive Hsf1 induction mutants, we started by looking for signs of disrupted protein homeostasis. As expected, most induction mutants with Hsf1 hyperactivity and fitness defects also had defects in cytosolic protein homeostasis, which the HSR is known to monitor and maintain. Therefore, Hsf1 hyperactivity in the induction mutants with the triple phenotype (defects in Hsf1 activity, fitness, and protein homeostasis) is due to disrupted cytosolic protein homeostasis.

The one exception was Gre3ΔHSE (Figure 3.5A), which had an overall fitness defect but normal cytosolic proteostasis (Hsp104 foci comparable to WT during stress). The Gre3ΔHSE phenotype indicates that the Hsf1 transcriptome may be sensing and maintaining additional processes outside of cytosolic protein homeostasis. Future investigations should explore the role of Hsf1 target gene induction in response to other stressors, which may disrupt processes outside of cytosolic protein homeostasis. Are different Hsf1 targets more important for HSR deactivation in osmotic stress or oxidative stress, compared to in heat stress? These investigations will further reveal whether the conserved induction of transcriptional targets in a regulon all have an adaptive role.

3.5 Methods

3.5.1 Strain construction

To create the library of P2A-mscarlet tagged strains, we introduce a P2A-mscarlet-KAN cassette with homologous flanking ends and plate on kanamycin selective media. Successful transformants were verified by flow cytometry. To create ΔHSE induction mutants, we delete the 9-25 bp Hsf1-binding consensus sequence by scarless CRISPR-Cas9 targeted deletion. The closest match to the Hsf1 binding motif (nnTTCnnGAA) is located under the 5 min heat shock Hsf1 ChIP-seq peak from our previous study[102]. Generally, we found one

strong consensus sequence under the singular Hsf1 ChIP-peak 200-300 bp ahead of the TSS. We delete the ChIP-verified consensus sequence, in the established library of P2A-mscarlet parent lines. Cell line construction involved cloning a guide RNA, which will target the Hsf1 binding site, into an episomal, URA3-marked, Cas9- containing plasmid. The guide RNA plasmid was co-transformed with a 100 bp double-stranded repair template to repair the double stranded break by homologous recombination, and yeast were plated on ura-selective media. HSE deletion was confirmed by Sanger sequencing. Finally, the cell lines were plated on 5-FOA selective media to expel the Cas9::ura3 plasmid.

Though our P2A-mscarlet reporter strategy is tagless, it caused abnormal basal Hsf1 activity in a few lines, probably because the C terminal linker inhibits protein function. So, another library of ΔHSE induction mutants in our original parent line w303a; HSE-mVenus is used in all experiments beyond the initial target gene transcription dynamics study (Figure 3.1, Figure 3.2B,C). All strains are derived from the W303a parent strain.

3.5.2 Heat shock time course

Cells were serially diluted and grown overnight on the benchtop at room temperature (25°C) in 1xSDC media. In the morning, cells were transferred to microcentrifuge tubes and aerated by shaking (1250 RPM) at 30°C for one hour.

Centrifuge tubes were then transferred to a shaking incubator at heat shock temperature (39°C). At each time point (0, 5,10,15, 30, 60, 90, 120, 180, 240 minutes), 50 uL of cells were transferred to a 96 well plate of 1xSDC at 50 ug/mL final concentration cycloheximide on the benchtop. After the time course, the plate was incubated at 30°C for 1 hour to promote fluorescent reporter maturation before flow cytometry.

3.5.3 Flow cytometry

Cells were measured with the BD Fortessa HTS 4-15 benchtop analyzer at the University of Chicago Cytometry and Antibody Technology Facility. Analysis was completed in FlowJo: fluorescence excitation value for each cell was normalized by side scatter for each cell to filter out signal from dead cells, and the median normalized fluorescence excitation value was calculated for each sample.

3.5.4 Quantitative growth assay

Cells were grown overnight shaking in 1xYPD at 30°C. In the morning, cells are diluted to OD_{600}=0.1 in 1xYPD and transferred to a 48-well plate. Cells are grown while shaking in the SPECTROstar Nano® Absorbance Plate Reader at 30°C for four hours, then at 37°C for 20 hours, and optical cell density is measured every 20 minutes. The initial four hour incubation at 30°C before heat shock yields more consistent results across biological replicates.

3.5.5 Heat shock time course and imaging

Cells were grown in 2xSDC media at 30°C shaking overnight. In the morning, cells are diluted to OD_{600}=0.1 and grown at 30°C shaking for 4 hours to reach log phase growth. 200 uL of cells are transferred to a microcentrifuge tube in the cell shaker at 39°C. At each time point, cells are fixed in 1% paraformaldehyde, then washed and imaged in KPIS media (1.2 M sorbitol, 0.1 M potassium phosphate, pH 7.5) Fixed cells are imaged on the Marianas Leica II Spinning Disk Confocal microscope at the University of Chicago Imaging Core. A single z stack is captured and analyzed for each frame. A minimum of 20 cells are quantified at each time point in ImageJ.

3.5.6 Image quantification

Imagej is used for all image quantification. Hsp104 foci in each cell are identified using Intermodes thresholding of each cell. Hsp70 and Sis1 foci are identified using the Triangle threshold. To determine the bounds of the nucleus, a ROI is drawn by hand based on the bounds of the nuclear membrane, marked by Sec61-mscarlet.

3.6 Supplementary Figures

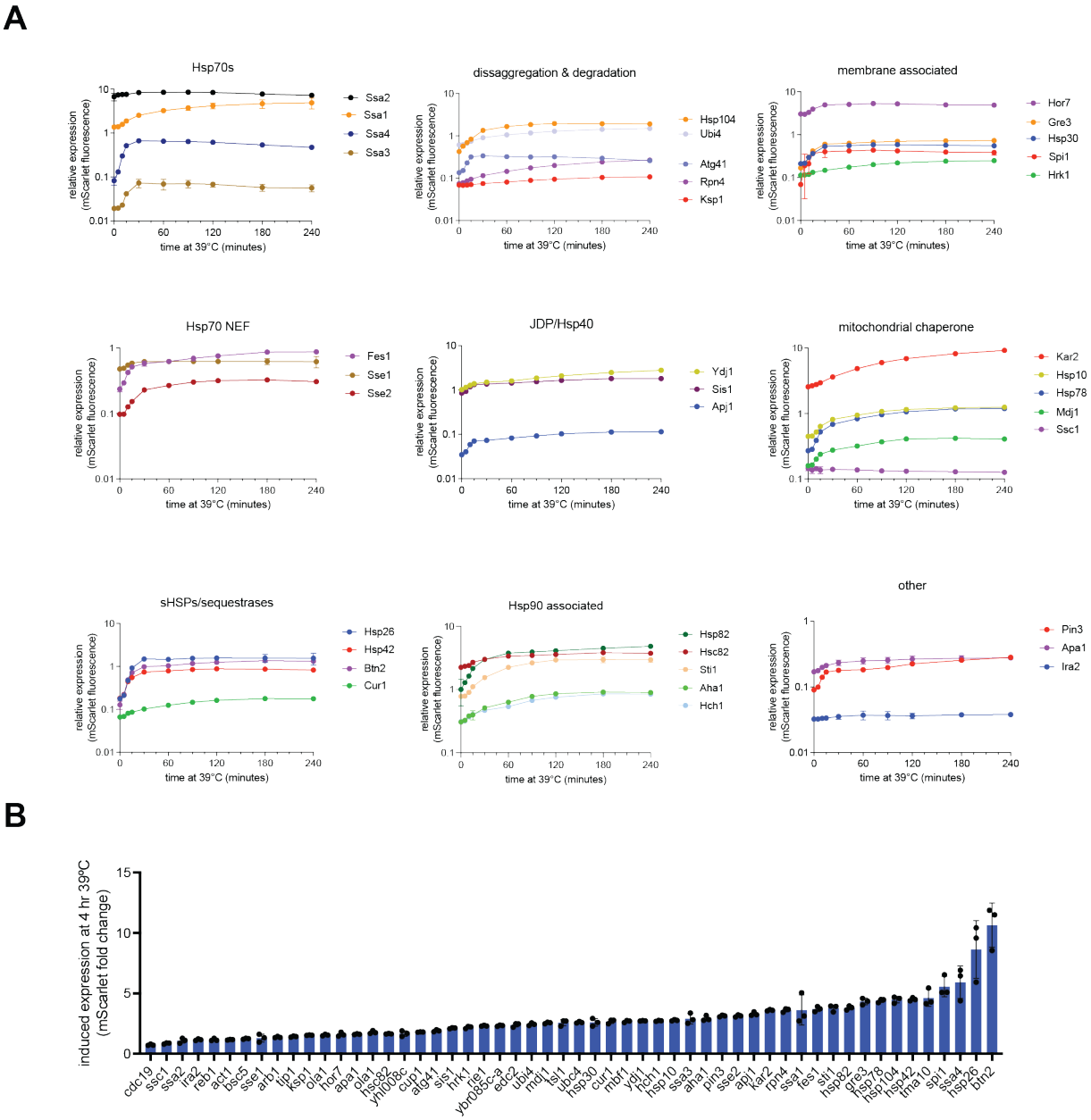

Figure 3.7: Wild type HS-induced expression dynamics of the Hsf1 target genes, grouped by function

A) Relative expression dynamics for Hsf1 target genes, captured with mScarlet fluorescent reporter, at 39°C. Hsf1 target genes are grouped by putative gene function. Average +/- SD, n=3. B) Fold change in mScarlet expression reporter for each Hsf1 target gene after 4 hr HS (normalized to non-stress mScarlet level). Average +/- SD, n=3.

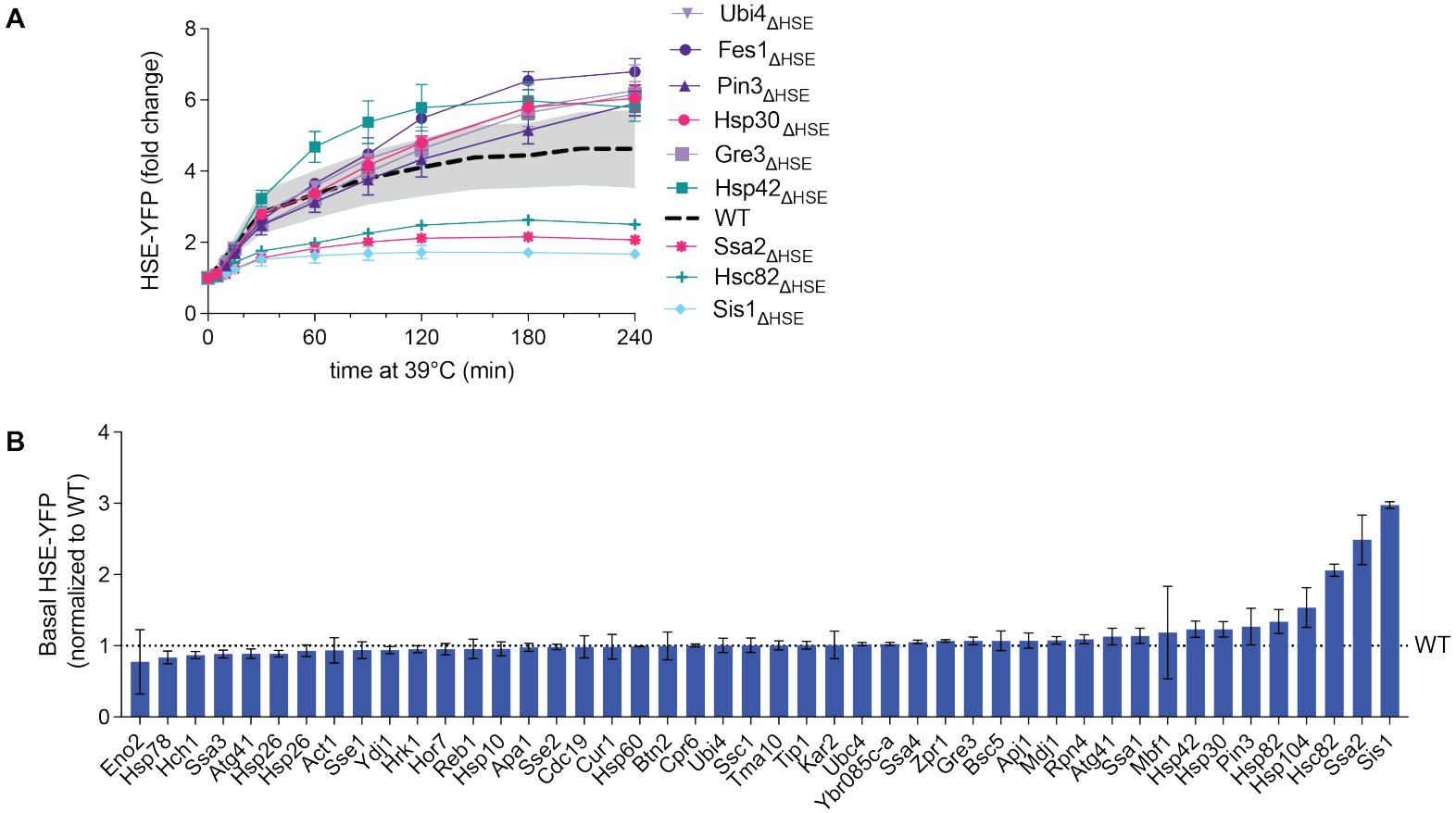

Figure 3.8: Hsf1 activity dynamics in ΔHSE induction mutants
A) HSE-YFP fold change during HS (39°C) for induction mutants with HSE-YFP dynamics outside of the WT range(gray, P<0.05). Average +/- SD, n=3. Dotted line is average WT, SD (gray shaded area), n=45. B) Relative non-stress levels of HSE-YFP reporter (normalized to WT) in each ΔHSE induction mutant. Average +/- SD, n=3.

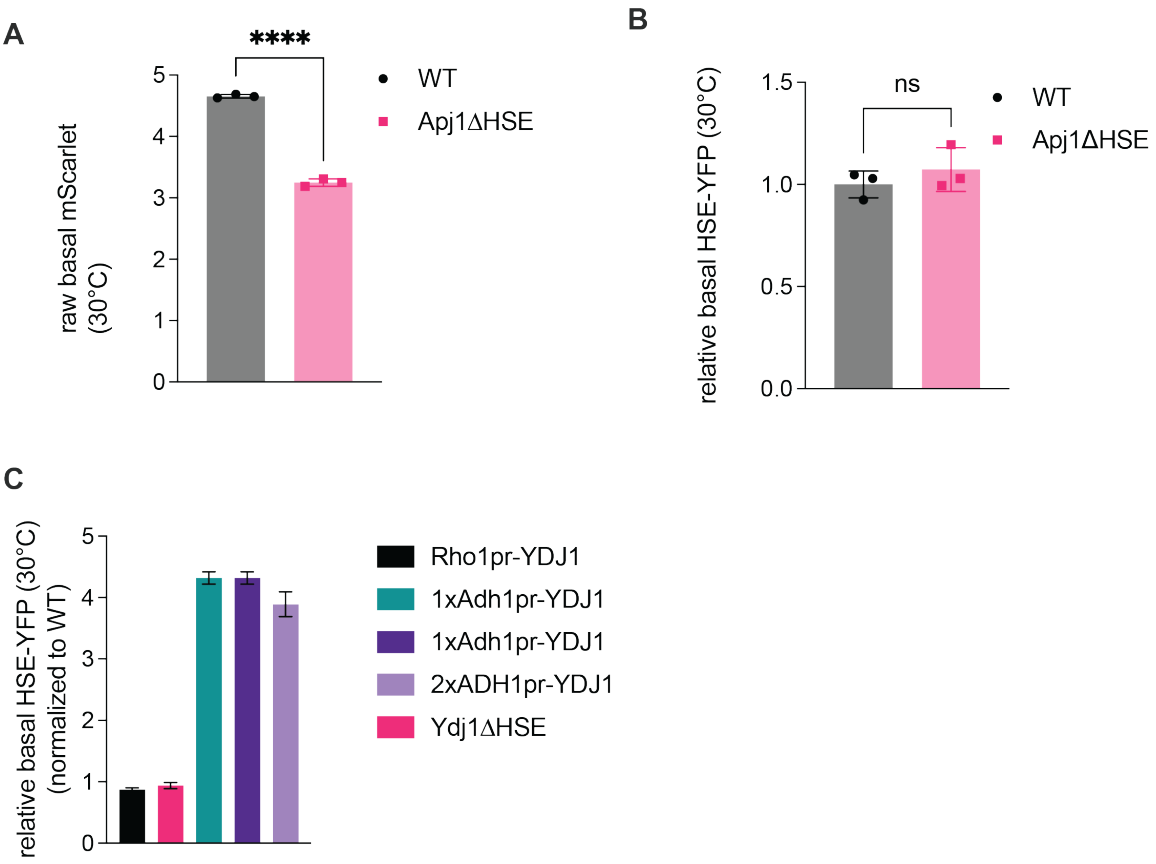

Figure 3.9: Validating Ydj1 and Apj1 induction mutants
A) Basal Apj1 expression measured by mScarlet fluorescence in Apj1ΔHSE vs WT. Average +/- SD, n=3. ****P<0.0001. B) Basal Hsf1 activity measured by HSE-YFP fluorescent reporter in Apj1ΔHSE vs WT. Average +/- SD, n=3. Non-significant (ns), P>0.05. C) Fine tuning Ydj1 expression level. Relative basal HSE-YFP (normalized to basal HSE-YFP in WT) when Ydj1 is expressed under non-inducible promoters of various strengths.

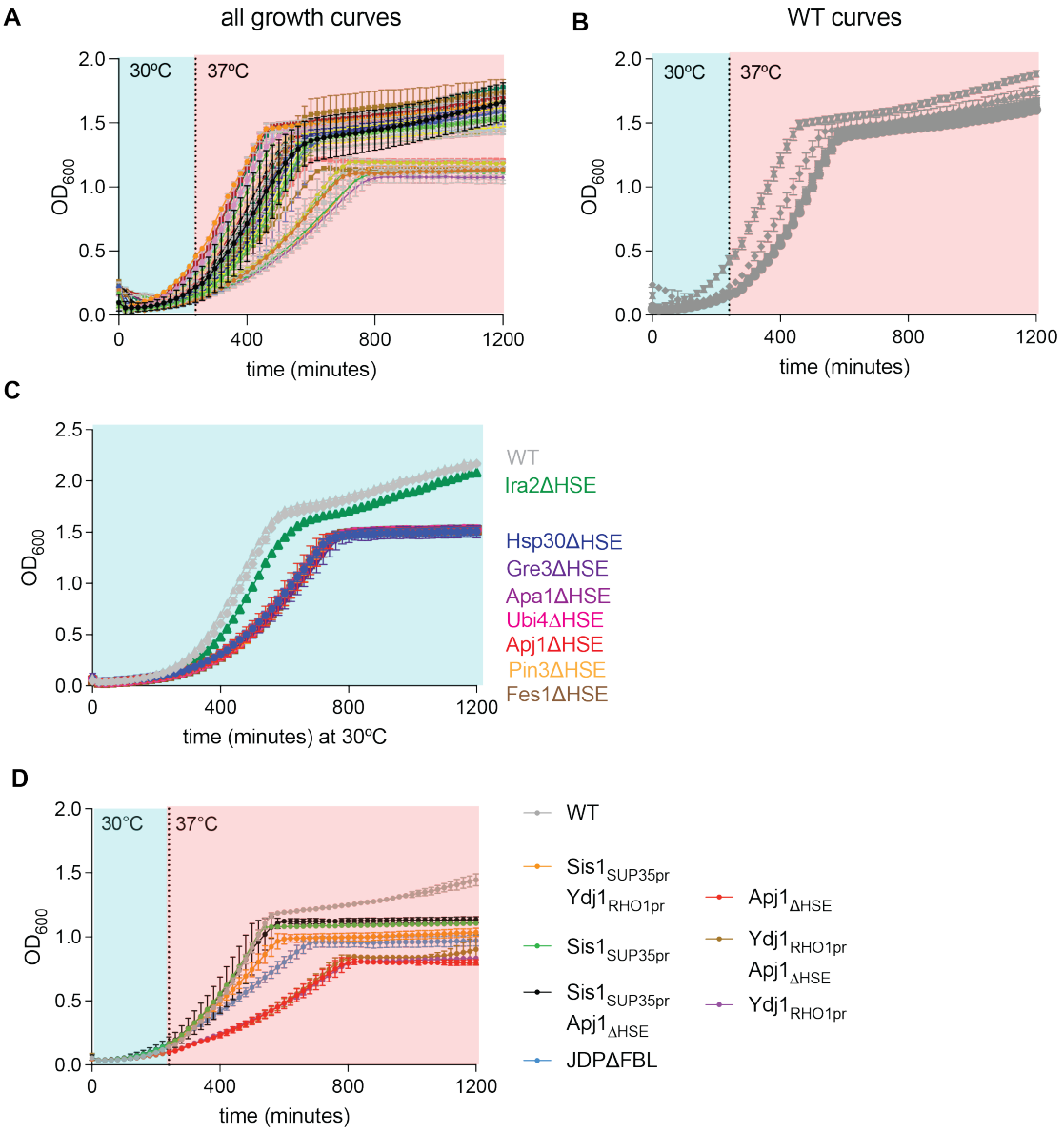

Figure 3.10: Additional quantitative growth assays
A-B) Quantitative growth assays during HS (37°C). C) Quantitative growth assay of the induction mutants (ΔHSE) that had fitness defects at 37°C. Lines are grown at optimal growth temperature (30°C). Average +/- SD, n=2. D) Quantitative growth assays of J domain induction mutants (single, double and triple mutants) during HS (37°C). Average +/- SD, n=2.

CHAPTER 4

ADAPTIVE PRESERVATION OF ORPHAN RIBOSOMAL PROTEINS DURING STRESS IN CHAPERONE-STIRRED CONDENSATES

This chapter is in revision at Nature Cell Biology and is available publicly as: Ali et al. 2023, bioRxiv. [6] I conducted the differential expression RNA-seq analysis and the quantitative growth assays that appear in this work.

4.1 Abstract

Ribosome biogenesis is among the most resource-intensive cellular processes, with ribosomal proteins accounting for up to half of all newly synthesized proteins in eukaryotic cells. During stress, cells shut down ribosome biogenesis in part by halting rRNA synthesis, potentially leading to massive accumulation of aggregation-prone "orphan" ribosomal proteins (oRPs). Here we show that during heat shock in yeast and human cells, oRPs accumulate as reversible condensates at the nucleolar periphery recognized by the Hsp70 co-chaperone Sis1/DnaJB6. oRP condensates are liquid-like in cell-free lysate but solidify upon depletion of Sis1 or inhibition of Hsp70. When cells recover from heat shock, oRP condensates disperse in a Sis1-dependent manner, and their ribosomal protein constituents are incorporated into functional ribosomes in the cytosol, enabling cells to efficiently resume growth.

4.2 Introduction

Cells must double their ribosome content each division cycle, and ribosome biogenesis may be rate-limiting for proliferation [73,82,119,137]. In yeast, where eukaryotic ribosome biogenesis has been most thoroughly studied, ribosomal proteins (RPs) account for >40% of all

newly synthesized proteins under nutrient-rich conditions [54,120]. This huge investment of resources results in the synthesis of more than 105 RPs each minute [120,137]. To assemble a mature yeast ribosome, 79 RPs must stoichiometrically associate with four ribosomal RNA (rRNA) molecules to form the large 60S and small 40S subunits [140]. Many RPs cannot adopt their native structures and are highly aggregation prone in the absence of rRNA [56]. This poses a challenge in the compartmentalized eukaryotic cell: rRNA is transcribed in the nucleolus, while RPs are synthesized on ribosomes in the cytosol. Most RPs translocate from the cytosol into the nucleolus, and specific karyopherins and dedicated chaperones known as escortins mediate their transport [101]. Transcription of rRNA and the mRNAs encoding RPs is coordinately regulated and rapidly repressed upon nutrient limitation or other environmental stressors such as heat shock [38,39,114,121]. Given the rate of RP synthesis, stress induced transcriptional attenuation would be predicted to result in an instantaneous buildup of a massive excess of RPs relative to rRNA.

Several cellular mechanisms have been described that respond to "orphan" RPs (oRPs), i.e., RPs that are mis-localized in the cell and/or not bound to rRNA [60]. Two distinct pathways, mediated by the Tom1/HUWE1 and UBE2O ubiquitin ligases, recognize oRPs and target them for proteasomal degradation [129,146]. Loss-of-function mutations in RP genes – which result in stoichiometric imbalance among RPs and accumulation of oRPs – lead to a class of human diseases known as "ribosomopathies" [93]. Mechanistically, the accumulation of oRPs in ribosomopathies is thought to result in the sequestration and inactivation of the ubiquitin ligase MDM2 that normally degrades p53, and the accumulation of p53 results in cell cycle arrest and apoptosis [57]. In yeast, which lacks p53, accumulation of oRPs activates a specific gene expression program [4,134]. This program involves downregulation of RP genes and induction of the heat shock response (HSR), a transcriptional regulon encoding chaperones and other protein homeostasis (proteostasis) factors [104]. The ability of oRPs to activate the HSR suggests there may be a physiological connection between oRPs

and the proteostasis network.

Here we demonstrate that oRPs accumulate and drive key early events in the cellular response to heat shock. We find that oRPs interact with the J-domain protein (JDP) Sis1, an essential regulator of the chaperone Hsp70. oRPs trigger the localization of Sis1 in yeast and its homolog DnaJB6 in human cells to the periphery of the nucleolus upon heat shock. Rather than targeting oRPs for degradation, Sis1 and Hsp70 maintain oRPs in dynamic condensates that remain liquid-like in cell-free lysate. Following recovery from heat shock, oRP condensates disperse, the RPs are incorporated into functional ribosomes in the cytosol, and cells efficiently resume proliferation. By actively maintaining condensate reversibility, Sis1 and Hsp70 preserve oRP functionality and conserve cellular resources during stress.

4.3 Results

4.3.1 Sis1 localizes to the nucleolar periphery during heat shock

To define the molecular species that drive the spatial reorganization of the proteostasis network during heat shock, we focused on the J-domain protein (JDP) Sis1. Subcellular re-localization of Sis1 represents the earliest known cell biological event following heat shock in yeast [30]. We developed a four-color yeast strain to monitor Sis1 localization in live cells with respect to the nucleolus, the nuclear boundary, the cortical endoplasmic reticulum, and cytosolic protein aggregates marked by Hsp104. We imaged this strain in three dimensions over a heat shock time course using lattice light sheet microscopy (Video S1). Prior to heat shock, Sis1 was concentrated in the nucleoplasm and diffuse throughout the cytosol (Figure 4.1A). Acute heat shock at 39ºC resulted in re-localization of Sis1 from the nucleoplasm to a region surrounding the nucleolus within 2.5 minutes (Figure 4.1A). Image analysis revealed increased Sis1 peri-nucleolar localization in nearly all cells following 2.5 and 10 minutes of heat shock (Figure 1B; Figure S1A; see methods). We additionally observed overlapping cy-

tosolic foci containing Sis1 and Hsp104 that formed with delayed kinetics compared to Sis1 peri-nucleolar localization (Figure 4.1A; Figure 4.7B). Ongoing protein synthesis and/or ribosome dynamics have been shown to contribute to activation of the heat shock transcriptional response and to re-localization of Sis1 and Hsp104 [30,36,84,132,133]. Sis1 localization to the nucleolar periphery and cytosolic foci formation was abolished following heat shock upon pre-treatment with the translation elongation inhibitor cycloheximide (CHX) (Figure 4.1A,B; Figure 4.7B). Thus, ongoing translation drives Sis1 spatial dynamics during heat shock – in the cytosol and within the nucleus.

4.3.2 Ribosomal proteins are a major class of Sis1 interactors during heat shock

To identify proteins that Sis1 interacts with during heat shock, we utilized proximity-dependent labeling and affinity capture coupled to mass spectrometry (MS). To achieve this, we endogenously fused Sis1 to the engineered peroxidase APEX2 [53]. We heat shocked cells expressing Sis1-APEX2 and performed the proximity labeling (see methods). Biological replicates showed strong concordance in the abundance of the 698 proximity labeled proteins reproduced across replicates and quantifiable above background (Figure 4.1C). The data revealed that during heat shock, Sis1 is proximal to other chaperones, metabolic enzymes, translation factors, ribosome biogenesis factors, and – most prominently – ribosomal proteins (RPs) (Figure 4.1C; Figure 4.7C).

To complement the proximity ligation approach, we performed immunoprecipitation (IP)-MS of Sis1-3xFlag following heat shock in the absence and presence of CHX. Of the 247 proteins we reproducibly pulled down during heat shock with Sis1, 210 were depleted in the CHX-treated cells relative to cells that were heat shocked in the absence of CHX (Figure 4.1D; Figure 4.7D). While interactions with other chaperones such as Hsp70 and Hsp104 were largely insensitive to CHX, the most abundant class of CHX-sensitive Sis1 interactors

was RPs. Comparison of the set of APEX2-labeled Sis1 interactors with the set of CHX-sensitive Sis1 interactors revealed an intersection of 178 proteins, 49 of which are RPs (Figure 4.1E,F). These proteomic results indicate that RPs are a major class of CHX-sensitive Sis1 interactors.

4.3.3 Sis1 interacts with orphan RPs at the nucleolar periphery upon heat shock

The CHX-sensitivity of the interaction between Sis1 and RPs could result either from interactions of Sis1 with actively cycling ribosomes (mature RPs) or from interactions of Sis1 with newly synthesized RPs. To distinguish these possibilities, we performed pulse-chase experiments to selectively label either mature or new RPs. We endogenously tagged RPs of the large (Rpl26a, Rpl25) and small ribosomal subunits (Rps4b, Rps9a) with the HaloTag to enable labeling with cell-permeable haloalkanes, either a non-fluorescent "blocker" (7-bromoheptanol) or fluorescent dye (JF646) (Figure 4.2A). To label mature RPs, we first pulsed with JF646 and subsequently chased with blocker to mask any new RPs. Conversely, we first added blocker to mask all the mature RPs and then added JF646 to label new RPs. We pulled down Sis1-3xFlag under these two labeling schemes in the presence or absence of heat shock. Despite the great excess of mature RPs in the input samples relative to the new RPs, Sis1 co-precipitated only with the new RPs and only during heat shock (Figure 4.2B,C; Figure 4.8A).

Next, we imaged RPs with respect to Sis1. We endogenously tagged three large subunit RPs (Rpl26a, Rpl25, and Rpl29) and three small subunit RPs (Rps4b, Rps9a, and Rps3) with the HaloTag in the Sis1-mVenus background. Using the pulse-chase labeling scheme described above, we imaged either mature or new RPs in live cells. Under nonstress conditions, all newly synthesized RPs were immediately localized to the cytosol, demonstrating the rapidity of ribosome biogenesis (Figure 4.8B). We heat shocked the cells for 10 minutes to cause both

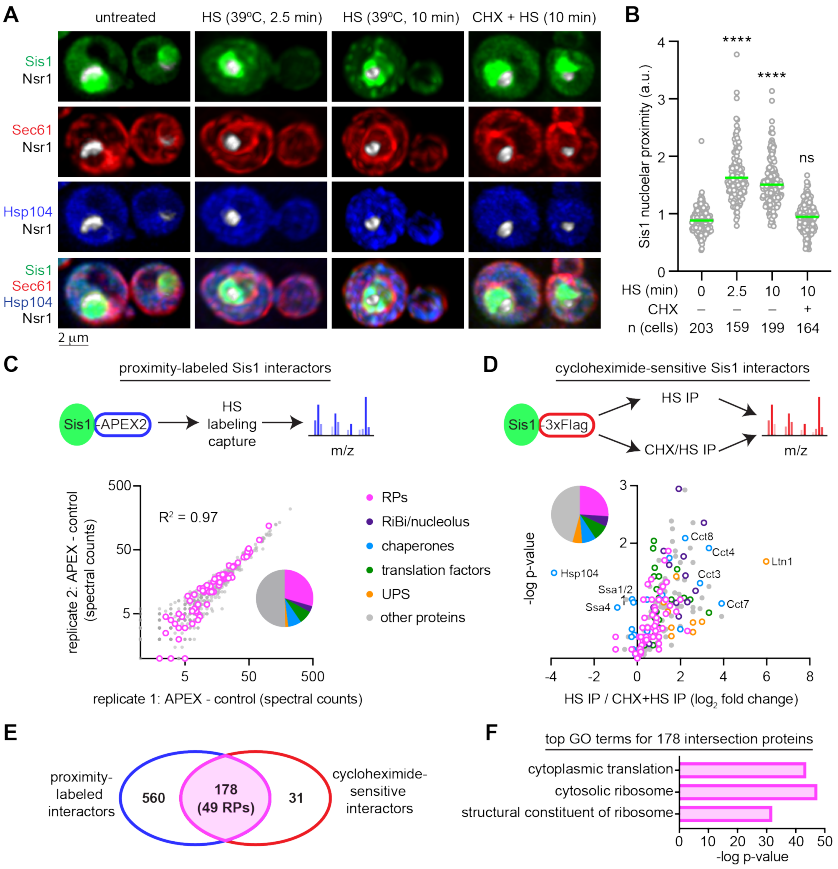

Figure 4.1: Sis1 localizes to the nucleolar periphery and interacts with ribosomal proteins during heat shock

A) Lattice light sheet live-imaging of yeast cells with endogenously tagged Sis1-mVenus (green), Hsp104-TFP (blue), Sec61-Halo (red) and Nsr1-mScarletI (white) under non-stress (30°C), heat shock (39°C, 2.5 and 10 min) and pre-treated with cycloheximide (CHX, 50μg/ml, 5min) followed by heat shock (39°C, 10 min). B) Single cell quantification of Sis1 nucleolar proximity defined as the ratio of mean Sis1 intensity in the half of the nucleus containing the nucleolus to the mean Sis1 intensity in the other half of the nucleus. Statistical significance was determined by Brown-Forsythe and Welch ANOVA test with multiple comparisons. ****P $<$ 0.0001, ns (non-significant). C) Top: Schematic of in vivo proximity labelling of Sis1-APEX2 followed by mass spectrometry analysis. Bottom: Enrichment of proteins labeled by Sis1-APEX2 following HS in two biological replicates. Ribosomal proteins highlighted in magenta. D) Top: Workflow to IP Sis1-3xFLAG following heat shock (39°C, 10 min) pretreated with either vehicle or cycloheximide (50μg/ml, 5 min). Bottom: Volcano plot demonstrating magnitude and statistical significance of cycloheximide sensitivity of Sis1 interactors. E) Venn diagram of proteins identified in (C) and (D). F) Gene ontology terms enriched among the 178 intersection proteins from (E).

Sis1 cytosolic foci formation and peri-nucleolar Sis1 accumulation. Mature RPs formed neither cytosolic foci nor peri-nucleolar structures, and the Sis1 cytosolic foci localized away from mature ribosomes (Figure 4.2D-G; Figure 4.8C-F). By contrast, new Rpl26a, Rpl25, Rps4b and Rps9b – which are all incorporated into ribosomal subunits in the nucleolus [140] – accumulated at the nucleolar periphery as mis-localized oRPs that colocalized with Sis1(Figure 4.2D-G; Figure 4.8C,D). However, new Rpl29 and Rps3 – which are incorporated into their respective ribosomal subunits at a late stage of biogenesis that occurs in the cytosol [140] – neither localized to the nucleolar periphery nor co-localized with Sis1 (Figure 4.8E,F). These observations suggest that oRPs accumulate at the nucleolar periphery with Sis1 during heat shock provided that the RP is incorporated into ribosome assembly in the nucleolus.

4.3.4 DnaJB6 co-localizes with newly synthesized RPL26 in human cells during heat shock

The human JDP DnaJB6 is likely to be the functional homolog of Sis1 in human cells [66]. To determine whether DnaJB6 co-localizes with RPs during heat shock, we obtained HCT116 human cells with a Halo-tagged copy of RPL26 integrated into the genome [7]. We followed a similar pulse-labeling protocol in the HCT116 cells as we used in yeast (Figure 4.2A), fixed the cells following heat shock, and stained with antibodies against DnaJB6 and NPM1 to mark the periphery of the nucleolus. As in yeast, mature RPL26 was primarily localized to the cytosol, though some was detectable colocalizing with NPM1 (Figure 4.2H). Mature RPL26 showed partial colocalization with DnaJB6 during heat shock (Figure 4.2H,I). However, as in yeast, newly synthesized RPL26 was highly concentrated at the periphery of the nucleolus and colocalized with DnaJB6 (Figure 4.2H,I). Thus, in yeast and human cells, heat shock triggers the peri-nucleolar accumulation of oRPs that colocalize with homologous JDPs.

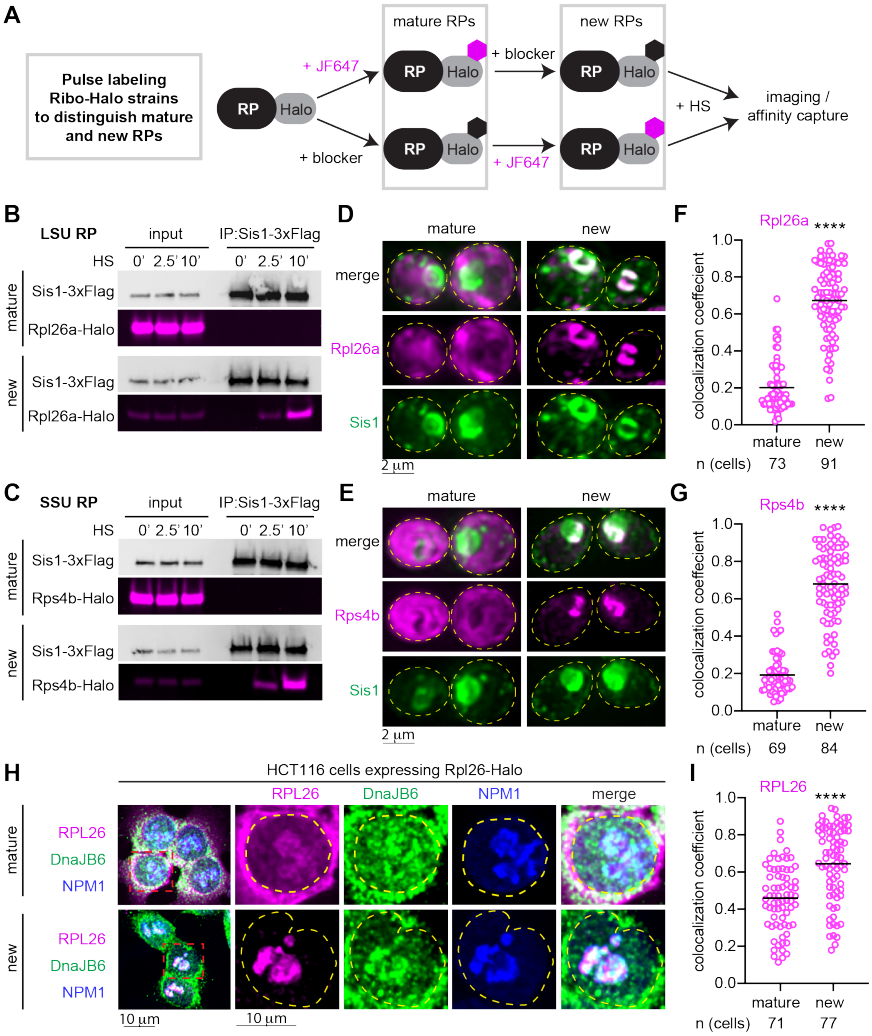

Figure 4.2: Orphan ribosomal proteins interact with Sis1/DnaJB6 at the nucleolar periphery

A) Workflow for in vivo pulse-labeling of mature and new ribosomal proteins. B) IP of Sis1-3xFLAG and either mature or new Rpl26a-Halo from cells left unstressed or heat shocked at 39°C for the indicated times. C) As in (B), but for Rps4b-Halo. D) Lattice light sheet live imaging of yeast under heat shock (39°C, 10 min) expressing Sis1-mVenus and labeled for either new or mature Rpl26a-Halo. The dashed line indicates the cellular boundary. E) As in (D), but for Rps4b-Halo. F) Colocalization (Mander's overlap coefficient) of Sis1-mVenus with either mature or new Rpl26a-Halo in heat shocked cells (39°C, 10 min). G) As in (F), but for Rps4b-Halo. P values were calculated with a two-tailed Welch's t-test. ****$P < 0.0001$. H) Human HCT116 cells stably expressing RPL26-Halo labeled for mature or new RPL26 and heat shocked (43°C for 30 min). Cells were fixed and immunostained for DnaJB6 and NPM1. Dashed line indicates the nuclear boundary. I) Colocalization (Mander's overlap coefficient) of DnaJB6 with either mature or new RPL26-Halo in heat shocked cells (43°C, 30 min). P values were calculated with a two-tailed Welch's t-test. ****$P < 0.0001$.

4.3.5 RP production is required for peri-nucleolar recruitment of Sis1/DnaJB6

To determine whether oRPs drive Sis1 peri-nucleolar localization during heat shock, we utilized auxin inducible degradation to acutely deplete Ifh1, a transcription factor required for the expression of RPs in yeast [115]. Depletion of Ifh1 impaired cell growth, and mRNA deep sequencing under nonstress conditions revealed that acute loss of Ifh1 resulted in reduced expression of RP mRNAs with few other changes to the transcriptome (Figure 4.3A,B). Upon heat shock, cells depleted for Ifh1 showed reduced transcriptional induction of Hsf1-regulated genes without alterations in other stress response genes (Figure 4.3C; Figure 4.9A,B). On average, Hsf1 targets were reduced 25% in Ifh1-depleted cells, suggesting that newly synthesized RPs contribute to activation of the heat shock response. While the effect of Ifh1-depletion on the heat shock response was relatively modest, loss of Ifh1 nearly abolished Sis1 localization to the nucleolar periphery during heat shock in most cells (Figure 4.3D,E). However, Ifh1 depletion did not prevent formation of Sis1 cytosolic foci during heat shock, demonstrating a specific effect on peri-nucleolar Sis1 (Figure 4.9C,D). In HCT116 cells, we used the mTOR inhibitor torin-1 to reduce expression of RPs [131], and this treatment prevented heat shock induced localization of DnaJB6 to the nucleolar periphery in most cells (Figure 4.3F,G). These data suggest that oRPs recruit Sis1/DnaJB6 to the nucleolar periphery during heat shock.

4.3.6 oRPs form dynamic condensates with Sis1 during heat shock

We next performed time-lapse 3D lattice light sheet imaging of new Rpl26a to observe spatiotemporal dynamics of oRPs during heat shock with respect to the nucleolus and Sis1. Over a sustained heat shock, new Rpl26a and Sis1 remained localized at the nucleolar periphery in dynamic clusters that rapidly reorganized via fission and fusion (Video S2; Figure 4A). The fluorescence signal remained nearly constant over time, suggesting that these clusters

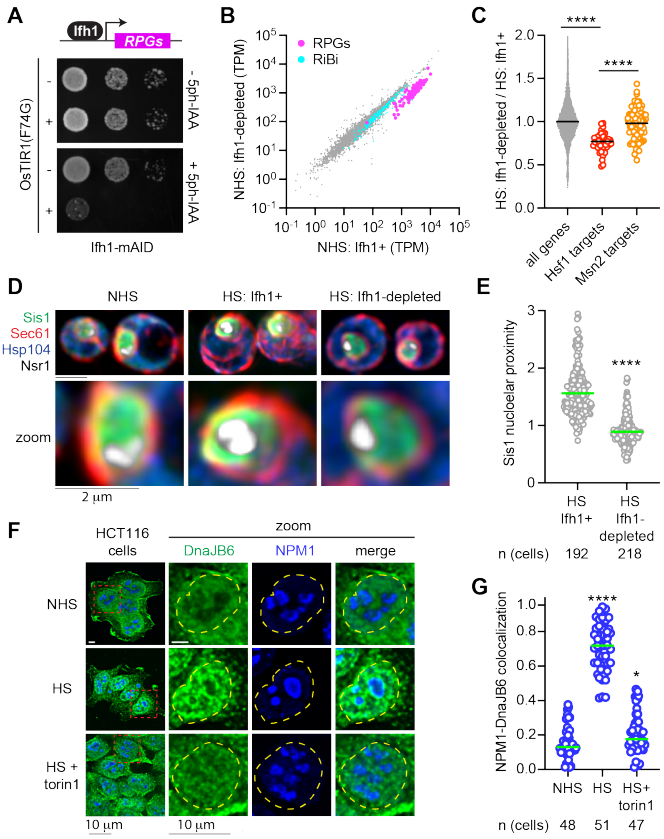

Figure 4.3: Ribosomal proteins drive Sis1/DnaJB6 localization to the nucleolar periphery A) Dilution series spot assay of yeast cells expressing Ifh1-mAID with or without estradiol inducible OsTIR1(F74G) spotted on to rich medium supplemented with either estradiol (1μM) alone or with 5ph-IAA (5μM) grown for 48 hr. B) Scatter plot of RNA seq data from Ifh1-mAID/OsTIR1(F74G) treated with estradiol alone or along with 5phIAA for 30 min. Ribosome biogenesis factors (RiBi, cyan) and ribosomal protein genes (RPGs, magenta) are highlighted. C) Ifh1-dependent fold change in expression in heat shocked cells showing a reduction in Hsf1 target gene induction but not Msn2 target induction. D) LLS imaging of the distribution of Sis1-mVenus in non-stressed cells, heat shocked cells, and heat shocked cells depleted for Ifh1. E) Quantification of Sis1 nucleolar proximity during heat shock in cells with Ifh1 and following Ifh1 depletion. Statistical significance was determined by Brown-Forsythe and Welch ANOVA test with multiple comparisons. ****P $<$ 0.0001, ns (non-significant). F) Immunostaining of HCT116 cell lines for DnaJB6 (green) and NPM1 (Blue) under nonstressed, heat shocked (43°C, 30min) and heat shock of cells pretreated with Torin1 (300nM, 30 min). G) Quantification of colocalization (Mander's overlap coefficient) of NPM1 and DnaJB6 in single cells in the conditions in (F). Statistical significance was determined by Brown-Forsythe and Welch ANOVA test with multiple comparisons. ****P $<$ 0.0001, *P 0.0248

are stable and are not sites of degradation (Figure 4.10A,B). We will refer to these clusters as "oRP condensates". To probe the sensitivity of oRP condensates to alcohols known to disrupt certain other biomolecular condensates, we treated cells with 2,5-hexanediol (HD) and 1,6-HD. 2,5-HD had no effect on Sis1 or new Rpl26a localization (Figure 4.4B). However, while treatment with 1,6-HD did not disrupt Rpl26a clustering, it resulted in loss of Sis1 peri-nucleolar localization (Figure 4.4B). This differential sensitivity to 1,6-HD suggests that the interactions that target Sis1 to oRPs are biophysically distinct from the interactions among the oRPs themselves. Remarkably, Sis1 localization to oRPs was restored upon washout of 1,6-HD (Figure 4.4B).

4.3.7 Hsp70 activity maintains the liquid-like dynamics of oRP condensates in cell-free extract

To interrogate the biochemical and biophysical properties of oRP condensates, we developed an assay to observe them in crude cell lysate. We labeled mature and new Rpl26a and Rps4b in cells co-expressing Sis1-mVenus, heat shocked the cells, and resuspended cryo-milled lysate in buffer with the chemical composition of yeast cytoplasm (see methods). In the lysate, mature RPs showed diffuse signal, but new Rpl26a and Rps4b were concentrated in round condensates that colocalized with Sis1-mVenus (Figure 4.4C). Condensates were nearly absent in lysate from non-heat shocked cells (Figure 4.10C). Addition of RNAse to the lysate did not disrupt the condensates, and addition of RNA-specific dye revealed that the condensates exclude RNA, demonstrating that the RPs are orphaned from rRNA (Figure 4.10D,E). We observed both fusion and fission of oRP condensates in the lysate (Figure 4.4D). To determine whether maintenance of oRP condensates required ATP, we added apyrase to hydrolyze ATP in the lysate. ATP depletion resulted in loss of round condensates and the formation of larger amorphous aggregates (Figure 4.4E). Since Sis1 activates ATP hydrolysis by Hsp70, we wondered whether Hsp70 activity might contribute to the requirement for ATP.

Indeed, addition of the Hsp70 inhibitor VER-155008 phenocopied ATP depletion, resulting in the formation of large irregular clumps of Rpl26a (Figure 4.4E).

We collected high frame rate time-lapse videos of the oRP condensates in lysate in the presence and absence of the Hsp70 inhibitor to measure the dynamics of oRPs within the condensates. Across a hundred timepoints from thousands of pixels, we quantified the variance in Rpl26a fluorescence over time for each pixel as a metric for the movement of molecules within a condensate. High variance indicates that a condensate is dynamically rearranging and therefore more liquid-like, while low variance indicates that a condensate is less dynamic and more solid-like. Pixels in individual condensates showed large variance in untreated lysate and much lower variance in the Hsp70-inhibited lysate (Figure 4.4F,G). Collective analysis of all pixels revealed that Hsp70 inhibition significantly reduced the pixel variance (Figure 4.4H). Thus, Hsp70 inhibition in lysate makes oRP condensates less dynamic and more solid-like.

The liquid-like character of the oRP condensates in lysate prompted us to ask whether they might be reversible upon recovery from stress in cells. We pulse labeled new Rpl26a and Rps4b with JF646, heat shocked the cells for 5 minutes, and chased with excess blocker in media either at 39°C for a sustained heat shock or 30°C to monitor recovery (Figure 4.5A). Imaging revealed that while the oRP condensates persisted at 39°C, cells allowed to recover at 30°C showed Rpl26a and Rps4b signal disperse to the cytosol within 7.5 minutes (Figure 4.5B-D;Figure 4.11A,B). Greater than 85% of the Rpl26a and Rps4b signals that were localized at the nucleolar periphery during heat shock can be accounted for in the stably in cytosol after recovery, suggesting there is little degradation of oRPs upon recovery (Figure 4.11C). We observed the same re-localization of the signal of pulse-labeled RPL26 from the nucleolar periphery to the cytosol in human HCT116 cells following recovery (Figure 4.5E,F).

Given the cytosolic localization of pulse labeled RPs following recovery, we hypothesized that the RPs were being incorporated into mature ribosomes. To test this, we performed

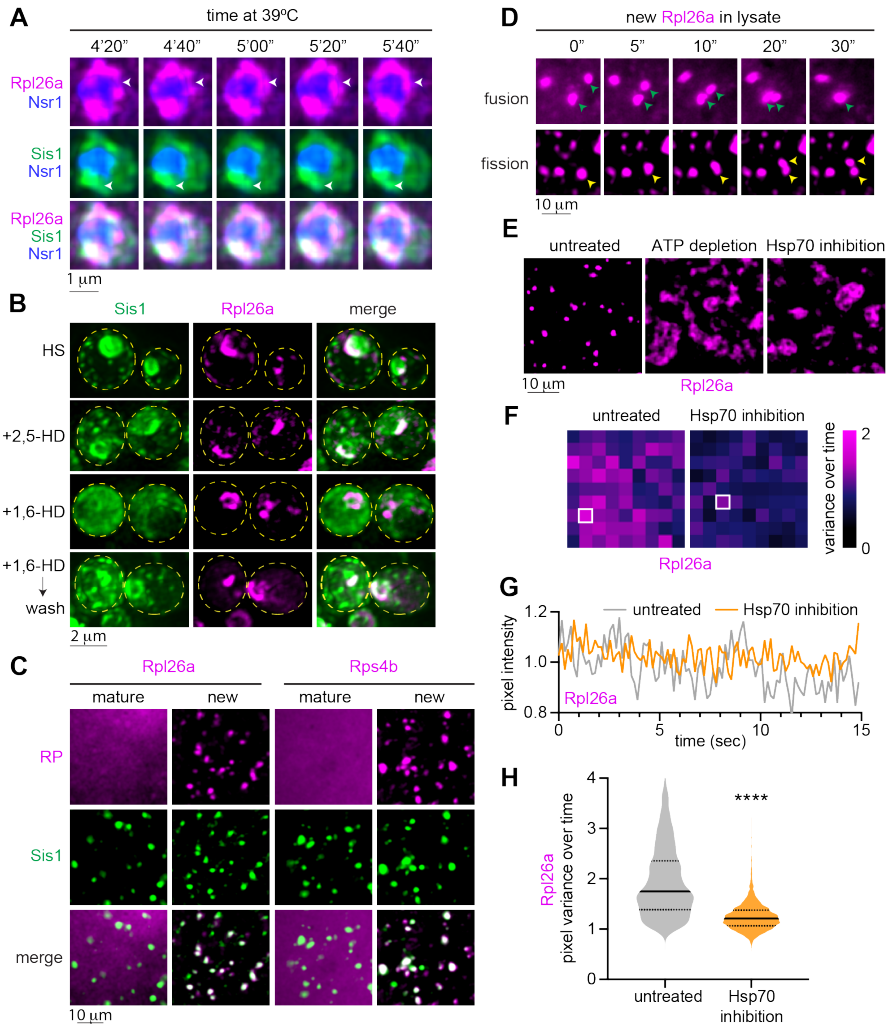

Figure 4.4: oRPs form dynamic condensates that are stable in cell-free extracts
A) 4D LLS imaging of Sis1-mVenus (green) and oRpl26 (magenta). B) Effect of 1,6-HD and 2,5-HD on Sis1 localization and oRP condensates. Cells were heat shocked for 10 min and incubated with either 5% 1,6 HD or 2,5 HD for 2 min. 1,6-HD was washed out for an additional 2 min at heat shock temperature and cells were imaged again. C) Imaging of mature and new Rpl26a-Halo and Rps4b-Halo along with Sis1-mVenus in cell-free lysate from heat shocked cells. D) Time lapse imaging of heat shocked cell-free lysate depicting fission and fusion of oRpl26a droplets. E) Depletion of ATP (apyrase, 0.05units/μl) or inhibition of Hsp70 (VER 155008, 50μM) activity in the lysate resulted in the formation of irregular clumps of oRpl26a. F) Heat map representing the variation in pixel intensity over time within the heat shock induced oRpl26a condensate and upon Hsp70 inhibition. G) Intensity over time of the most variable pixel in an oRpl26a condensate in lysate with and without Hsp70 inhibition. H) Distribution of pixel variance of oRpl26a in condensates over time in lysate with and without Hsp70 inhibition. P values were calculated with a two-tailed Welch's t-test. ****P $<$ 0.0001.

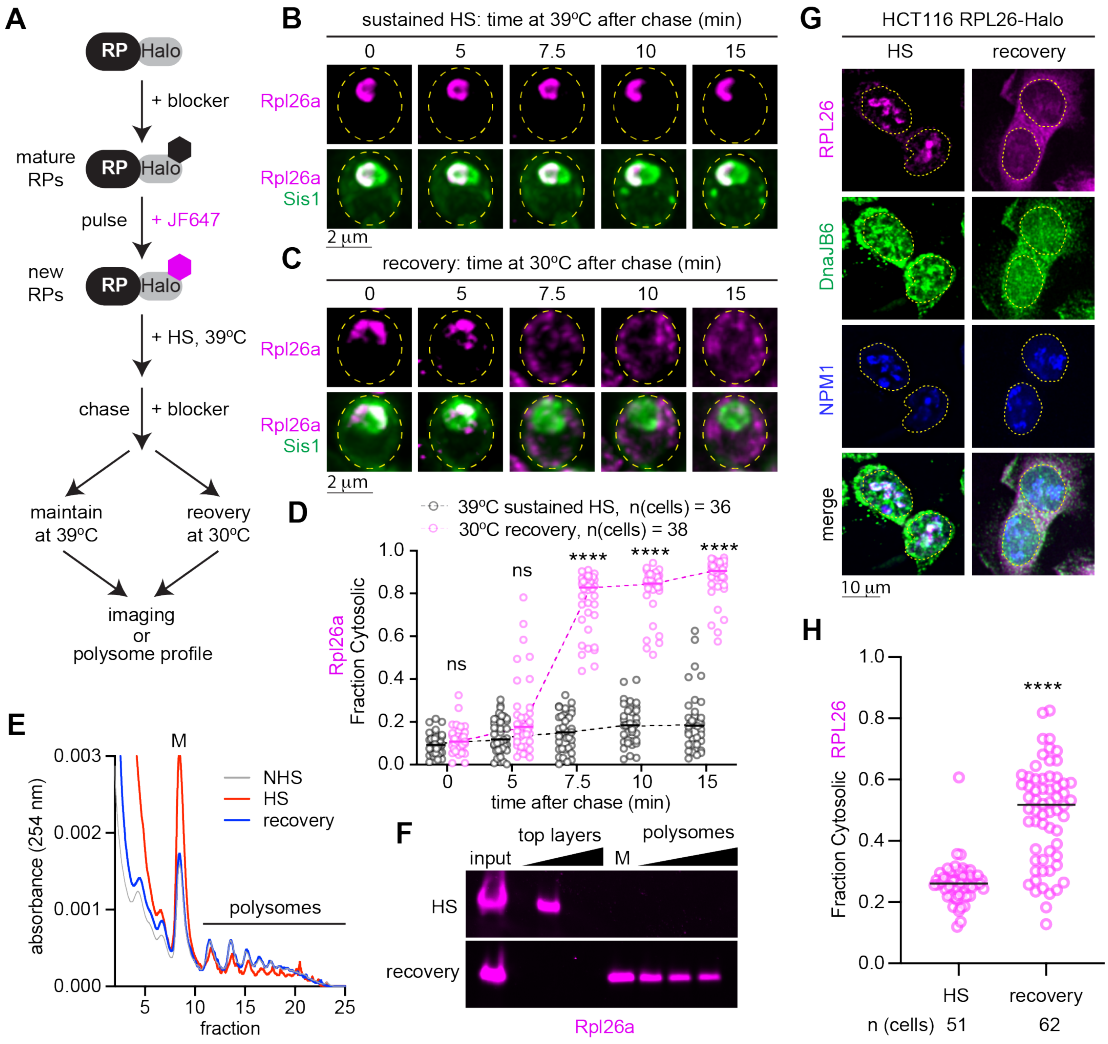

Figure 4.5: oRP condensates are reversible upon recovery from heat shock
A) Workflow to evaluate the fate of oRPs during sustained heat shock or recovery. B) Representative live-cell time lapse images of the spatial distribution of oRpl26a (magenta) and Sis1-mVenus (green) during sustained heat shock. C) As in (B) but following recovery from heat shock. D) Quantification of the fraction of cytosolic Rpl26a signal under sustained HS or recovery. Statistical significance was determined by Brown-Forsythe and Welch ANOVA test with multiple comparisons. ****P $<$ 0.0001, ns (non-significant). E) Polysome profiles of yeast expressing Rpl26a-Halo during nonstress, heat shock and recovery conditions. F) In-gel fluorescence of oRpl26a across the polysome profile in heat shock and recovery. G) Localization of oRPL26 (magenta) in HCT116 cells following heat shock and recovery. Cells were fixed and immunostained for DnaJB6 (green) and NPM1 (blue). H) Quantification of the fraction of cytosolic RPL26 in HCT116 cells under sustained HS or recovery.

polysome profiling of lysate from unstressed yeast cells, heat shocked cells, and cells that had been heat shocked and allowed to recover. Consistent with previous reports [21,46], we observed an increase in monosomes and a decrease in polysomes in heat shocked cells compared to unstressed cells that was completely reversed upon recovery (Figure 4.5G). In the heat shocked sample, we observed pulse labeled Rpl26a in the top layer fraction of cellular components not incorporated in or associated with ribosomes, consistent with it being an oRP (Figure 4.5H). By contrast, Rpl26a sedimented in the heavy polysome fractions in cells allowed to recover after heat shock (Figure 4.5H). Together, the cytosolic localization and co-sedimentation with polysomes suggest that RPs orphaned at the nucleolar periphery during heat shock are incorporated into functional ribosomes upon recovery.

Since Sis1 localizes to the oRP condensates, and Hsp70 activity was required to maintain the liquid-like character of the oRP condensates in lysate, we next asked whether the Sis1/Hsp70 chaperone system was also required for the dispersal of the condensates when cells recover from heat shock. Rather than mutating or inhibiting Hsp70 – which would have pleiotropic effects due to the diversity of processes in which Hsp70 participates – we utilized the "anchor away" approach we had previously established to conditionally deplete Sis1 from the nucleus [30]. We generated RP-Halo strains in the Sis1 anchor away background and either left the cells untreated (Sis1+) or depleted Sis1 from the nucleus (Sis1-depleted). Then we pulse labeled new Rpl26a and Rps4b, heat shocked the cells at 39^{o}C, returned the cells to the recovery temperature of 30^{o}C, and imaged the RPs with respect to the nucleolus over time. In the Sis1+ condition, Rpl26a and Rps4b rapidly dispersed from the nucleolar periphery into the cytosol (Figure 4.6A,B;Figure 4.12A,B). However, in the Sis1-depleted cells, the RPs remained adjacent to the nucleolus upon recovery (Figure 4.6A,B;Figure 4.12A,B). Consistent with a connection between the reversibility of the oRP condensate and their liquid-like internal dynamics, new Rpl26a formed amorphous solid-like aggregates in lysate from Sis1-depleted cells (Figure 4.6C,D). These data suggest that Sis1 recruitment to the

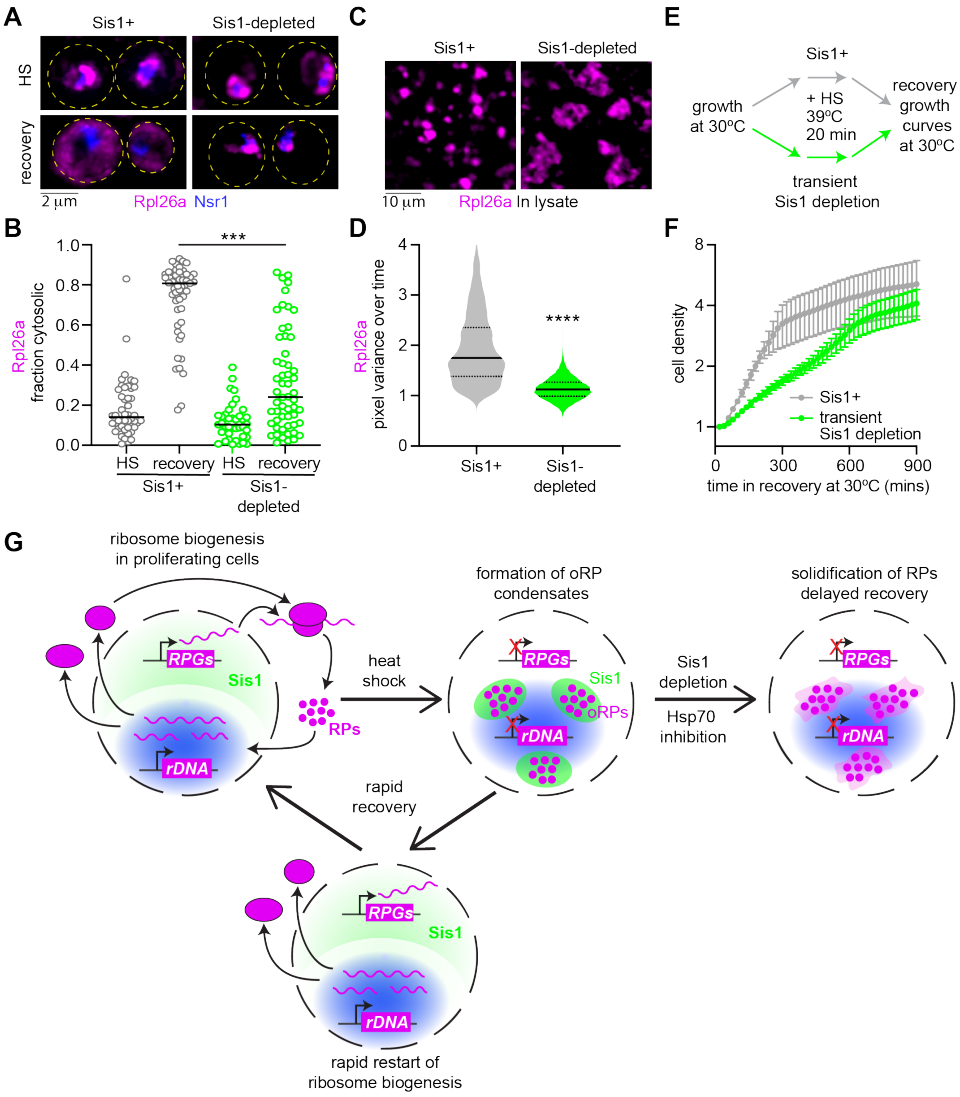

Figure 4.6: oRP condensate reversibility requires Sis1 and promotes fitness
A) LLS imaging of oRPl26a (magenta) and the nucleolar marker Nsr1 (blue) during heat shock and recovery in the absence or presence of Sis1 depletion. B) Quantification of the fraction of cytosolic Rpl26a under sustained HS or recovery in the absence or presence of Sis1 depletion. P values were calculated with a two-tailed Welch's t-test. ****P $<$ 0.0001. C) Depletion of Sis1 resulted in formation of irregular clumps of Rpl26a in lysate. D) Distribution of pixel variance of Rpl26a in condensates over time in control lysate and lysate with Sis1 depletion. Control lysate distribution replotted from Figure 4.4A. P values were calculated with a two-tailed Welch's t-test. ****P $<$ 0.0001. E) Workflow of growth assay following recovery. F) Growth curve of cells following recovery from heat shock in the absence or presence of transient Sis1 depletion. Mean and standard deviation of 3 biological replicates are plotted.

nucleolar periphery during heat shock is required to maintain the liquid-like properties of oRP condensates and enable them to be dispersed and utilized to restart ribosome biogenesis upon recovery from stress.

To determine whether preserving oRPs during stress might promote fitness, we performed growth measurements of cells during recovery from heat shock (Figure 4.6E). We either left Sis1 in the nucleus or transiently depleted it and heat shocked the cells. After 20 minutes of heat shock, we allowed Sis1 to return to the nucleus in the cells in which it had been depleted and measured growth over time under non-heat shock conditions. In the Sis1+ cells, we observed immediate resumption of growth at a constant doubling rate that persisted until the cells plateaued after 300 minutes (Figure 4.6F). The cells in which Sis1 was transiently depleted showed slower growth and did not plateau until after 600 minutes (Figure 4.6F). This result suggests that reversibility of oRP condensates contributes to resumption of rapid growth upon recovery from stress (Figure 4.6G).

4.4 Discussion

Upon exposure to a broad range of environmental stressors, cells rapidly inactivate ribosome biogenesis by repressing transcription of rRNA and RP mRNAs [38,39,114,121]. Limiting production of ribosomes limits proliferation [137], providing a general mechanism for cells to simultaneously slow growth during stress and free up resources to mount an adaptive response. However, instantaneous transcriptional repression may leave newly synthesized RPs orphaned from rRNA due to the compartmentalization of RP synthesis in the cytosol and rRNA production in the nucleolus. Here we show that heat shock triggers the accumulation of oRPs at the periphery of the nucleolus in yeast and human cells. Rather than being degraded or forming toxic aggregates, we find that oRPs form dynamic condensates that preserve RPs for future use upon recovery from stress. oRP condensates retain their liquid-like dynamics in lysate and their reversibility in cells by virtue of the Sis1 and Hsp70 chaperones.

We propose that a "chaperone-stirring" mechanism enables cells to rapidly restart ribosome biogenesis and efficiently resume proliferation when conditions improve.

Like stress-induced condensates formed by the translation factors Pab1 and Ded1 [55,107], oRP condensates appear to play an adaptive role in the yeast stress response. For Pab1 and Ded1, the ability to undergo temperature-dependent phase separation has been linked to fitness. For oRPs, it does not appear to be formation of the condensates per se but their reversibility that confers a fitness advantage. Our data suggest that active engagement of Sis1 and Hsp70 with the condensates maintains the RPs in a usable state. We envision that a sudden buildup of oRPs drives initial condensation, but such assemblies would quickly become amorphous aggregates without Sis1 and Hsp70. Sis1 and Hsp70 in collaboration with other chaperones have been shown to efficiently disperse Pab1 condensates [148], and Hsp70 has been implicated in repressing transcriptional condensates formed by the HSR regulator Hsf1 [23]. The additional role we identify here in maintenance of oRP condensates suggests that Sis1 and Hsp70 may broadly surveil and remodel biomolecular condensates during stress.

We have yet to perform detailed analysis of the conservation, composition, properties, and regulation of oRP condensates. We provide initial evidence that formation of reversible oRP condensates during heat shock is conserved in human cells, but we have not monitored the human oRP condensates live, nor have we assessed their biophysical properties in human cell lysate. The relationship between oRP condensates and the nucleolus – which has itself been shown to function as a proteostasis compartment in human cells [33] – should also be explored. In yeast, we do not know whether any other proteins in addition to Sis1 co-localize with oRP condensates. Moreover, we did not distinguish whether each RP species forms its own homotypic condensates or whether multiple distinct RPs intermix in heterotypic assemblies. If the condensates do contain multiple RPs, do they organize into sub-assemblies that are incorporated together in the ribosome biogenesis process? While

RNA is not a constituent of the oRP condensates, rRNA may drive condensate dispersal by specifically binding to the RPs. We have not yet assessed the range of heat shock temperatures that drive condensate formation, nor how pH or other physicochemical features of the environment affect the condensates. Beyond heat shock, it will be important to determine whether other perturbations trigger oRP condensate formation and whether repression of rRNA transcription is sufficient. Finally, it will be necessary to establish rules for when the ubiquitin-proteasome system degrades oRPs and when they form condensates.

Our data suggest a direct connection between the biophysical properties of oRP condensates and fitness. We established this connection by depleting Sis1 from the nucleus, which solidified oRP condensates in lysate, rendered them irreversible in cells, and slowed proliferation upon recovery from heat shock. A caveat to these experiments is that depleting Sis1 may have pleiotropic effects on the proteostasis network. However, if our interpretation is correct, then solidification of oRPs impairs growth. Loss of liquid-like properties has been associated with neurodegenerative disease-associated condensates [2,3], so it is possible that solidification of oRP condensates may play an analogous role in ribosomopathies. Alternatively, solid oRP aggregates may be nontoxic but simply unusable, slowing growth by wasting resources. In healthy cells, oRP condensates define proteostasis hubs that play an adaptive role in the stress response. The chaperone-stirring mechanism that sustains the liquid-like properties of the oRP condensates may function more broadly to transform potentially deleterious aggregates into benign condensates with adaptive potential.

4.5 Acknowledgements

We thank V. Bindokas and C. Labno at the University of Chicago Integrated Light Microscopy Core for imaging assistance. We are especially grateful to B. Glick and lab members for the yeast HaloTag construct and advice on using JF dyes in yeast. We thank S. Kron for use of gel imaging instruments, and K. Lin for assistance aligning the Squires Lab custom

wide-field setup and camera calibration. We also thank members of the Pincus, Squires, and Drummond labs for helpful discussions. J.A.M.B. acknowledges fellowship support from the Helen Hay Whitney Foundation. This work was supported by NIH grants R01 GM138689 to D.P., R35 GM144278 to D.A.D., support from the Neubauer Family Foundation to A.H.S., and NSF QLCI QuBBE grant OMA-2121044 to D.P. and A.H.S.

4.6 Author Contributions

Conceptualization: A. A. and D. P.; Methodology: S. C., A. S. K., D. S. G. and D. P; Formal Analysis: A. A., O. S., K. H., A. H. S., D. P.; Investigation: A. A., R. G., O. S., J. A. M. B., S. K., K. D., S. L-W.; Resources: A. A., J. A. M. B., D. A. D., A. S. H., D. P.; Writing – original draft: A. A. and D. P.; Writing – Review and Editing: all authors.; Visualization: A. A., O. S., K. H., D. P.; Supervision: D. A. D., A. H. S., D. P.; Funding Acquisition: D. A. D., A. H. S., D. P.

4.7 Methods

4.7.1 Yeast strain construction and cell growth

Yeast strains used in this study are catalogued in Table S1. All strains are derivatives of W303, and fluorescent protein and epitope tags are integrated into the genome mostly using scarless CRISPR/Cas9 gene editing method. Yeasts were cultured in rich glucose medium (YPD) or appropriate synthetic complete (SC) drop-out media at 30°C. For lattice light sheet imaging cells were cultured in SDC-riboflavin and folic acid to minimize autofluorescence.

4.7.2 Pulse labeling of newly synthesized or mature Halo-tagged ribosomal proteins (yeast)

To visualize newly synthesized ribosomal proteins, corresponding strains having ribosomal proteins fused with HaloTag7 (codon optimized for *S. cerevisiae*) were grown till O.D 0.3-0.6 and incubated with non-fluorescent Halo tag ligand 7-bromo-1-heptanol (7BRO, 100μM, VWR #AAH54762) for 10 min to irreversibly mask all the pre-existing ribosomal proteins. Subsequently excess ligands were extensively washed away (3X) with fresh media under shaking for 1 min. Cells were incubated with the Janelia Fluor 646 Halo tag ligand (JF646, 1μM, Promega#GA1120) in media at 30°C or 39°C and started live-imaging. Conversely, to label and visualize old ribosomal proteins yeast were incubated with 10μM JF646 Halo dye for 10 mins. Excess dyes were washed away, and further labeling with dye is prevented by addition of 100μM 7BRO.

4.7.3 Acute depletion of Ifh1

Genomic IFH1 was fused in frame with mini auxin inducible degron (miniAID) at its C termini using CRISPR/Cas9 gene editing. Estradiol inducible OsTIR1(F74G) was introduced at the leu2 locus. Acute and non-leaky depletion of Ifh1 is achieved by co-treatment with β-estradiol (1μM, Sigma #E8875) and 5ph-IAA (5μM, MedChemExpress #HY-134653) for 30 min.

4.7.4 Transient Sis1 depletion and quantitative growth assay

1 μM rapamycin (Sigma #R8781) was used to anchor away Sis1-FRB in a rapamycin-resistant background (TOR1-1 fpr1Δ) having Rpl25-FKBP. Three biological replicates of Sis1-FRB/Rpl25-FKBP strain were grown at 30°C overnight in 2xSDC media, then diluted to OD 0.05 in the morning. Cells were growth for 5 hours at 30°C until OD reached 0.2. Each

biological replicate was split into two tubes, corresponding to conditions DMSO pretreated followed by HS (39°C, 20 min) only or rapamycin pre-treated (1μM, 10 min) followed by HS (39°C, 20 min). All cell samples were then washed three times with 2xSDC media, resuspended in 2xSDC to final OD 0.1, and OD measurements taken every 20 minutes for the next 24 hours while shaking at 30°C.

4.7.5 Human cell culture

HCT116 and HCT116 RPL26-Halo were grown in Dulbecco's modified Eagle's medium (DMEM, high glucose and pyruvate) supplemented with 10% (vol/vol) fetal bovine serum, 1X GlutaMAX and 100 units of penicillin and streptomycin, and maintained in a 5% CO2 incubator at 37°C. All cell lines were found to be free of mycoplasma using the MycoAlert® PLUS Mycoplasma Detection Kit (Lonza #LT07-703).

4.7.6 Conditioned media heat shock treatment

Heat shock with conditioned media was performed essentially following Mahat et al. 2016 [80]. Briefly, two sets of cell plates were grown identically at 70-80% confluence. Conditioned media from the first cell plate was collected and prewarmed to 43°C in bead bath. The cells on this plate were discarded. Once the conditioned media were heated to 43°C, conditioned media from the second cell plate were discarded and replaced with heated conditioned media collected from the first cell plate and immediately placed in a 43°C incubator with 5 % CO2.

4.7.7 Pulse labeling of new or mature Halo-tagged ribosomal proteins (human cell lines)

HCT116-RPL26-Halo strain were seeded on 24-well plates 30 hr prior to experiment. To visualize newly synthesized RPL26 cells, pre-existing RPL26 were masked by incubation with

non-fluorescent irreversible Halo ligand (7-bromo-1-hepatanol, 100μM) for 15 min. Cells were washed with complete DMEM for 3 times under shaking for 2 min. Cells were then treated with JF646 Halo dye (1μM) mixed with prewarmed conditioned media and heat shocked as indicated. Conversely to label pre-existing RPL26, cells were incubated with JF646 Halo dye (10μM) for 15 min. After extensive washing further labelling is prevented by addition of 100μM 7BRO.

4.7.8 Immunofluorescence of HCT116 cells

HCT116 RPL26-Halo cells were seeded at 0.8 × 105 cells/ml on poly-Lysine-coated coverslips 30h prior to experiment. Cells were fixed with fixative solution (4% paraformaldehyde, 4% sucrose in 1XPBS) for 5 min. Fixed cells were washed with 1XPBS and fixation was quenched with 125mM glycine. Thereafter, cells were permeabilized with 0.1% Triton-X100 followed by blocking with 5% normal goat serum in 1X PBS. DnaJB6 was stained by incubating cells overnight with 1:100 dilution polyclonal rabbit DnaJB6 antibody (ThermoFisher #PA5-27577). Nucleolus was stained by incubating with 1:1000 dilution of mouse monoclonal NPM1 antibody (ThermoFisher #FC-61991). Cells were then washed with 1XPBS and fluorescently labeled with goat–anti-rabbit 488 and goat–anti-mouse 594 secondary antibodies (Invitrogen). Cells were then washed with 1XPBS, mounted on microscope slides using ProLong Gold Antifade Mountant with DAPI (Invitrogen #P36930) and imaged the following day. Images were taken using a 3i Marianas Spinning Disk Confocal with 100X oil objective and pseudo colored with Fiji.

4.7.9 Lattice light-sheet imaging and analysis

Lattice light-sheet imaging of live yeast were executed using a phase 2 system manufactured by Intelligent Imaging Innovations (3i) and run in SlideBook 6.0 software. The design is a commercially produced clone of the original [19] with greater automation and stability. The

imaging camera used was a Hamamatsu Fusion chilled sCMOS run at default speed/quality. The annulus mask was set for a 20-μm beam length (outer NA, 0.55; inner NA, 0.493) with 400-nm thickness, with dither set at 9 μm. Laser intensities were optimized to balance signal and bleaching rates. Temperature was controlled by a built-in Peltier device (empirically set to indicated temperatures). Optics were aligned daily before the experiment, and the bead PSFs (at the respective temperature and media) were collected before yeast were imaged. Objective scan images were collected in x (100-nm), y (100-nm) and z (100-nm) directions. Graphics processing unit–based Richardson-Lucy deconvolution (Yacu Decu) was used to denoise and enhance z stack images using measured PSFs or theoretical PSF via Brian Northan's "Ops" implementation (https://github.com/imagej/ops-experiments). 3D reconstructions and videos were assembled using MPI-CBG developed ClearVolume [111] plugin of Fiji.

4.7.10 APEX2 proximity labeling

Sis1-Apex2 strains were grown in 300 ml SDC media until O.D 0.3-0.6. Cells were heat shocked at 39°C for 15 mins by immediate mixing with the 300ml of pre-warmed media at 50°C. Post-treatments cells were fixed with 1% Paraformaldehyde for 5 min. The fixation was quenched with 125mM glycine and cells were vacuum filter collected and washed with potassium phosphate buffer saline (KpiS) buffer three times. Cells were resuspended in KpiS Buffer supplemented with 100T zymolyse to lyse cell wall. Cell membrane were permeabilized with 0.1% TritonX100 in KpiS Buffer. Spheroplast were incubated with biotin phenol (0.5mM) for 20 mins at 30°C. To activate APEX2 labelling reactions Hydrogen peroxide (1mM) was added to the medium for 1 min. For background correction one set without peroxide treatment was identically processed. The reactions were immediately quenched with a cocktail of Trolox (2.5mM), Sodium Ascorbate (10mM) and Sodium azide (10mM) in 1XPBS. Cells were harvested by centrifugation and pellet was flash frozen in liquid nitrogen.

Cell pellet were cryo-milled, and lysate were dissolved in 1XRIPA buffer. Proteins were precipitated with ice cold methanol at -80°C for overnight. Protein precipitants were dissolved in 2% SDS RIPA Buffer solution under 95°C for 20 mins. Biotinylated proteins were affinity captured with streptavidin magnetic beads. Washed with RIPA ×2, 1M KCl, 0.1M Na2CO3, 2M urea in HEPES buffer ×2 and RIPA ×2. Completely dried beads were then resuspended in 50 μl of hexafluoro isopropanol (HFIP), incubated for 5 min with shaking and eluted by spinning. Fifty microliters of HFIP were added to the beads again, and the eluates were combined and dried in a speedvac for 10 min. This sample was used for LC/MS analysis.

4.7.11 Sis1 co-IP from cells labeled for mature and new ribosomal proteins

Corresponding Rp-Halo strains with Sis1-3xFlag were grown to mid log phase in 300 ml SDC media. Cells were labeled for either mature or new form respective ribosomal proteins as described earlier. Cells were kept unstressed, or heat shocked (39°C) for indicated time by mixing with equal volume media at 50°C. Following treatment cells were harvested by vacuum filtration and flash frozen in liquid nitrogen. Cells were lysed by cryo-milling at 6x90sx30Hz pulses in a Retsch MM100 mixer mill under liquid nitrogen. Samples were dissolved in physiological buffer (20mM NaCl, 50mM KCl, 150mM K+Glutamate, 50mM HK2PO4, 0.5mM MgCl2, 25mM HEPES-KOH, 25mM MES pH 7.4). Sis1-3xFlag were immunoprecipitated using anti-Flag M2 Magnetic bead (Sigma #M8823) from the cell lysates. Bead bound complexes were released with competition for 3xFlag peptide (Sigma #F4799). IP eluates were run on SDS-PAGE gel and visualized using fluorescence gel imager. Gels were then blotted and probed with anti-Flag (Sis1). All Co-IP experiments were performed in biological triplicate.

4.7.12 Proteomics sample preparation

Samples were run on SDS-PAGE and gel bands were subjected for in-gel digestion. Gel bands were washed in 100mM Ammonium Bicarbonate (AmBic)/Acetonitrile (ACN) and reduced with 10mM dithiothreitol at 50°C for 45 minutes. Cysteines were alkylated with 100 mM iodoacetamide in the dark for 45 minutes in room temperature (RT). Gel bands were washed in 100mM AmBic/ACN prior to adding 1μg trypsin (Promega #V5111) for overnight incubation at 37°C. Supernatant containing peptides were collected into a new tube. Gel pieces were washed with gentle shaking in 50% ACN/1% FA at RT for ten minutes, and supernatant was collected in the previous tubes. Final peptide extraction step was done with 80% ACN/1% FA, and 100% ACN, and all supernatant was collected. The peptides were dried at speedvac and reconstituted with 5% ACN/0.1% FA in water before injecting into the LC-MS/MS.

4.7.13 LC-MS/MS analysis

Peptides were analyzed by LC-MS/MS using a Dionex UltiMate 3000 Rapid Separation nanoLC coupled to a Q-Exactive HF (QE) Quadrupole-Obitrap mass spectrometer (Thermo Fisher Scientific Inc, San Jose, CA). Samples were loaded onto the trap column, which was 150 μm x 3 cm in-house packed with 3 um ReproSil-Pur® beads. The analytical column was a 75 um x 10.5 cm PicoChip column packed with 3 um ReproSil-Pur® beads (New Objective, Inc. Woburn, MA). The flow rate was kept at 300nL/min. All fractions were eluted from the analytical column at a flow rate of 300 nL/min using an initial gradient elution of 5% B from 0 to 5 min, transitioned to 40% over 100 min, 60% for 4 mins, ramping up to 90% B for 3 min, holding 90% B for 3 min, followed by re-equilibration of 5% B at 10 min with a total run time of 120 min. Mass spectra (MS) and tandem mass spectra (MS/MS) were recorded in positive-ion and high-sensitivity mode with a resolution of 60,000 full-width half-maximum. The 15 most abundant precursor ions in each MS1 scan were selected for

fragmentation by collision-induced dissociation (CID) at 35% normalized collision energy in the ion trap. Previously selected ions were dynamically excluded from re-selection for 60 s. Proteins were identified from the MS raw files using the Mascot search engine (Matrix Science, London, UK. version 2.5.1). MS/MS spectra were searched against the SwissProt Saccharomyces cerevisiae database. All searches included carbamidomethyl cysteine as a fixed modification and oxidized Methionine, deamidated asparagine and aspartic Acid, and acetylated N-term as variable modifications. Three missed tryptic cleavages were allowed. A 1% false discovery rate cutoff was applied at the peptide level. Only proteins with a minimum of two peptides above the cutoff were considered for further study. Identified peptides/protein were visualized by Scaffold software (version 5.0, Proteome Software Inc., Portland, OR).

4.7.14 Polysome profiling

Polysome analyses by sucrose gradient fractionation were performed based on a protocol in Aboulhouda et al. 2017. Rpl26a-Halo strains were grown in SDC media (160 ml) to mid-log phase (OD 600 0.5). Pre-existing ribosomes were masked by incubation with 7BRO (100μM, 5 mins). Cells were washed with fresh media (5x volume) 3 times under shaking for 2 min. Newly synthesized Rpl26a were labeled by incubation with JF646 Halo ligand (2μM). Following which cells were heat shocked at 39°C (10 min) by mixing with equal volume media at 50°C. One half of the cells were harvested by vacuum filter and denoted as heat shock sample. Another half were allowed to recover at 30°C in the presence of blocker (100μM) for 30 min. Similarly, this sample was vacuum filter collected and marked as recovery sample.

The cell pellet was transferred to a 2 mL Eppendorf "Safe-Lok" tube and flash frozen in liquid nitrogen. Cells were lysed by a pre-chilled 7 mM stainless steel ball (Retsch #05.368.0035) with 4x90sx30Hz pulses in a Retsch MM100 mixer mill, chilling in liquid nitrogen (LN) between pulses. Sample was resuspended in 500 μL lysis buffer (20mM

HEPES-KOH (pH 7.4), 100mM KCl, 5mM MgCl2, 200μg/mL heparin (Sigma #H3149), 1% triton X-100, 0.5mM TCEP, 100μg/mL cycloheximide, 20 U/mL superase-IN (Invitrogen#AM2696), 1:200 millipore protease inhibitor IV#539136). The lysate was clarified by centrifugation at 3000 g for 30 s, and the supernatant was transferred to new tube and aliquots were flash frozen in LN.

A 10–50% continuous sucrose gradient in polysome gradient buffer (5mM HEPES-KOH (pH 7.4), 140mM KCl, 5mM MgCl2, 100μg/mL cycloheximide, 10 U/mL superase-in, 0.5 mM TCEP) was prepared in SW 28.1 tubes (Seton #7042) using a Biocomp Gradient Master and allowed to cool to 4 °C. 200 μl of clarified lysate was loaded on top of the gradient, and gradients were spun in a SW28.1 rotor at 27500 rpm for 3.5 hr at 4 °C. Gradients were fractionated into 15 fractions using a Biocomp Piston Gradient Fractionator with UV monitoring at 260 nm, and fractions were flash frozen in LN. UV traces were normalized to the total signal starting with the 40S peak. For in gel-fluorescence samples were treated with 0.02% sodium deoxy cholate and precipitated by adding 10% TCA for 1 hr on ice. Pellets were extensively washed with ice-cold acetone, and then resuspended in 2X Laemmli sample buffer.

4.7.15 Cell-free lysate droplet assay

Corresponding newly synthesized or matured ribosomal protein-stained yeast cultures were heat shocked, filter collected, cryo-lyzed and dissolved in 1:2 volume of physiological buffer (20mM NaCl, 50mM KCl, 150mM K+Glutamate, 50mM HK2PO4, 0.5mM MgCl2, 25mM HEPES-KOH, 25mM MES pH 7.4, 5mM PMSF and 1:200 millipore Protease Inhibitor Cocktail). Cellular debris and un-lysed cells were clarified by centrifugation at 6000 rpm for 5 min. Cleared lysates were immediately loaded onto a homemade chamber comprising a glass slide with a coverslip attached by two parallel strips of double-sided tape. Slides were then imaged with an epifluorescence microscope with 60X objective. Images presented are of

droplets settled on the glass coverslip.

4.7.16 Sis1 nucleolar proximity analysis

From the maximum intensity projections, nuclei were segmented by drawing oval masks around the peri-nuclear ring of Sec61-Halo using Fiji software. This was used as an input to custom-written Python code, which carried out the rest of the analysis. For each nucleus, the geometric center was computed from the mask, and a family of lines drawn at varying angles θ to bisect the nuclear area into two halves. For each θ, the fold-change in Nsr1 and Sis1 intensity between the two halves was computed, and the angle $\theta = \theta_n$ with a maximal fold-change in Nsr1 intensity was identified as splitting the nucleus into Nsr1-proximal and Nsr1-distal. The fold-change in Sis1 signal along the bisecting angle θ_n was recorded for each nucleus.

4.7.17 Colocalization analysis

To quantify colocalization between Sis1 and Rps signal Coloc2 plugin of Fiji was utilized. Minimum error thresholding (MET) method coupled with watershed algorithm were used to generate mask for individual cell. Automatic Otsu (maximum between-cluster variance) thresholding was used for pixel intensity-based mask creation and segmentation of high intensity peri nucleolar Sis1 signal and cytosolic foci from the low intensity diffused signal. Mander's overlap coefficient was calculated to determine the fraction of the mature or new form of RP signals overlap with Sis1 signals.

For human cells, colocalization analysis of DnaJB6 with RP signals with the Coloc2 plugin of FIJI was also utilized. Huang threshold method coupled with fill hole and watershed algorithm was utilized upon DAPI signal to create a mask and segment nuclei. Created masks were binary dilated to segment the cytosol. The ROI generated was used to calculate the Mander's overlap coefficient between RPL26 (mature or new) and DnaJB6 signal.

4.7.18 Yeast cytosol image segmentation

Deconvolved z stack images were maximum intensity projected. Estimated mask for whole cell were obtained using the Minimum error thresholding (MET) methods coupled with watershed algorithm upon Sis1 signal. Nsr1 signal were used for segmentation of yeast nucleoli. Nucleolar mask was binary dilated to enlarge and cover the nucleolar proximity region. Cytosolic signals were extracted by subtracting the nucleoalar+perinucleolar signal (approx. nuclei) with whole cell signal. Fraction cytosolic is determined by dividing the integrated density of whole cell over cytosol signal.

4.7.19 Human cell cytosol image segmentation

Z series images were background subtracted and projected over 2D for maximum intensity. DAPI signal was used to mask and segment the nuclei using Li threshold coupled with watershed and fill hole algorithm (Fiji). DAPI mask were binary dilated and segment for whole cell were created. Fraction cytosolic RPL26 signal was calculated by dividing the whole cell integrated density with cytosol intergraded density.

4.7.20 Condensate pixel variance analysis

To determine the relative dynamicity of the condensates using videos taken with a wide-field microscope, the time-dependent variance in condensate brightness was quantified. In comparison to the solid-state condensates, the liquid-like condensates were found to exhibit higher variance in pixel brightness over time, which is consistent with higher mobility of heterogeneously labeled contents, such as aggregates of fluorescent protein, moving around within a liquid-like environment. The time-dependent depletion of ATP or tethering of heat shock proteins was found to produce a solid-like state, indicating that ATPases such as Hsp70 might be responsible for maintaining a liquid-like state. Analysis was undertaking for videos of condensates under identical illumination using a bespoke Python script:

Pixel count values were converted to photon counts according to a previously calibrated gain matrix unique to the sCMOS camera used (Photometrics Prime95B). Converted videos were cropped to include only areas within the condensate. For each pixel at location (i, j) in the condensate, normalized pixel variance over time ${\bar{\sigma}_{ij}}^2$ was calculated from the photon counts observed in each of N frames, $x_{ij}(t)$, and the expected variance of the signal according to a Poisson distribution of photon counts, $\left\langle {\bar{\sigma}_{ij}}^2 \right\rangle = \left\langle x_{ij} \right\rangle^2$, Equation 1.

$$ {\bar{\sigma}_{ij}}^2 = \frac{\sum_{t=0}^{N} \left(x_{ij}(t) - \left(x_{ij} \right) \right)^2}{N \left(x_{ij} \right)^2} \quad \text{Eqn. 1} $$

The resulting two-dimensional array of normalized variances for each condensate, $\overline{\boldsymbol{\sigma}}^2$, was generated and displayed as a heatmap. Normalized variance values from multiple condensate videos of each condensate type were aggregated to enable robust comparison among treatment conditions, displayed as a violin plot. The expected normalized variance for solid objects is 1 , since any variability in the signal would be due to shot noise generated from photon counting by the detector. Similarly, fluctuations above the expected shot noise variance would have values greater than 1 , indicating that the object is exhibiting fluctuations in addition to those predicted from shot noise.

4.8 Supplementary Information

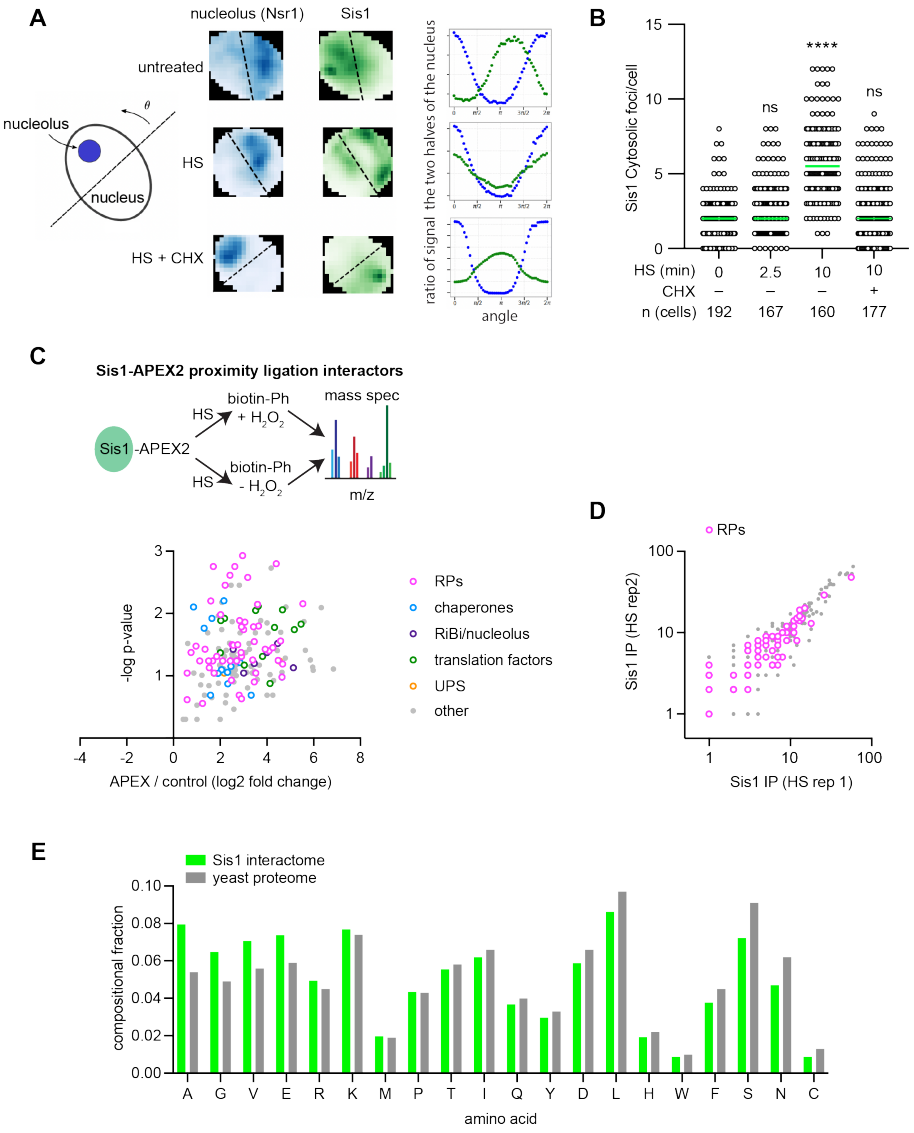

Figure 4.7: Sis1 localization and interactions during heat shock
A)Left: Schematic of how to bisect the nucleus with the nucleolus on one side by finding the line angle with the maximum difference in signal of the nucleolar marker in the two halves. Middle: Representative 2D projections of cells showing Nsr1 (blue) to mark the nucleolus and Sis1 (green). Line is set to maximize the difference in nucleolar signal and the ratio of Sis1 in the two halves is calculated. Right: Sis1 ratio as a function of the line angle rotated as depicted in the schematic to the left. B) Quantification of Sis1 cytosolic foci per cell in the conditions listed. Foci were identified using the FindFoci plugin in ImageJ. Statistical significance was determined by Brown-Forsythe and Welch ANOVA test with multiple comparisons. ****P < 0.0001. C) Volcano plot of Sis1-APEX2 interactors during heat shock. D) Biological replicates of Sis1-3xFLAG IP interactors.

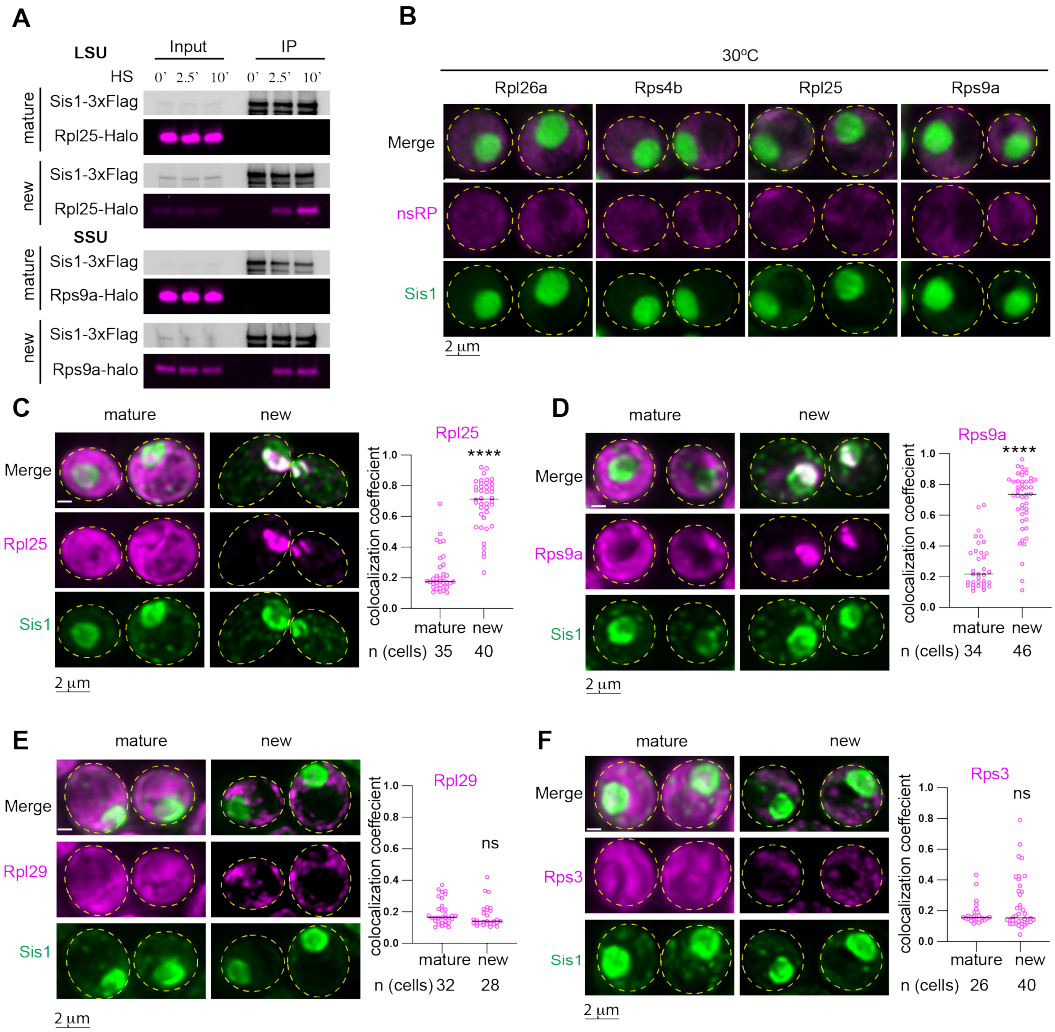

Figure 4.8: Interaction and localization of pulse-labeled ribosomal proteins with Sis1
A) IP of Sis1-3xFlag and either mature or new Rpl25-Halo and Rps9a-Halo from cells left unstressed or heat shocked at 39°C for the indicated times. B) In the absence of heat shock, pulse-labeled RPs localize immediately to the cytosol. C) Left Panel: Lattice light sheet live imaging of yeast under heat shock (39°C, 10 min) expressing Sis1-mVenus and labeled for either new or mature Rpl25-Halo. Right Panel: Dot plot representing the colocalization coefficient (Mander's overlap coefficient) of Sis1-mVenus with either mature or new Rpl25-Halo in heat shocked cells (39°C, 10 min). D) As in (C) but for Rps9a-Halo. E) As in (C) but for the late joining subunit Rpl29-Halo. F) As in (C) but for the late joining subunit Rps3-Halo. P values were calculated with a two-tailed Welch's t-test. ****P $<$ 0.0001. ns, (non-significant).

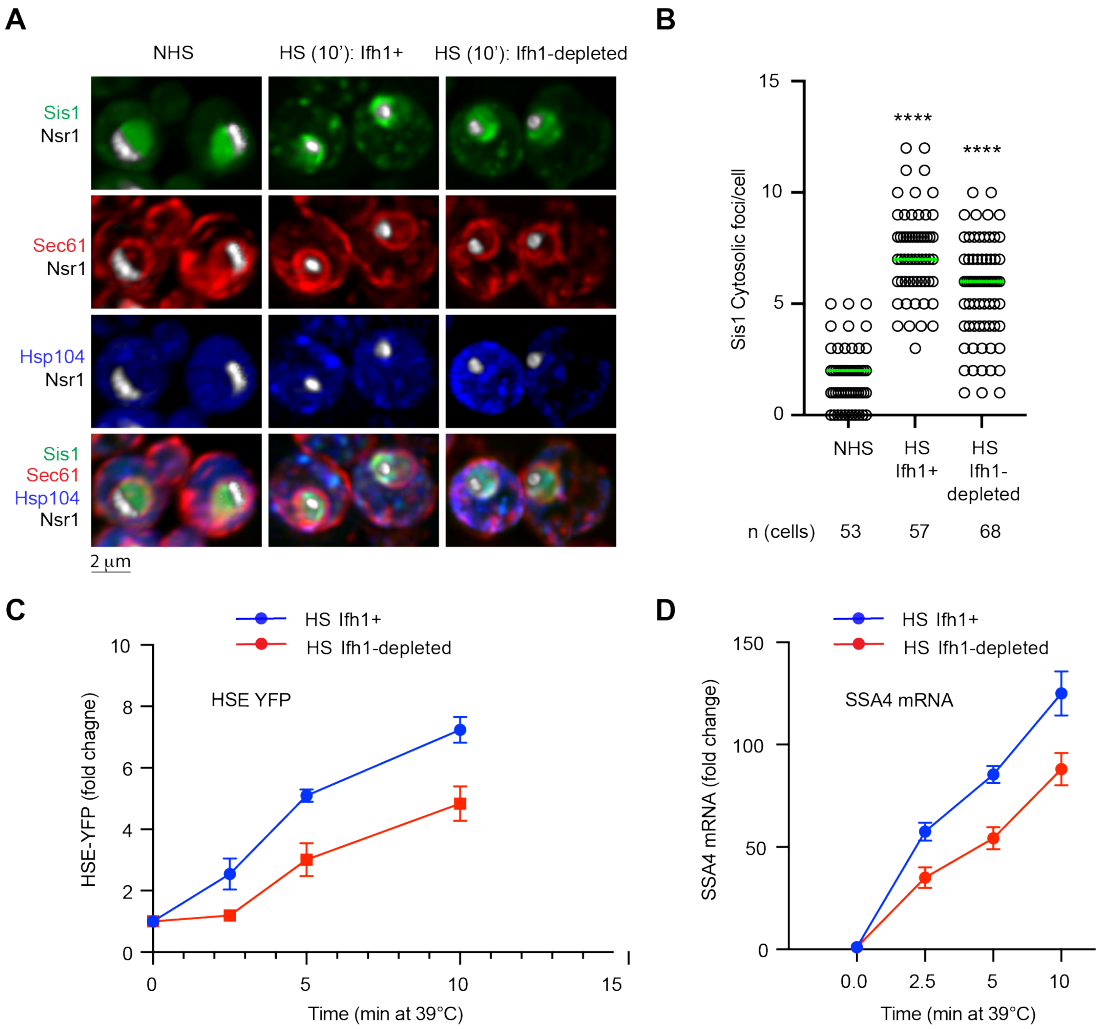

Figure 4.9: Cell biological and transcriptional effects of Ifh1 depletion
A) LLS live-imaging of yeast cells with endogenously tagged Sis1-mVenus (green), Hsp104-TFP (blue), Sec61-Halo (red) and Nsr1-mScarletI (white) under non-stress (30°C) and heat shock (39°C, 10 min) in the absence and presence of Ifh1 depletion. B) Quantification of Sis1 cytosolic foci per cell in the conditions shown in (A). Statistical significance was determined by Brown-Forsythe and Welch ANOVA test with multiple comparisons. ****$P < 0.0001$. C) HSE-YFP reporter heat shock time course showing reduced HSR induction when Ifh1 is depleted. D) RT-qPCR of the HSR target gene transcript SSA4 over a heat shock time course in the absence and presence of Ifh1 depletion.

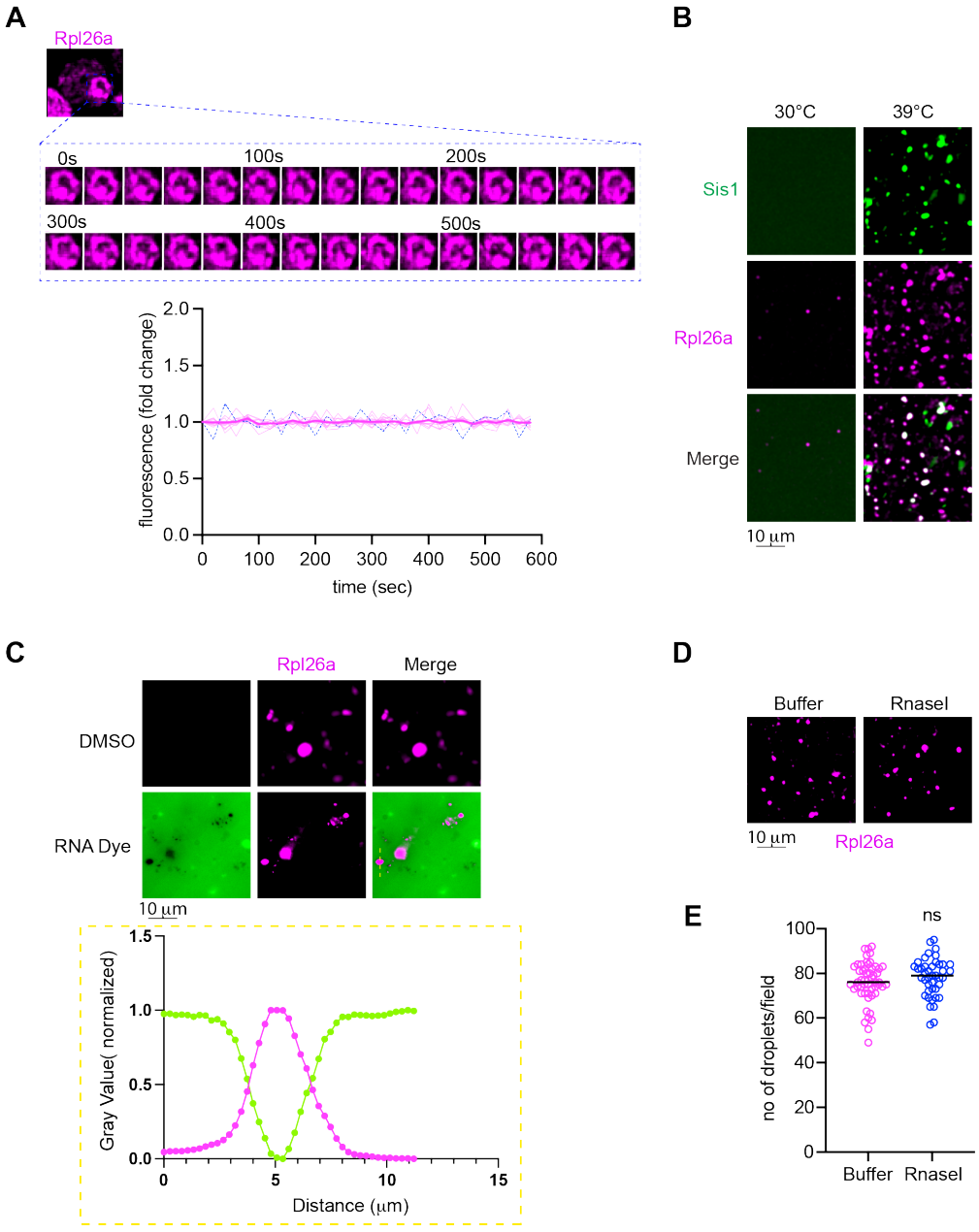

Figure 4.10: oRPs condensates are stable, heat shock-dependent, and RNA-free
A) oRP proteins are stable (not degraded) in condensates in cells. B) oRP condensates are more abundant in lysate from heat-shocked cells. C) RNA dye (SYTO RNASelect, 0.5mM, 10 min) is excluded from the oRP condensate. D) oRP condensates are resistant to RNaseIf (5 units/μl, 15 min, RT). E) Quantification of number of droplets per field in buffer or RNaseIf treatment to the lysate. P values were calculated with a two-tailed Welch's t-test. ns, (non-significant).

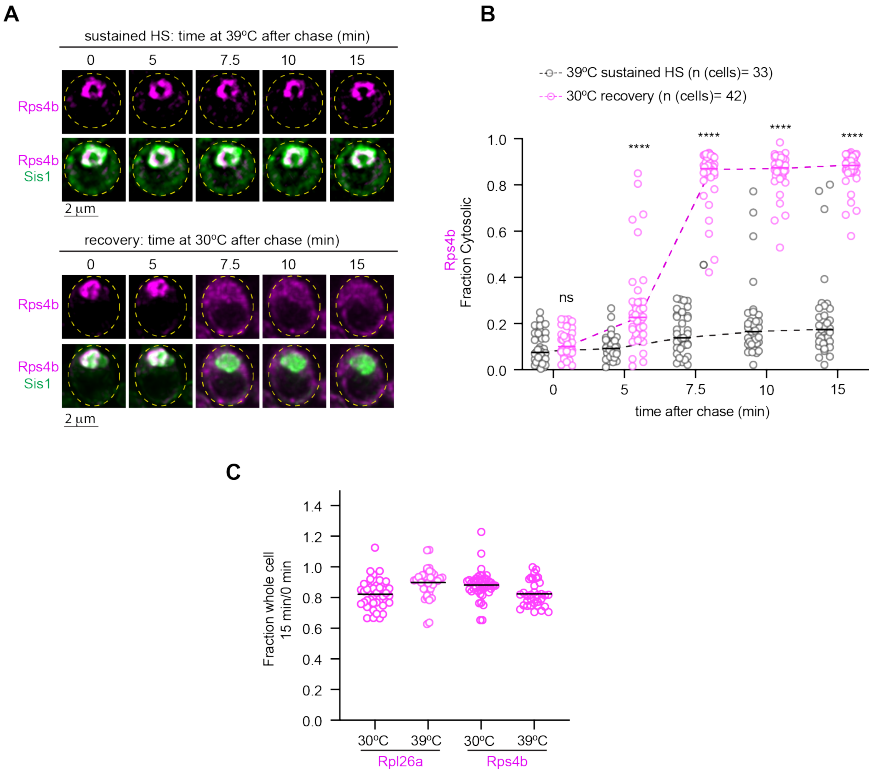

Figure 4.11: Peri-nucleolar oRps4b condensates get exported to cytosol upon recovery from heat shock
A) Live cell time lapse imaging of the spatial distribution of oRps4b (magenta) and Sis1-mVenus (green) during sustained heat shock and recovery B) Quantification of the fraction of cytosolic oRps4b signal under sustained HS or recovery. Statistical significance was determined by Brown-Forsythe and Welch ANOVA test with multiple comparisons. ****P < 0.0001, ns (non-significant).

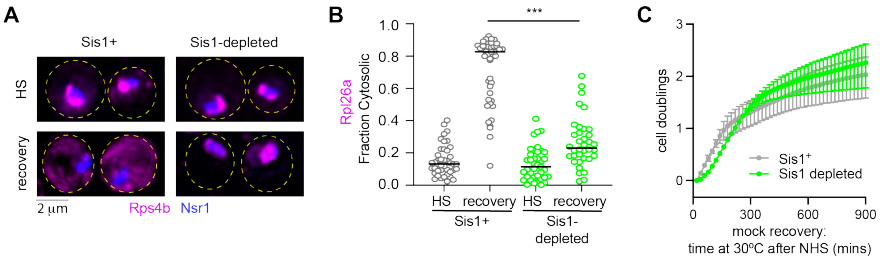

Figure 4.12: oRP condensate reversibility depends upon Sis1 availability
A) LLS live cell imaging of oRps4b (magenta) and the nucleolar marker Nsr1 (blue) during heat shock and recovery in the absence or presence of Sis1 depletion. B) Quantification of the fraction of cytosolic Rpl26a under sustained HS or recovery in the absence or presence of Sis1 depletion. P values were calculated with a two-tailed Welch's t-test. ****P < 0.0001.

CHAPTER 5

CONCLUSIONS AND FUTURE DIRECTIONS

I hope this thesis project is a tribute to investigations that build directly upon previous work, and the importance of investigating, and publishing, 'negative' results (Chapter 2). My work capitalized on the excellent investigations and genome-wide data sets generated from the lab, especially by David Pincus, Zoe Feder, Joanna Krakowiak, Surabhi Chowdhary, and Asif Ali.

5.1 How is Hsf1 Tuned in Healthy Cells?

In my initial research proposal, I asked how Hsf1 is regulated in the healthy *S. cerevisiae* cell. Hsf1 is misregulated in both directions in human disease, indicating its tight tuning must be highly adaptive. By default, Hsp70 binds and represses Hsf1 in the nucleus. But when protein homeostasis is disrupted, proteins aggregate in the cytosol, which recruits Hsp70, releasing Hsf1 to induce its targets in the cytoplasm. After just a few minutes of activity, protein homeostasis is restored and Hsf1 is repressed again, in spite of ongoing environmental stress. Though Hsp70 induction is necessary for Hsf1 deactivation, the ubiquity and promiscuity of Hsp70 in the eukaryotic cell (1000:1 Hsp70:Hsf1) implied that Hsp70 induction could not be sufficient. At the outset, we foresaw a few possible scenarios:

(1) Hsp70 availability is controlled by another Hsf1 target gene whose induction controls how much Hsp70 is actually available for protein aggregate clearance and Hsf1 binding.

(2) Most of the 42 Hsf1 target genes each provide small additive contributions to Hsf1 negative feedback regulation, cumulatively deactivating Hsf1 via the Hsp70 negative feedback loop (likely controlling Hsp70 by performing diverse roles in protein homeostasis).

(3) Many Hsf1 target genes provide feedback regulation to Hsf1 via Hsp70-independent feedback loops.

(4) None of the other Hsf1 targets provide feedback regulation to Hsf1. In this case,

factors that control Hsp70 availability must lie outside of the Hsf1 transcriptional regulon.

Our screen for negative feedback regulators of Hsf1 revealed that six Hsf1 target genes provide feedback regulation on Hsf1, but none as dramatically as Hsp70 (Chapter 3). Fes1 induction affects Hsp70's ability to return to the nucleus, so Fes1 controls Hsf1 activity via Hsp70 availability, as proposed in option 1. However, the Hsf1 activity defect in Fes1ΔHSE is not large; Fes1 induction must only be partially responsible for controlling Hsp70 availability. I imagine that option 4 is also at play: factors outside of the Hsf1 transcriptional regulation deactivate Hsf1 by controlling Hsp70 availability.

Clarifying the vague notion of "cytosolic protein aggregates" and "condensates" will help elucidate the other pathways which control Hsf1 activity via Hsp70 availability. Endogenous stress-induced aggregates vary in their contents, functions and timelines of formation and intracellular location. While the ubiquitous and abundant Hsp70 is probably recruited to all aggregates, Hsp70-interacting proteins (like co-chaperone Sis1) are likely recruited to specific types of aggregates and control Hsp70 recruitment and release from these sites [29,88]. Though the Hsp70 co-chaperone Sis1 appears to relocalize with Hsp70 to Hsp104-marked cytosolic aggregates and to ORP condensates at the nucleolar periphery, other factors may strongly influence Hsp70 recruitment to, and release from, other kinds of protein aggregates or even the inner cell membrane [11], in turn affecting Hsf1 activity [6].

5.2 Alternative Stressors

It is still unclear why many of the Hsf1 target genes are conserved targets in the HSR, perhaps because the HSR has been primarily studied in heat shock. The HSR is activated in response to many stressors, elevated pH, osmotic stress, nutrient starvation, and defective internal processes such as disrupted mitochondrial import. A parallel study to this one, which exposes cells to diverse stressors, may reveal that different target genes in the regulon have adaptive roles in restoring homeostasis or providing feedback regulation on Hsf1 in

different conditions. For example, induction of two Hsf1 targets (Hrk1 and Hsp30) which are membrane proton pumps probably become important in acidic conditions, which are known to induce protein aggregation [45,105,132]. If these genes are responsible for the restoration of protein homeostasis during pH stress, they probably affect Hsp70 availability, in turn regulating Hsf1.

I imagine that a parallel study to this one, in alternative stressors, will not only reveal additional Hsf1 regulators and more about the logistics of Hsf1 regulation, but also could uncover how the constituents of protein aggregates differ under different stressors.

5.3 Alternative Roles for Induced Hsp70

In our Hsp70ΔFBL line, Hsf1 is very hyperactive, but Hsp104-marked protein aggregates are resolved and long term fitness is similar to WT. Imaging shows that Hsp104 aggregates are resolved efficiently, suggesting that the basal pool of Hsp70 and Sis1 is freed from aggregates and available to repress Hsf1 in the Hsp70ΔFBL. It would be surprising if Hsp70 is induced solely to deactivate Hsf1, during stress, when resources are limited; if true, this result would highlight how important and adaptive HSR autoregulation is. Alternatively, induced Hsp70 may be necessary for other processes in the cell, like restoring lipid homeostasis or facilitating protein transport across membranes or dissolving Hsf1 transcriptional condensates [23,25,27]. Finding out which processes Hsp70 maintains will help us understand which processes Hsf1 senses via Hsp70 availability, outside of cytosolic protein homeostasis.

5.4 Mechanisms of Transcriptional Regulation

The characterization of the HSR revealed that the single transcription factor, Hsf1, induced a diversity of transcriptional profiles within minutes (Figure 4.1). The determinants of transcriptional dynamics and amplitude are not well understood. Though one in vitro study

on Msn2 binding indicates a combination of factors - the number of binding sites ahead of the gene of interest, chromatin accessibility and distance of binding site to promoter - determine the lag between stimulus and transcription initiation and the threshold of activation [48], we know little about what determines how sustained or transient gene induction is, and how highly a gene is expressed. These questions are especially salient in the heat shock response, where genes are induced in a dose-dependent manner, depending on the intensity of stress, but the response appears to be invariably transient (Figure 2.2).

Perhaps, the transient Hsf1 transcriptional hubs, which form during the first five minutes of heat shock, affect transcriptional dynamics [23]. Our characterization of transcriptional dynamics in the heat shock response showed that genes have a range of transcriptional profiles during heat shock (Figure 2.3). Genes that are strongly and transiently induced are transcribed in the Hsf1 transcriptional condensates that last for the first ten minutes of heat shock, while genes that are weakly induced with sustained dynamics are excluded entirely, or only included in the dynamic Hsf1 transcriptional hubs at a lower frequency. It has yet to be determined which Hsf1 target genes coalesce into Hsf1 transcriptional condensates, beyond the few highly-expressed genes which all form intergenic contacts with one another: Hsp104, Ssa2, and Hsp82 [22]. TaqI-3C can be used to measure the frequency with which Hsf1 target genes make contact with one another, to form a comprehensive picture of 3D genome architecture during stress. Then, by referring back to the transcriptional profiles generated in this project, we can divine how 3D genome architecture controls transcriptional dynamics.

5.5 Evolution of Basal and Stress-Induced Target Gene Induction

The decreased basal target expression in many of the ΔHSE induction mutants suggests that most of the Hsf1 target genes (more than the 18 we originally expected) are dependent on

Hsf1 for not only stress-induced expression, but basal expression as well. Basal and induced expression seem to be coupled processes. This makes sense because eukaryotic cells are constantly tuning HSR level along a continuum, and the same proteins that are needed in more stressful conditions are also needed, to some extent, in more optimal growth conditions, when the HSR is less activated.

Notably, basal expression and induction fold change have no correlation across the Hsf1 target genes. Ssa2, for example, is dependent on Hsf1 for its high basal expression and is essential for cell growth, but it is only slightly induced during heat shock. The levels of basal expression and stress-induced expression fold change are tuned independently, over evolution, by mechanisms we don't yet understand.

There are many avenues for further investigation: the mechanisms of transcriptional regulation, the evolution of a transcriptional network over time, and the protein aggregates which perform diverse, stress-protective functions across the eukaryotic cell.

CHAPTER 6

UNPUBLISHED RESULTS

These experiments were prompted by interesting findings in Chapter 3, but did not make it to the manuscript.

6.1 Ira2 at the interface between stress responses

Ira2 is an Hsf1 target gene that is important for fitness during heat shock (Figure 3.4A,B) and has a known role in the Ras-PKA pathway, which regulates growth according to glucose availability. Therefore, we wondered whether the induction of Ira2 during the HSR had a role in coordinating with other pathways important for cell fitness during heat shock or other stressors that activate the HSR [12,35]. To explore whether Ira2 mediates cross talk between the HSR and the osmotic stress response, we simultaneously measured fluorescent reporters of the osmotic stress response (HOR7-GFP) and of the HSR (HSE-mApple) when Ira2 induction was depleted (Ira2ΔHSE) and cells were exposed to osmotic shock (Figure 6.1B), glucose deprivation (Figure 6.1A) or heat shock (Figure 6.1C). Ira2ΔHSE had heat shock response and osmotic stress response like WT, indicating Ira2 induction is dispensable for these osmotic stress response regulation (Figure 6.1). To test for Ira2 regulation of the Msn2-controlled environmental stress response (ESR), which is activated by many stressors, we measured the GFP-tagged Msn2 target gene, Hsp12. However, the ESR was almost identical in WT and Ira2ΔHSE in each stressor tested (Figure 6.2).

Though Ira2 induction did not appear to affect feedback regulation of stress responses in any conditions, we already knew from the initial fitness screen that Ira2 induction affected fitness during heat shock. It was likely, therefore, that Ira2 induction affected growth resumption in other environmental stressors, as well as heat shock. We quantified long term fitness by quantitative growth assay in Ira2ΔHSE and WT, in heat shock, osmotic stress,

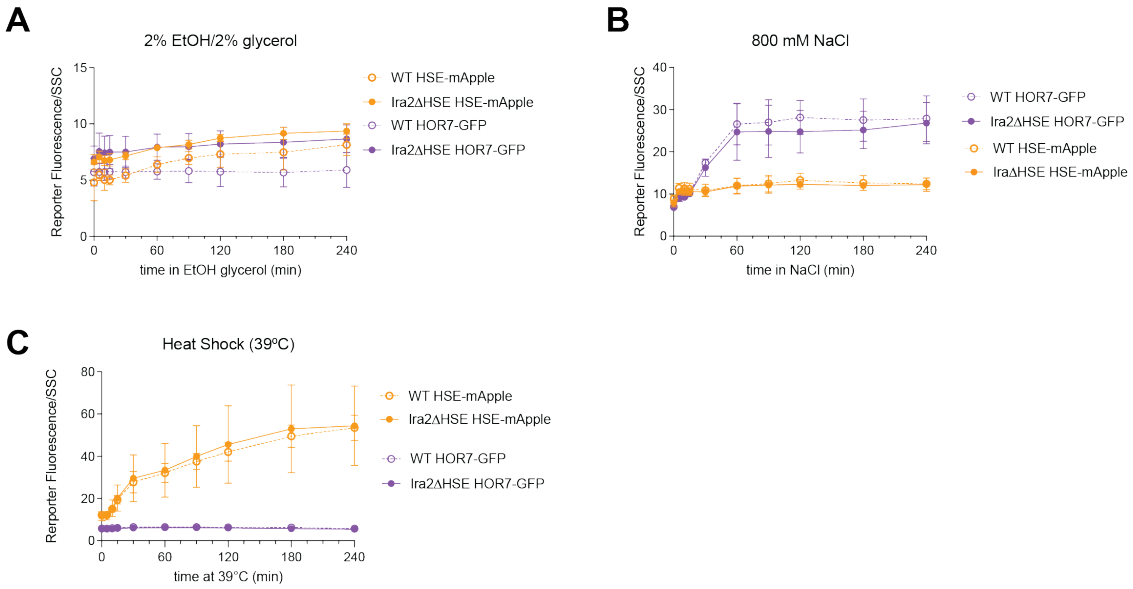

Figure 6.1: Ira2 induction by Hsf1 is dispensable for osmotic stress response and heat shock response regulation in diverse stressors
Cells were deprived of glucose (A), exposed to osmotic shock (B), or heat shock (C) and fluorescent reporters for HSR (HSE-mApple) and osmotic stress response (HOR7-GFP) levels were quantified by flow cytometry. (D) All graphs combined. Average +/- SD, n=3.

and glucose deprivation. Ira2ΔHSE had decreased fitness in osmotic stress (800 mM NaCl) (Figure 6.3), glucose deprivation (subtle defect), and heat shock (Figure 3.4) compared to WT.

In summary, Ira2 induction does not provide feedback regulation to the heat shock response or other stress responses but does support long term fitness in osmotic shock, heat shock and glucose deprivation. In conclusion, Ira2 is a conserved Hsf1 target gene because it maintains fitness in a diversity of stressors. To understand how Ira2 promotes fitness, future experiments might test whether Ira2 induction supports optimal stress response prioritization (i.e. when cells are exposed to heat shock and glucose deprivation at once).

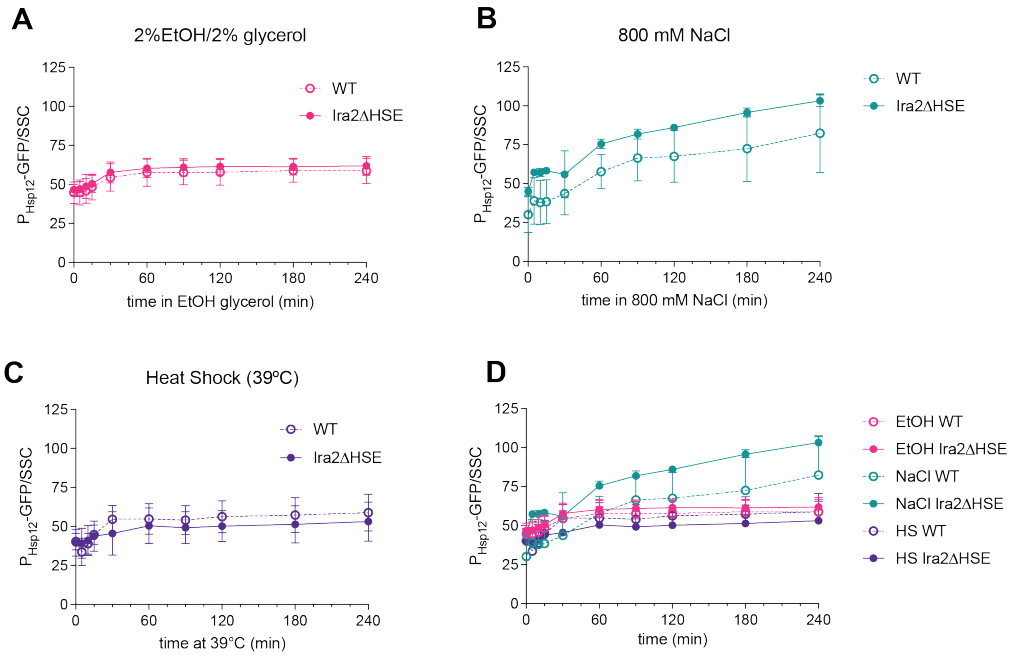

Figure 6.2: Ira2 induction is dispensable for the environmental stress response
Cells were deprived of glucose (A), exposed to osmotic shock (B), or heat shock (C) and fluorescent reporter of ESR (Hsp12-GFP) was measured by flow cytometry. Average +/- SD, n=3.

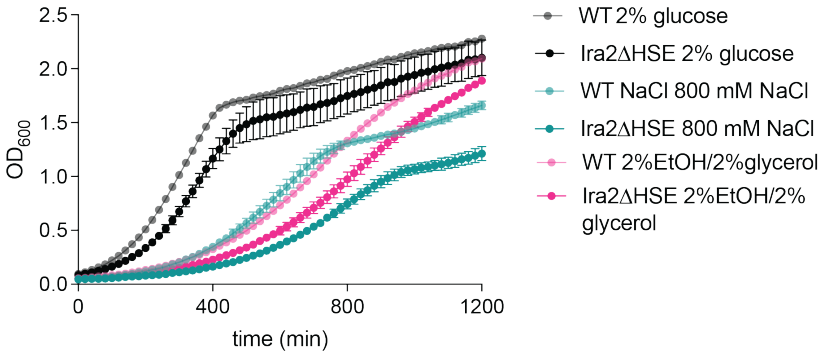

Figure 6.3: Ira2 induction affects fitness in the osmotic and heat shock responses
Quantitative growth assay of Ira2ΔHSE and WT in a variety of conditions. Average +/- SD, n=3.

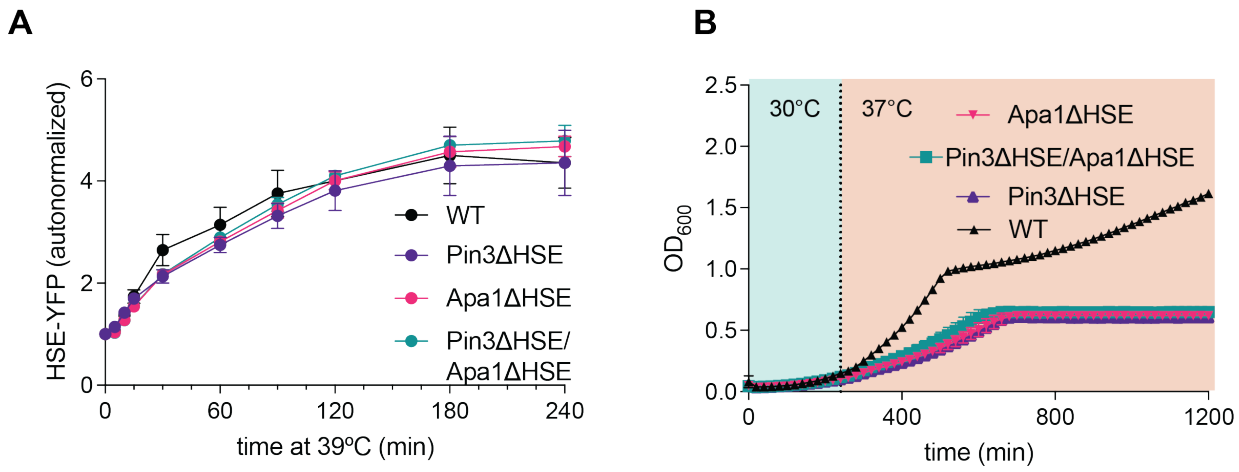

Figure 6.4: Apa1 and Pin3 are dispensable for Hsf1 regulation but necessary for fitness A) HSE-YFP measured over a heat shock time course (39°C). Each data point represents the mean of the three biological replicates. Conducted 11.8.22. B) Quantitative growth assay conducted during heat shock during heat shock (37°C). Average +/- SD, n=2. Conducted 11.18.22.

6.2 Apa1 and Pin3

We hypothesized that Apa1 and Pin3 function redundantly in Hsf1 regulation, given that Apa1 and Pin3 both have large, persistent Hsp104-marked protein aggregates, and both affect fitness during heat shock. However, the double induction mutant had Hsf1 activity similar to WT (Figure 6.4A). We can only conclude that Apa1 induction and Pin3 induction do not have a significant effect on Hsf1 regulation independently, or in combination. Also, the double mutant had an identical fitness defect to the two single mutants (Figure 6.4B). Because so many Hsf1 target gene induction mutants had almost identical fitness defects, it would be overconfident to make any conclusions (about Apa1 and Pin3 epistasis) from the double mutant fitness defect, which looks exactly like each single mutant.

6.3 Hsp42 and Fes1

Our initial results showed that both Fes induction and Hsp42 induction are necessary for normal Hsf1 activity (Figure 3.2). Fes1 and Hsp42's established functions are not known to

overlap or interact. Also, Fes1ΔHSE and Hsp42ΔHSE induction mutants have distinctive defects in Hsf1 activity regulation: Fes1ΔHSE has hyperactive Hsf1 after three hours of heat shock, while Hsp42ΔHSE has hyperactive Hsf1 mainly during the first few minutes of heat shock. We hypothesized that Fes1 and Hsp42 might work in completely independent tracks of Hsf1 regulation. If true, the double induction mutant would have an additive Hsf1 hyperactivity defect, in both early and late heat shock. Though Hsf1 was misregulated and hyperactive in the double mutant, the Hsf1 activity defect in the double mutant was somewhere between what is expected if the proteins cooperate to regulate Hsf1 (epistatic interaction, double mutant is similar to each single mutant) and what is expected if they regulate Hsf1 independently (additive interaction, the double mutant Hsf1 activity defect is the sum of the single mutant phenotypes) (Figure 6.5).

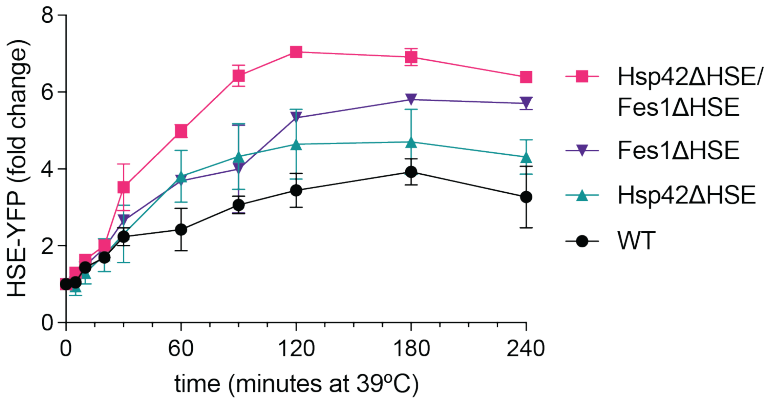

Figure 6.5: Hsp42 and Fes1 function somewhat epistatically in Hsf1 regulation
HSE-YFP measured over a heat shock time course (39°C). Average +/- SD, n=3. Conducted 11.21.22

Table 6.1: Cell lines used in unpublished results.

Strain	**Genotype**	**Description**	**Figure**
DPY1857	w303a; 4xHSE-mvenus::LEU;Ira2ΔHSE410-418,383-394	Ira2ΔHSE	6.3
DPY144	w303a; 4xHSE-Venus::LEU	WT	6.3 - 6.5
DPY1983	w303a; PHSP12-GFP::LEU; Ira2ΔHSE-383-394,410-418	Ira2ΔHSE	6.2
DPY146	w303a; PHSP12-GFP::LEU	WT	6.2
DPY1973	Leu::HSE-mApple; Trp::pHOR7-GFP; His::pStre-HALO; Ira2ΔHSE410-418,383-394	Ira2ΔHSE	6.1
AD7	Leu::HSE-mApple; Trp::pHOR7-GFP; His::pStre-HALO	WT	6.1
DPY1925	w303a; 4xHSE-Venus::LEU; Pin3ΔHSE303-321	Pin3ΔHSE	6.4
DPY1917	w303a; 4xHSE-Venus::LEU; Apa1ΔHSE204-190	Apa1ΔHSE	6.4
DPY1993	w303a; 4xHSE-Venus::LEU; Apa1Δ204-190-APA1;Pin3ΔHSE303-321	Apa1ΔHSE/ Pin3ΔHSE	6.5
DPY1987	w303a; 4xHSE-mvenus::LEU; Fes1ΔHSE 158-171;Hsp42ΔHSE225-243-HSP42	Fes1ΔHSE/ Hsp42ΔHSE	6.5
DPY1913	w303a; 4xHSE-Venus::LEU; Hsp42ΔHSE225-243-HSP42	Hsp42ΔHSE	6.5
DPY1856	w303a; 4xHSE-mvenus::LEU;Fes1ΔHSE158-171	Fes1ΔHSE	6.5

REFERENCES

[1] Jennifer L Abrams, Jacob Verghese, Patrick A Gibney, and Kevin A Morano. Hierarchical functional specificity of cytosolic heat shock protein 70 (hsp70) nucleotide exchange factors in yeast. *The Journal of Biological Chemistry*, 289(19):13155–13167, May 2014.

[2] Benjamin Albert, Isabelle C Kos-Braun, Anthony K Henras, Christophe Dez, Maria Paula Rueda, Xu Zhang, Olivier Gadal, Martin Kos, and David Shore. A ribosome assembly stress response regulates transcription to maintain proteome homeostasis. *eLife*, 8, May 2019.

[3] Simon Alberti and Dorothee Dormann. Liquid-liquid phase separation in disease. *Annual Review of Genetics*, 53:171–194, Dec 2019.

[4] Simon Alberti and Anthony A Hyman. Biomolecular condensates at the nexus of cellular stress, protein aggregation disease and ageing. *Nature Reviews. Molecular Cell Biology*, 22(3):196–213, Mar 2021.

[5] Brian D Alford, Eduardo Tassoni-Tsuchida, Danish Khan, Jeremy J Work, Gregory Valiant, and Onn Brandman. Reporterseq reveals genome-wide dynamic modulators of the heat shock response across diverse stressors. *eLife*, 10, Jul 2021.

[6] Asif Ali, Rania Garde, Olivia C Schaffer, Jared A M Bard, Kabir Husain, Samantha Keyport Kik, Kathleen A Davis, Sofia Luengo-Woods, D Allan Drummond, Allison H Squires, and et al. Adaptive preservation of orphan ribosomal proteins in chaperone-stirred condensates. *BioRxiv*, Nov 2022.

[7] Heeseon An, Alban Ordureau, Maria Körner, Joao A Paulo, and J Wade Harper. Systematic quantitative analysis of ribosome inventory during nutrient stress. *Nature*, 583(7815):303–309, Jul 2020.

[8] Julius Anckar and Lea Sistonen. Regulation of hsf1 function in the heat stress response: implications in aging and disease. *Annual Review of Biochemistry*, 80:1089–1115, 2011.

[9] Claes Andréasson, Jocelyne Fiaux, Heike Rampelt, Matthias P Mayer, and Bernd Bukau. Hsp110 is a nucleotide-activated exchange factor for hsp70. *The Journal of Biological Chemistry*, 283(14):8877–8884, Apr 2008.

[10] William E Balch, Richard I Morimoto, Andrew Dillin, and Jeffery W Kelly. Adapting proteostasis for disease intervention. *Science*, 319(5865):916–919, Feb 2008.

[11] Zsolt Balogi, Gabriele Multhoff, Thomas Kirkegaard Jensen, Emyr Lloyd-Evans, Tetsumori Yamashima, Marja Jäättelä, John L Harwood, and László Vígh. Hsp70 interactions with membrane lipids regulate cellular functions in health and disease. *Progress in lipid research*, 74:18–30, Apr 2019.

[12] Fiorella Belotti, Renata Tisi, Chiara Paiardi, Marco Rigamonti, Silvia Groppi, and Enzo Martegani. Localization of ras signaling complex in budding yeast. *Biochimica et Biophysica Acta*, 1823(7):1208–1216, Jul 2012.

[13] Scott E Berger, Anna M Nolte, Erina Kamiya, and Justin K Hines. Three j-proteins impact hsp104-mediated variant-specific prion elimination: a new critical role for a low-complexity domain. *Current Genetics*, 66(1):51–58, Feb 2020.

[14] Edgar E Boczek, Lasse G Reefschläger, Marco Dehling, Tobias J Struller, Elisabeth Häusler, Andreas Seidl, Ville R I Kaila, and Johannes Buchner. Conformational processing of oncogenic v-src kinase by the molecular chaperone hsp90. *Proceedings of the National Academy of Sciences of the United States of America*, 112(25):E3189–98, Jun 2015.

[15] Sagie Brodsky, Tamar Jana, and Naama Barkai. Order through disorder: The role of intrinsically disordered regions in transcription factor binding specificity. *Current Opinion in Structural Biology*, 71:110–115, Dec 2021.

[16] Martin S Buckley, Hojoong Kwak, Warren R Zipfel, and John T Lis. Kinetics of promoter pol ii on hsp70 reveal stable pausing and key insights into its regulation. *Genes & Development*, 28(1):14–19, Jan 2014.

[17] D Carmona-Gutierrez, T Eisenberg, S Büttner, C Meisinger, G Kroemer, and F Madeo. Apoptosis in yeast: triggers, pathways, subroutines. *Cell Death and Differentiation*, 17(5):763–773, May 2010.

[18] Bi-Chang Chen, Wesley R Legant, Kai Wang, Lin Shao, Daniel E Milkie, Michael W Davidson, Chris Janetopoulos, Xufeng S Wu, John A Hammer, Zhe Liu, and et al. Lattice light-sheet microscopy: imaging molecules to embryos at high spatiotemporal resolution. *Science*, 346(6208):1257998, Oct 2014.

[19] Han-Jou Chen, Jacqueline C Mitchell, Sergey Novoselov, Jack Miller, Agnes L Nishimura, Emma L Scotter, Caroline A Vance, Michael E Cheetham, and Christopher E Shaw. The heat shock response plays an important role in tdp-43 clearance: evidence for dysfunction in amyotrophic lateral sclerosis. *Brain: A Journal of Neurology*, 139(Pt 5):1417–1432, May 2016.

[20] Valeria Cherkasov, Sarah Hofmann, Silke Druffel-Augustin, Axel Mogk, Jens Tyedmers, Georg Stoecklin, and Bernd Bukau. Coordination of translational control and protein homeostasis during severe heat stress. *Current Biology*, 23(24):2452–2462, Dec 2013.

[21] Surabhi Chowdhary, Amoldeep S Kainth, and David S Gross. Heat shock protein genes undergo dynamic alteration in their three-dimensional structure and genome organization in response to thermal stress. *Molecular and Cellular Biology*, 37(24), Dec 2017.

[22] Surabhi Chowdhary, Amoldeep S Kainth, Sarah Paracha, David S Gross, and David Pincus. Inducible transcriptional condensates drive 3d genome reorganization in the heat shock response. *Molecular Cell*, 82(22):4386–4399.e7, Nov 2022.

[23] Surabhi Chowdhary, Amoldeep S Kainth, David Pincus, and David S Gross. Heat shock factor 1 drives intergenic association of its target gene loci upon heat shock. *Cell reports*, 26(1):18–28.e5, Jan 2019.

[24] Elizabeth A Craig. Hsp70 at the membrane: driving protein translocation. *BMC Biology*, 16(1):11, Jan 2018.

[25] Paolo De Los Rios and Alessandro Barducci. Hsp70 chaperones are non-equilibrium machines that achieve ultra-affinity by energy consumption. *eLife*, 3:e02218, May 2014.

[26] Antonio De Maio and Lawrence Hightower. The interaction of heat shock proteins with cellular membranes: a historical perspective. *Cell Stress & Chaperones*, 26(5):769–783, Sep 2021.

[27] Fabian den Brave, Lucas V Cairo, Chandhuru Jagadeesan, Carmen Ruger-Herreros, Axel Mogk, Bernd Bukau, and Stefan Jentsch. Chaperone-mediated protein disaggregation triggers proteolytic clearance of intra-nuclear protein inclusions. *Cell reports*, 31(9):107680, Jun 2020.

[28] Rabin Dhakal, Chunyi Tong, Sean Anderson, Anna S Kashina, Barry Cooperman, and Haim H Bau. Dynamics of intracellular stress-induced trna trafficking. *Nucleic Acids Research*, 47(4):2002–2010, Feb 2019.

[29] Stéphanie Escusa-Toret, Willianne I M Vonk, and Judith Frydman. Spatial sequestration of misfolded proteins by a dynamic chaperone pathway enhances cellular fitness during stress. *Nature Cell Biology*, 15(10):1231–1243, Oct 2013.

[30] Zoë A Feder, Asif Ali, Abhyudai Singh, Joanna Krakowiak, Xu Zheng, Vytas P Bindokas, Donald Wolfgeher, Stephen J Kron, and David Pincus. Subcellular localization of the j-protein sis1 regulates the heat shock response. *The Journal of Cell Biology*, 220(1), Jan 2021.

[31] James E Ferrell. Perfect and near-perfect adaptation in cell signaling. *Cell Systems*, 2(2):62–67, Feb 2016.

[32] Monique Floer, Gene O Bryant, and Mark Ptashne. Hsp90/70 chaperones are required for rapid nucleosome removal upon induction of the gal genes of yeast. *Proceedings of the National Academy of Sciences of the United States of America*, 105(8):2975–2980, Feb 2008.

[33] F Frottin, F Schueder, S Tiwary, R Gupta, R Körner, T Schlichthaerle, J Cox, R Jungmann, F U Hartl, and M S Hipp. The nucleolus functions as a phase-separated protein quality control compartment. *Science*, 365(6451):342–347, Jul 2019.

[34] Giorgio Gaglia, Rumana Rashid, Clarence Yapp, Gaurav N Joshi, Carmen G Li, Susan L Lindquist, Kristopher A Sarosiek, Luke Whitesell, Peter K Sorger, and Sandro Santagata. Hsf1 phase transition mediates stress adaptation and cell fate decisions. *Nature Cell Biology*, 22(2):151–158, Feb 2020.

[35] F Galello, S Moreno, and S Rossi. Interacting proteins of protein kinase a regulatory subunit in saccharomyces cerevisiae. *Journal of Proteomics*, 109:261–275, Sep 2014.

[36] Rania Garde, Abhyudai Singh, Asif Ali, and David Pincus. Induction of sis1 promotes fitness but not feedback in the heat shock response. *BioRxiv*, Apr 2022.

[37] Rania Garde, Abhyudai Singh, Asif Ali, and David Pincus. Transcriptional regulation of sis1 promotes fitness but not feedback in the heat shock response. *eLife*, 12, May 2023.

[38] A P Gasch, P T Spellman, C M Kao, O Carmel-Harel, M B Eisen, G Storz, D Botstein, and P O Brown. Genomic expression programs in the response of yeast cells to environmental changes. *Molecular Biology of the Cell*, 11(12):4241–4257, Dec 2000.

[39] Audrey P Gasch and Margaret Werner-Washburne. The genomics of yeast responses to environmental stress and starvation. *Functional & Integrative Genomics*, 2(4–5):181–192, Sep 2002.

[40] Olivier Genest, Sue Wickner, and Shannon M Doyle. Hsp90 and hsp70 chaperones: Collaborators in protein remodeling. *The Journal of Biological Chemistry*, 294(6):2109–2120, Feb 2019.

[41] Hannah Girstmair, Franziska Tippel, Abraham Lopez, Katarzyna Tych, Frank Stein, Per Haberkant, Philipp Werner Norbert Schmid, Dominic Helm, Matthias Rief, Michael Sattler, and et al. The hsp90 isoforms from s. cerevisiae differ in structure, function and client range. *Nature Communications*, 10(1):3626, Aug 2019.

[42] J R Glover and S Lindquist. Hsp104, hsp70, and hsp40: a novel chaperone system that rescues previously aggregated proteins. *Cell*, 94(1):73–82, Jul 1998.

[43] Rocio Gomez-Pastor, Eileen T Burchfiel, Daniel W Neef, Alex M Jaeger, Elisa Cabiscol, Spencer U McKinstry, Argenia Doss, Alejandro Aballay, Donald C Lo, Sergey S Akimov, and et al. Abnormal degradation of the neuronal stress-protective transcription factor hsf1 in huntington's disease. *Nature Communications*, 8:14405, Feb 2017.

[44] Davi Gonçalves, Alec Santiago, and Kevin A Morano. When ph comes to the rescue. *eLife*, 9, Sep 2020.

[45] A Goossens, N de La Fuente, J Forment, R Serrano, and F Portillo. Regulation of yeast h(+)-atpase by protein kinases belonging to a family dedicated to activation of plasma membrane transporters. *Molecular and Cellular Biology*, 20(20):7654–7661, Oct 2000.

[46] Tomas Grousl, Pavel Ivanov, Ivana Malcova, Petr Pompach, Ivana Frydlova, Renata Slaba, Lenka Senohrabkova, Lenka Novakova, and Jiri Hasek. Heat shock-induced accumulation of translation elongation and termination factors precedes assembly of stress granules in s. cerevisiae. *Plos One*, 8(2):e57083, Feb 2013.

[47] Ji-Sook Hahn and Dennis J Thiele. Activation of the saccharomyces cerevisiae heat shock transcription factor under glucose starvation conditions by snf1 protein kinase. *The Journal of Biological Chemistry*, 279(7):5169–5176, Feb 2004.

[48] Anders S Hansen and Erin K O'Shea. cis determinants of promoter threshold and activation timescale. *Cell reports*, 12(8):1226–1233, Aug 2015.

[49] Denes Hnisz, Daniel S Day, and Richard A Young. Insulated neighborhoods: structural and functional units of mammalian gene control. *Cell*, 167(5):1188–1200, Nov 2016.

[50] Chi-Ting Ho, Tomas Grousl, Oren Shatz, Areeb Jawed, Carmen Ruger-Herreros, Marije Semmelink, Regina Zahn, Karsten Richter, Bernd Bukau, and Axel Mogk. Cellular sequestrases maintain basal hsp70 capacity ensuring balanced proteostasis. *Nature Communications*, 10(1):4851, Oct 2019.

[51] Victoria Hung, Namrata D Udeshi, Stephanie S Lam, Ken H Loh, Kurt J Cox, Kayvon Pedram, Steven A Carr, and Alice Y Ting. Spatially resolved proteomic mapping in living cells with the engineered peroxidase apex2. *Nature Protocols*, 11(3):456–475, Mar 2016.

[52] Nicholas T Ingolia, Sina Ghaemmaghami, John R S Newman, and Jonathan S Weissman. Genome-wide analysis in vivo of translation with nucleotide resolution using ribosome profiling. *Science*, 324(5924):218–223, Apr 2009.

[53] Christiane Iserman, Christine Desroches Altamirano, Ceciel Jegers, Ulrike Friedrich, Taraneh Zarin, Anatol W Fritsch, Matthäus Mittasch, Antonio Domingues, Lena Hersemann, Marcus Jahnel, and et al. Condensation of ded1p promotes a translational switch from housekeeping to stress protein production. *Cell*, 181(4):818–831.e19, May 2020.

[54] Allison James, Yubo Wang, Himanshu Raje, Raphyel Rosby, and Patrick DiMario. Nucleolar stress with and without p53. *Nucleus (Austin, Tex.)*, 5(5):402–426, 2014.

[55] Gopal G Jayaraj, Mark S Hipp, and F Ulrich Hartl. Functional modules of the proteostasis network. *Cold Spring Harbor Perspectives in Biology*, 12(1), Jan 2020.

[56] Felix Jonas, Miri Carmi, Beniamin Krupkin, Joseph Steinberger, Sagie Brodsky, Tamar Jana, and Naama Barkai. The molecular grammar of protein disorder guiding genome-binding locations. *Nucleic Acids Research*, Mar 2023.

[57] Szymon Juszkiewicz and Ramanujan S Hegde. Quality control of orphaned proteins. *Molecular Cell*, 71(3):443–457, Aug 2018.

[58] Stefan Jäkel, José-Manuel Mingot, Petra Schwarzmaier, Enno Hartmann, and Dirk Görlich. Importins fulfil a dual function as nuclear import receptors and cytoplasmic chaperones for exposed basic domains. *The EMBO Journal*, 21(3):377–386, Feb 2002.

[59] Daniel Kaganovich, Ron Kopito, and Judith Frydman. Misfolded proteins partition between two distinct quality control compartments. *Nature*, 454(7208):1088–1095, Aug 2008.

[60] Jayasankar Mohanakrishnan Kaimal, Ganapathi Kandasamy, Fabian Gasser, and Claes Andréasson. Coordinated hsp110 and hsp104 activities power protein disaggregation in saccharomyces cerevisiae. *Molecular and Cellular Biology*, 37(11), Jun 2017.

[61] Ganapathi Kandasamy and Claes Andréasson. Hsp70-hsp110 chaperones deliver ubiquitin-dependent and -independent substrates to the 26s proteasome for proteolysis in yeast. *Journal of Cell Science*, 131(6), Mar 2018.

[62] Sunyoung Kim and David S Gross. Mediator recruitment to heat shock genes requires dual hsf1 activation domains and mediator tail subunits med15 and med16. *The Journal of Biological Chemistry*, 288(17):12197–12213, Apr 2013.

[63] Roman Kityk, Markus Vogel, Rainer Schlecht, Bernd Bukau, and Matthias P Mayer. Pathways of allosteric regulation in hsp70 chaperones. *Nature Communications*, 6:8308, Sep 2015.

[64] Courtney L Klaips, Michael H M Gropp, Mark S Hipp, and F Ulrich Hartl. Sis1 potentiates the stress response to protein aggregation and elevated temperature. *Nature Communications*, 11(1):6271, Dec 2020.

[65] Szymon W Kmiecik, Laura Le Breton, and Matthias P Mayer. Feedback regulation of heat shock factor 1 (hsf1) activity by hsp70-mediated trimer unzipping and dissociation from dna. *The EMBO Journal*, 39(14):e104096, Jul 2020.

[66] Joanna Krakowiak, Xu Zheng, Nikit Patel, Zoë A Feder, Jayamani Anandhakumar, Kendra Valerius, David S Gross, Ahmad S Khalil, and David Pincus. Hsf1 and hsp70 constitute a two-component feedback loop that regulates the yeast heat shock response. *eLife*, 7, Feb 2018.

[67] Arun Kumar, Veena Mathew, and Peter C Stirling. Nuclear protein quality control in yeast: The latest inquiries. *The Journal of Biological Chemistry*, 298(8):102199, Aug 2022.

[68] Lilian T Lamech and Cole M Haynes. The unpredictability of prolonged activation of stress response pathways. *The Journal of Cell Biology*, 209(6):781–787, Jun 2015.

[69] Michelle D Leach, Rhys A Farrer, Kaeling Tan, Zhengqiang Miao, Louise A Walker, Christina A Cuomo, Robert T Wheeler, Alistair J P Brown, Koon Ho Wong, and

Leah E Cowen. Hsf1 and hsp90 orchestrate temperature-dependent global transcriptional remodelling and chromatin architecture in candida albicans. *Nature Communications*, 7:11704, May 2016.

[70] Kiwon Lee, Chris C-S Hsiung, Peng Huang, Arjun Raj, and Gerd A Blobel. Dynamic enhancer-gene body contacts during transcription elongation. *Genes & Development*, 29(19):1992–1997, Oct 2015.

[71] Harri Lempiäinen and David Shore. Growth control and ribosome biogenesis. *Current Opinion in Cell Biology*, 21(6):855–863, Dec 2009.

[72] Bentley Lim, Ryoji Miyazaki, Saskia Neher, Deborah A Siegele, Koreaki Ito, Peter Walter, Yoshinori Akiyama, Takashi Yura, and Carol A Gross. Heat shock transcription factor σ_{32} co-opts the signal recognition particle to regulate protein homeostasis in e. coli. *PLoS Biology*, 11(12):e1001735, Dec 2013.

[73] S Lindquist. The heat-shock response. *Annual Review of Biochemistry*, 55:1151–1191, 1986.

[74] John T Lis. A 50 year history of technologies that drove discovery in eukaryotic transcription regulation. *Nature Structural & Molecular Biology*, 26(9):777–782, Sep 2019.

[75] Robbie Loewith and Michael N Hall. Target of rapamycin (tor) in nutrient signaling and growth control. *Genetics*, 189(4):1177–1201, Dec 2011.

[76] M S Longtine, A McKenzie, D J Demarini, N G Shah, A Wach, A Brachat, P Philippsen, and J R Pringle. Additional modules for versatile and economical pcr-based gene deletion and modification in saccharomyces cerevisiae. *Yeast*, 14(10):953–961, Jul 1998.

[77] Georgyi V Los, Lance P Encell, Mark G McDougall, Danette D Hartzell, Natasha Karassina, Chad Zimprich, Monika G Wood, Randy Learish, Rachel Friedman Ohana, Marjeta Urh, and et al. Halotag: a novel protein labeling technology for cell imaging and protein analysis. *ACS Chemical Biology*, 3(6):373–382, Jun 2008.

[78] Wenxiu Ma, William S Noble, and Timothy L Bailey. Motif-based analysis of large nucleotide data sets using meme-chip. *Nature Protocols*, 9(6):1428–1450, May 2014.

[79] O. Maaløe and N.O. Kjeldgaard. *Control of Macromolecular Synthesis: A Study of DNA, RNA, and Protein Synthesis in Bacteria*. Microbial and molecular biology series. Benjamin, 1966.

[80] Dig B Mahat, H Hans Salamanca, Fabiana M Duarte, Charles G Danko, and John T Lis. Mammalian heat shock response and mechanisms underlying its genome-wide transcriptional regulation. *Molecular Cell*, 62(1):63–78, Apr 2016.

[81] Anna E Masser, Michela Ciccarelli, and Claes Andréasson. Hsf1 on a leash - controlling the heat shock response by chaperone titration. *Experimental Cell Research*, 396(1):112246, Nov 2020.

[82] Anna E Masser, Wenjing Kang, Joydeep Roy, Jayasankar Mohanakrishnan Kaimal, Jany Quintana-Cordero, Marc R Friedländer, and Claes Andréasson. Cytoplasmic protein misfolding titrates hsp70 to activate nuclear hsf1. *eLife*, 8, Sep 2019.

[83] M.L. Mendillo, David Pincus, and R. Scherz-Shouval. *HSF1 and Molecular Chaperones in Biology and Cancer*. Springer Nature, 2020.

[84] Ronald A Merrill, Jianing Song, Rikki A Kephart, Annette J Klomp, Claire E Noack, and Stefan Strack. A robust and economical pulse-chase protocol to measure the turnover of halotag fusion proteins. *The Journal of Biological Chemistry*, 294(44):16164–16171, Nov 2019.

[85] Stephanie B M Miller, Chi-Ting Ho, Juliane Winkler, Maria Khokhrina, Annett Neuner, Mohamed Y H Mohamed, D Lys Guilbride, Karsten Richter, Michael Lisby, Elmar Schiebel, and et al. Compartment-specific aggregases direct distinct nuclear and cytoplasmic aggregate deposition. *The EMBO Journal*, 34(6):778–797, Mar 2015.

[86] Stephanie B M Miller, Axel Mogk, and Bernd Bukau. Spatially organized aggregation of misfolded proteins as cellular stress defense strategy. *Journal of Molecular Biology*, 427(7):1564–1574, Apr 2015.

[87] Axel Mogk, Damon Huber, and Bernd Bukau. Integrating protein homeostasis strategies in prokaryotes. *Cold Spring Harbor Perspectives in Biology*, 3(4), Apr 2011.

[88] Richard I Morimoto. Proteotoxic stress and inducible chaperone networks in neurodegenerative disease and aging. *Genes & Development*, 22(11):1427–1438, Jun 2008.

[89] Tania Morán Luengo, Matthias P Mayer, and Stefan G D Rüdiger. The hsp70-hsp90 chaperone cascade in protein folding. *Trends in Cell Biology*, 29(2):164–177, Feb 2019.

[90] Dale Muzzey, Carlos A Gómez-Uribe, Jerome T Mettetal, and Alexander van Oudenaarden. A systems-level analysis of perfect adaptation in yeast osmoregulation. *Cell*, 138(1):160–171, Jul 2009.

[91] Anupama Narla and Benjamin L Ebert. Ribosomopathies: human disorders of ribosome dysfunction. *Blood*, 115(16):3196–3205, Apr 2010.

[92] Daniel W Neef, Alex M Jaeger, and Dennis J Thiele. Heat shock transcription factor 1 as a therapeutic target in neurodegenerative diseases. *Nature Reviews. Drug Discovery*, 10(12):930–944, Dec 2011.

[93] Gen Nonaka, Matthew Blankschien, Christophe Herman, Carol A Gross, and Virgil A Rhodius. Regulon and promoter analysis of the e. coli heat-shock factor,

sigma32, reveals a multifaceted cellular response to heat stress. *Genes & Development*, 20(13):1776–1789, Jul 2006.

[94] Sae-Hun Park, Yury Kukushkin, Rajat Gupta, Taotao Chen, Ayano Konagai, Mark S Hipp, Manajit Hayer-Hartl, and F Ulrich Hartl. Polyq proteins interfere with nuclear degradation of cytosolic proteins by sequestering the sis1p chaperone. *Cell*, 154(1):134–145, Jul 2013.

[95] Monobesh Patra, Sourav Singha Roy, Rakhi Dasgupta, and Tarakdas Basu. Groel to dnak chaperone network behind the stability modulation of σ32 at physiological temperature in escherichia coli. *FEBS Letters*, 589(24 Pt B):4047–4052, Dec 2015.

[96] Sara Peffer, Davi Gonçalves, and Kevin A Morano. Regulation of the hsf1-dependent transcriptome via conserved bipartite contacts with hsp70 promotes survival in yeast. *The Journal of Biological Chemistry*, 294(32):12191–12202, Aug 2019.

[97] Ion Petre, Andrzej Mizera, Claire L. Hyder, Annika Meinander, Andrey Mikhailov, Richard I. Morimoto, Lea Sistonen, John E. Eriksson, and Ralph-Johan Back. A simple mass-action model for the eukaryotic heat shock response and its mathematical validation. *Natural computing*, 10(1):595–612, Mar 2011.

[98] M W Pfaffl. A new mathematical model for relative quantification in real-time rt-pcr. *Nucleic Acids Research*, 29(9):e45, May 2001.

[99] Benjamin Pillet, Valentin Mitterer, Dieter Kressler, and Brigitte Pertschy. Hold on to your friends: Dedicated chaperones of ribosomal proteins: Dedicated chaperones mediate the safe transfer of ribosomal proteins to their site of pre-ribosome incorporation. *Bioessays: News and Reviews in Molecular, Cellular and Developmental Biology*, 39(1):1–12, Jan 2017.

[100] David Pincus. Regulation of hsf1 and the heat shock response. *Advances in Experimental Medicine and Biology*, 1243:41–50, 2020.

[101] David Pincus, Jayamani Anandhakumar, Prathapan Thiru, Michael J Guertin, Alexander M Erkine, and David S Gross. Genetic and epigenetic determinants establish a continuum of hsf1 occupancy and activity across the yeast genome. *Molecular Biology of the Cell*, 29(26):3168–3182, Dec 2018.

[102] David Pincus, Michael W Chevalier, Tomás Aragón, Eelco van Anken, Simon E Vidal, Hana El-Samad, and Peter Walter. Bip binding to the er-stress sensor ire1 tunes the homeostatic behavior of the unfolded protein response. *PLoS Biology*, 8(7):e1000415, Jul 2010.

[103] P W Piper, C Ortiz-Calderon, C Holyoak, P Coote, and M Cole. Hsp30, the integral plasma membrane heat shock protein of saccharomyces cerevisiae, is a stress-inducible regulator of plasma membrane h(+)-atpase. *Cell Stress & Chaperones*, 2(1):12–24, Mar 1997.

[104] Mikael Christer Puustinen and Lea Sistonen. Molecular mechanisms of heat shock factors in cancer. *Cells*, 9(5), May 2020.

[105] Joshua A Riback, Christopher D Katanski, Jamie L Kear-Scott, Evgeny V Pilipenko, Alexandra E Rojek, Tobin R Sosnick, and D Allan Drummond. Stress-triggered phase separation is an adaptive, evolutionarily tuned response. *Cell*, 168(6):1028–1040.e19, Mar 2017.

[106] F Ritossa. A new puffing pattern induced by temperature shock and dnp in drosophila. *Experientia*, 18(12):571–573, Dec 1962.

[107] Lukas Rohland, Roman Kityk, Luka Smalinskaitė, and Matthias P Mayer. Conformational dynamics of the hsp70 chaperone throughout key steps of its atpase cycle. *Proceedings of the National Academy of Sciences of the United States of America*, 119(48):e2123238119, Nov 2022.

[108] Davide Roncarati and Vincenzo Scarlato. Regulation of heat-shock genes in bacteria: from signal sensing to gene expression output. *FEMS Microbiology Reviews*, 41(4):549–574, Jul 2017.

[109] Loic A Royer, Martin Weigert, Ulrik Günther, Nicola Maghelli, Florian Jug, Ivo F Sbalzarini, and Eugene W Myers. Clearvolume: open-source live 3d visualization for light-sheet microscopy. *Nature Methods*, 12(6):480–481, Jun 2015.

[110] Isabelle Sagot and Damien Laporte. The cell biology of quiescent yeast - a diversity of individual scenarios. *Journal of Cell Science*, 132(1), Jan 2019.

[111] Sandro Santagata, Rong Hu, Nancy U Lin, Marc L Mendillo, Laura C Collins, Susan E Hankinson, Stuart J Schnitt, Luke Whitesell, Rulla M Tamimi, Susan Lindquist, and et al. High levels of nuclear heat-shock factor 1 (hsf1) are associated with poor prognosis in breast cancer. *Proceedings of the National Academy of Sciences of the United States of America*, 108(45):18378–18383, Nov 2011.

[112] Ritwick Sawarkar. Transcriptional lockdown during acute proteotoxic stress. *Trends in Biochemical Sciences*, 47(8):660–672, Aug 2022.

[113] Stephan B Schawalder, Mehdi Kabani, Isabelle Howald, Urmila Choudhury, Michel Werner, and David Shore. Growth-regulated recruitment of the essential yeast ribosomal protein gene activator ifh1. *Nature*, 432(7020):1058–1061, Dec 2004.

[114] Jeremy D Scheff, Jonathan D Stallings, Jaques Reifman, and Vineet Rakesh. Mathematical modeling of the heat-shock response in hela cells. *Biophysical Journal*, 109(2):182–193, Jul 2015.

[115] Brenda A Schilke and Elizabeth A Craig. Essentiality of sis1, a j-domain protein hsp70 cochaperone, can be overcome by tti1, a specialized pikk chaperone. *Molecular Biology of the Cell*, 33(3):br3, Mar 2022.

[116] Kara L Schneider, Thomas Nyström, and Per O Widlund. Studying spatial protein quality control, proteopathies, and aging using different model misfolding proteins in s. cerevisiae. *Frontiers in Molecular Neuroscience*, 11:249, Jul 2018.

[117] Matthew Scott, Stefan Klumpp, Eduard M Mateescu, and Terence Hwa. Emergence of robust growth laws from optimal regulation of ribosome synthesis. *Molecular Systems Biology*, 10(8):747, Aug 2014.

[118] David Shore and Benjamin Albert. Ribosome biogenesis and the cellular energy economy. *Current Biology*, 32(12):R611–R617, Jun 2022.

[119] David Shore, Sevil Zencir, and Benjamin Albert. Transcriptional control of ribosome biogenesis in yeast: links to growth and stress signals. *Biochemical Society Transactions*, 49(4):1589–1599, Aug 2021.

[120] Carrie L Simms, Benjamin H Hudson, John W Mosior, Ali S Rangwala, and Hani S Zaher. An active role for the ribosome in determining the fate of oxidized mrna. *Cell reports*, 9(4):1256–1264, Nov 2014.

[121] A Smith, M P Ward, and S Garrett. Yeast pka represses msn2p/msn4p-dependent gene expression to regulate growth, stress response and glycogen accumulation. *The EMBO Journal*, 17(13):3556–3564, Jul 1998.

[122] Eric J Solís, Jai P Pandey, Xu Zheng, Dexter X Jin, Piyush B Gupta, Edoardo M Airoldi, David Pincus, and Vladimir Denic. Defining the essential function of yeast hsf1 reveals a compact transcriptional program for maintaining eukaryotic proteostasis. *Molecular Cell*, 63(1):60–71, Jul 2016.

[123] Emily Mitchell Sontag, Rahul S Samant, and Judith Frydman. Mechanisms and functions of spatial protein quality control. *Annual Review of Biochemistry*, 86:97–122, Jun 2017.

[124] Claudio Soto. Unfolding the role of protein misfolding in neurodegenerative diseases. *Nature Reviews. Neuroscience*, 4(1):49–60, Jan 2003.

[125] Tatiana M Souza-Moreira, Clara Navarrete, Xin Chen, Cleslei F Zanelli, Sandro R Valentini, Maysa Furlan, Jens Nielsen, and Anastasia Krivoruchko. Screening of 2a peptides for polycistronic gene expression in yeast. *FEMS Yeast Research*, 18(5), Aug 2018.

[126] A M Stock, V L Robinson, and P N Goudreau. Two-component signal transduction. *Annual Review of Biochemistry*, 69:183–215, 2000.

[127] Min-Kyung Sung, Tanya R Porras-Yakushi, Justin M Reitsma, Ferdinand M Huber, Michael J Sweredoski, André Hoelz, Sonja Hess, and Raymond J Deshaies. A conserved quality-control pathway that mediates degradation of unassembled ribosomal proteins. *eLife*, 5, Aug 2016.

[128] K Tanaka, B K Lin, D R Wood, and F Tamanoi. Ira2, an upstream negative regulator of ras in yeast, is a ras gtpase-activating protein. *Proceedings of the National Academy of Sciences of the United States of America*, 88(2):468–472, Jan 1991.

[129] Carson C Thoreen, Lynne Chantranupong, Heather R Keys, Tim Wang, Nathanael S Gray, and David M Sabatini. A unifying model for mtorc1-mediated regulation of mrna translation. *Nature*, 485(7396):109–113, May 2012.

[130] Catherine G Triandafillou, Christopher D Katanski, Aaron R Dinner, and D Allan Drummond. Transient intracellular acidification regulates the core transcriptional heat shock response. *eLife*, 9, Aug 2020.

[131] Blake W Tye and L Stirling Churchman. Hsf1 activation by proteotoxic stress requires concurrent protein synthesis. *Molecular Biology of the Cell*, 32(19):1800–1806, Sep 2021.

[132] Blake W Tye, Nicoletta Commins, Lillia V Ryazanova, Martin Wühr, Michael Springer, David Pincus, and L Stirling Churchman. Proteotoxicity from aberrant ribosome biogenesis compromises cell fitness. *eLife*, 8, Mar 2019.

[133] Ambro van Hoof, Pamela A Frischmeyer, Harry C Dietz, and Roy Parker. Exosome-mediated recognition and degradation of mrnas lacking a termination codon. *Science*, 295(5563):2262–2264, Mar 2002.

[134] Ambro van Hoof and Eric J Wagner. A brief survey of mrna surveillance. *Trends in Biochemical Sciences*, 36(11):585–592, Nov 2011.

[135] Edward W J Wallace, Jamie L Kear-Scott, Evgeny V Pilipenko, Michael H Schwartz, Pawel R Laskowski, Alexandra E Rojek, Christopher D Katanski, Joshua A Riback, Michael F Dion, Alexander M Franks, and et al. Reversible, specific, active aggregates of endogenous proteins assemble upon heat stress. *Cell*, 162(6):1286–1298, Sep 2015.

[136] Ge Wang, Pengxiu Cao, Yumei Fan, and Ke Tan. Emerging roles of hsf1 in cancer: Cellular and molecular episodes. *Biochimica et biophysica acta. Reviews on cancer*, 1874(1):188390, Jul 2020.

[137] J R Warner. The economics of ribosome biosynthesis in yeast. *Trends in Biochemical Sciences*, 24(11):437–440, Nov 1999.

[138] Kerstin S Wendt and Frank G Grosveld. Transcription in the context of the 3d nucleus. *Current Opinion in Genetics & Development*, 25:62–67, Apr 2014.

[139] Luke Whitesell and Susan L Lindquist. Hsp90 and the chaperoning of cancer. *Nature Reviews. Cancer*, 5(10):761–772, Oct 2005.

[140] John L Woolford and Susan J Baserga. Ribosome biogenesis in the yeast saccharomyces cerevisiae. *Genetics*, 195(3):643–681, Nov 2013.

[141] Jeremy J Work and Onn Brandman. Adaptability of the ubiquitin-proteasome system to proteolytic and folding stressors. *The Journal of Cell Biology*, 220(3), Mar 2021.

[142] Jerry L Workman. Nucleosome displacement in transcription. *Genes & Development*, 20(15):2009–2017, Aug 2006.

[143] Lidia Wrobel, Ulrike Topf, Piotr Bragoszewski, Sebastian Wiese, Malgorzata E Sztolsztener, Silke Oeljeklaus, Aksana Varabyova, Maciej Lirski, Piotr Chroscicki, Seweryn Mroczek, and et al. Mistargeted mitochondrial proteins activate a proteostatic response in the cytosol. *Nature*, 524(7566):485–488, Aug 2015.

[144] Si Wu, Liu Hong, Yuqing Wang, Jieqiong Yu, Jie Yang, Jie Yang, Hong Zhang, and Sarah Perrett. Kinetics of the conformational cycle of hsp70 reveals the importance of the dynamic and heterogeneous nature of hsp70 for its function. *Proceedings of the National Academy of Sciences of the United States of America*, 117(14):7814–7823, Apr 2020.

[145] Ayako Yamamoto, Junko Ueda, Noritaka Yamamoto, Naoya Hashikawa, and Hiroshi Sakurai. Role of heat shock transcription factor in saccharomyces cerevisiae oxidative stress response. *Eukaryotic Cell*, 6(8):1373–1379, Aug 2007.

[146] Kota Yanagitani, Szymon Juszkiewicz, and Ramanujan S Hegde. Ube2o is a quality control factor for orphans of multiprotein complexes. *Science*, 357(6350):472–475, Aug 2017.

[147] Haneul Yoo, Jared A M Bard, Evgeny V Pilipenko, and D Allan Drummond. Chaperones directly and efficiently disperse stress-triggered biomolecular condensates. *Molecular Cell*, 82(4):741–755.e11, Feb 2022.

[148] Haneul Yoo, Jared A.M. Bard, Evgeny Pilipenko, and D. Allan Drummond. Chaperones directly and efficiently disperse stress-triggered biomolecular condensates. *BioRxiv*, May 2021.

[149] Kenneth S Zaret. Pioneer transcription factors initiating gene network changes. *Annual Review of Genetics*, 54:367–385, Nov 2020.

[150] Kenneth S Zaret and Jason S Carroll. Pioneer transcription factors: establishing competence for gene expression. *Genes & Development*, 25(21):2227–2241, Nov 2011.

[151] Hongchen Zhang, Shipeng Shao, Yong Zeng, Xiaotian Wang, Yizhi Qin, Qiunan Ren, Shengqi Xiang, Yuxin Wang, Junyu Xiao, and Yujie Sun. Reversible phase separation of hsf1 is required for an acute transcriptional response during heat shock. *Nature Cell Biology*, Mar 2022.

[152] Xu Zheng, Joanna Krakowiak, Nikit Patel, Ali Beyzavi, Jideofor Ezike, Ahmad S Khalil, and David Pincus. Dynamic control of hsf1 during heat shock by a chaperone switch and phosphorylation. *eLife*, 5, Nov 2016.

[153] J Zou, Y Guo, T Guettouche, D F Smith, and R Voellmy. Repression of heat shock transcription factor hsf1 activation by hsp90 (hsp90 complex) that forms a stress-sensitive complex with hsf1. *Cell*, 94(4):471–480, Aug 1998.